HYDROGEN ISOTOPE GEOCHEMISTRY OF THE MANTLE: CONSTRAINTS FROM BACK ARC BASIN BASALTS AND MANTLE XENOLITHS

Thesis by

Julie Ann O'Leary

In Partial Fulfillment of the Requirements for the

Degree of

Doctor of Philosophy

CALIFORNIA INSTITUTE OF TECHNOLOGY

Pasadena, California

2007

(Defended September 5, 2006)

ACKNOWLEDGEMENTS

I would like to thank my advisor, John Eiler, for the encouragement, advice, scientific opportunities, and good humor that he is always willing to share. I would also like to thank George Rossman for his guidance and the joy that he brings to science. I thank Paul Asimow for acting as my academic advisor and Ken Farley for acting as a both an advisor and friend.

I thank Nami Kitchen and Wang Zhengrong for being great co-workers and for teaching me how to work in a lab. The geochemistry and petrology group at Caltech is full of many talented and helpful people. I would particularly like to thank Mike Baker, Hagit Afek, Magnus Eek, Liz Miura Boyd, Jed Mosenfelder, Lindsay Hedges, John Beckett, Paula Smith, Laura Baker, Sarah Miller, Sally Newman, and Ma Chi for their generosity with time, expertise, and materials.

I would like to the Yoshi Tamura, Robert Stern, and JAMSTEC for the opportunity to participate in a research expedition to the Marianas. During my undergraduate education I was fortunate to be encouraged to pursue geology by Gordon Medaris, Clark Johnson, John Valley, Brian Beard, and William Peck.

I would like to thank the Gordon and Betty Moore foundation for fellowship support for four years of graduate school.

It has been a pleasure to become friends with many bright, offbeat people during grad school. I will miss them terribly when I leave and look forward to seeing them again. I would particularly like to say thanks to Lucia Fernandez-Ballester, Eunjung Choi, Paul

Wiggins, David Shuster, Nicole and Nathan Smith Downey, Laura Baker, Julie Fry, John Crounse, Jesse Kroll, and Sarah Miller.

Lastly, I would like to thank my family. My parents, Phil and Carol O'Leary, my brother, Dan O'Leary, and grandmother, Ruth Wilson, have supported me at every stage of my life. I would not have been able to finish this thesis without the.

DEDICATION

I dedicate this thesis to the Rooseloons, for all the fun times we have had together.

ABSTRACT

A new technique for measuring the hydrogen isotopic compositions of small quantities of hydrous and nominally anhydrous silicate materials was developed. The hydrogen isotopic composition of mantle derived basalts and nominally anhydrous minerals were measured to examine the systematics of the hydrogen isotope geochemistry of the mantle and to better constrain the mantle water cycle.

Back arc basin basalts (BABB) from the Mariana Trough are variably enriched in deuterium relative to mid ocean ridge basalts (MORBs). The δD values of 15 Mariana Trough BABB samples range from -74 ‰ to -34 ‰. High δD values in BABB lavas are associated with the trace element signature of H_2O rich fluids derived from the altered oceanic crust that is subducting into the mantle. We calculate a mixing model to constrain the isotopic composition and trace element chemistry of the fluid infiltrating the back arc lava source region. The δD value of the infiltrating fluid is close to -30 ‰. When the composition of the infiltrating fluid is compared to a forward calculation of the hydrogen isotopic evolution of altered oceanic crust it indicates that hydrous fluids in the back arc source region originate from the hydrated lithospheric mantle section of altered oceanic crust. Forward model calculations predict that hydrogen deeply subducted into the mantle may have an isotopic composition that is highly fractionated from the initial composition of altered oceanic crust.

Pyroxenes from mantle xenoliths are deuterium depleted relative to all mantle materials, with δD values ~50 ‰ lower than average MORB. Using continuous flow mass

spectrometry we analyzed the hydrogen isotopic composition of clinopyroxene and orthopyroxene from mantle xenoliths. Our results confirm the previous observations of very low δD values for xenoliths from continental interiors but found δD values similar to MORB in Central American arc xenoliths. The relationship between δD and water content observed in pyroxenes suggests that most mantle xenoliths have undergone extensive degassing (40 % – 60 %) and therefore the hydrogen content of upper mantle minerals may be higher than previously thought.

TABLE OF CONTENTS

FIGURES

Number *Page*

Chapter 1

Chapter 2

Chapter 3

Chapter 4

TABLES

Number *Page*

Appendix 3

Chapter 1

Introduction

The concentration and distribution of water in the mantle influences the formation of oceanic crust and is a dominant factor in arc magmatism. Water concentrations measured in mid ocean ridge basalts (MORB), back arc basin basalts (BABB) and mantle xenoliths indicate that the upper mantle is heterogeneous in water content, varying from tens to hundreds of ppm water (by weight, as H_2O). However, the mantle hydrogen cycle has not been quantitatively described. There is a large range in the hydrogen isotopic composition of mantle samples (>100‰ reported in values of δD_{VSMOW}); these differences should be able to offer constraints on the source of mantle reservoirs of hydrogen (see figure 1.1). This thesis investigates the range of hydrogen isotopic compositions found in mantle reservoirs and attempts to quantitatively describe processes that control isotopic heterogeneity in back arc basin basalts and mantle xenoliths.

Hydrogen on Earth is divided between the hydrosphere, consisting of the oceans, biomass, freshwater, and groundwater and the lithosphere, where hydrogen is contained in hydrous and nominally anhydrous minerals. Estimates of water stored in the mantle range from 0.5 to 5.5 times the mass of water in the modern hydrosphere (Ahrens 1989; Jambon 1994; Jambon and Zimmermann 1990). Mantle minerals have the capacity to store large amounts of hydrogen, up to 0.4 wt % H_2O (Hirschmann, Aubaud, and Withers 2005) in upper mantle lithologies. Measurements of mantle derived basalts and xenoliths suggest that the water content of the upper mantle is much less than the storage capacity,

500 between 90 ppm and 450 ppm H_2O (Bell and Rossman 1992b; Danyushevsky et al. 2000; Jambon 1994; Michael 1988; Peslier and Luhr 2006). Hydrogen is exchanged between the mantle and the hydrosphere primarily in two geologic environments: mid ocean ridges and subduction zones. Melting at mid ocean ridges extracts hydrogen dissolved in basaltic melts, a process that releases 1-2 × 10^{11} kg H_2O/year to the hydrosphere (Ito, Harris, and Anderson 1983). This outward flux is countered by water subducted in altered oceanic crust. The proportion of water in altered oceanic crust that is deeply subducted is unknown, estimates range from 40% (Rupke et al. 2004) to less then 5% (Dixon et al. 2002) of the initial water is retained in deeply subducted oceanic lithosphere.

Hydrogen has two stable isotopes, protium (^{1}H) and deuterium (^{2}H or D), that are fractionationated by chemical and physical processes. Ocean water, with D/H = 0.00015576, δD = 0‰, is used as the reference frame for hydrogen isotope compositions of natural materials (Hagemann 1970). Hydrogen fractionations between water and hydrogen bound as hydroxyl in hydrous minerals are large, typically water in equilibrium with hydrous minerals are D enriched by 10‰ to 50‰ (Chacko et al. 2001). The magnitudes of mineral-fluid fractionation factors are sensitive to temperature, pressure, mineral phase, and composition of the water.

Mid ocean ridge basalts (MORBs) contain a restricted range in isotopic composition with a mode of -75‰, thought to be typical of upper mantle hydrogen(Chaussidon and Jambon 1994; Chaussidon et al. 1991; Craig and Lupton 1976; Garcia 1989; Kyser and O'Neil 1984; Pineau and Javoy 1994; Poreda et al. 1986). Back-arc basin basalts are higher, on average, in δD compared to MORB but vary widely

(range of -74‰ to -34‰; mode of -44‰) (Poreda 1985b; Honma et al. 1991; Chapter 2). This difference likely reflects the addition to the sources of arc-related lavas of D-enriched fluids and/or hydrous melts from subducted oceanic lithosphere. Ocean island basalts are the most heterogeneous in δD, with some measured compositions below the MORB average and some above (range of -165‰ to -33‰ (Garcia 1989; Hauri 2002; Kingsley et al. 2002; Poreda et al. 1986)). These variations have also been attributed to the addition of subduction-derived hydrogen to the mantle sources of OIB. Mantle pyroxenes and garnets are among the lowest- δD mantle materials (-129 to -89‰) (Bell and Ihinger 2000; O'Leary et al. 2005). The origin of their exotic and variable δD values is unclear, and represents a central mystery in our understanding of the mantle hydrogen budget. In this thesis I present a new method for measuring the hydrogen isotope composition of geologic materials and use this method to investigate hydrogen isotope chemistry of mantle materials.

Chapter 2 is an investigation of the hydrogen and oxygen isotope chemistry of the Mariana Arc system. Basalts from the Mariana Trough vary in water content from concentrations similar to those found in mid ocean ridge basalts (MORB) to ten times those concentrations and previous studies found δD values up to ~40‰ higher than average MORB. The high water content of back arc basin basalts (BABB) plausibly reflects the addition of fluid derived from subducted ocean crust to the mantle wedge. The hydrogen isotope composition of Marianas trough lavas vary between -74‰ and -34‰; this is a larger range than previous measured in related lavas (-46‰ to -32‰ (Poreda 1985a)) and is similar to the previously observed range for back arc basin basalts generally (-70‰ to -32‰ (Honma et al. 1991; Poreda 1985a)). Two-thirds of our sample

suite span a small range in δD (-40 ± 4‰) that we suggest is representative of the Marianas Trough. Correlations between the trace element content, δD value, and $\delta^{18}O$ value of basalts were used to calculate a mixing model that indicates the Mariana Trough basalt source region was fluxed by a low $\delta^{18}O$, high δD siliceous fluid. This result was then compared to a forward model of hydrogen released from hydrated ocean crust during subduction.

In chapter 3 a technique for measuring the water content of nominally anhydrous minerals is described. Hydrogen extraction followed by manometry and mass spectrometry is a standard method for absolute water content and hydrogen isotope measurements, but requires large masses of sample (typically 10s of mg to grams). Major contributions have been made by measuring relative concentration on very small samples using infrared spectroscopy and secondary ionization mass spectrometry, but these methods must be calibrated by absolute methods. In collaboration with John Eiler and George Rossman, I developed methods to measure the absolute hydrogen content and isotope composition of minerals using continuous flow mass spectrometry. This approach is independent of mineral species and requires ~1/1000 the absolute amount of H required by conventional mass spectrometry, making this technique attractive for analyzing mantle materials, where there are often only small quantities available.

Chapter 4 uses the techniques developed in chapter 3 to measure the hydrogen isotopic composition of clinopyroxene and orthopyroxene from mantle xenoliths. Nominally anhydrous minerals from mantle xenoliths are the most deuterium depleted of all mantle materials, with δD values ~50‰ lower than average MORB (Bell and Ihinger 2000). These variations suggest large hydrogen fractionations within the mantle but

available data were limited to large, high-quality samples needed for conventional measurement techniques. Using our continuous flow technique we analyzed the hydrogen isotopic composition of clinopyroxene and orthopyroxene from mantle xenoliths. Our results confirm the previous observations of very low δD values for xenoliths from continental interior but found δD values similar to MORB in Central American arc xenoliths. The relationship between δD and water content observed in pyroxenes suggests that most mantle xenoliths have undergone extensive degassing (40%-60%) and therefore the hydrogen content of upper mantle minerals may be higher than previously thought.

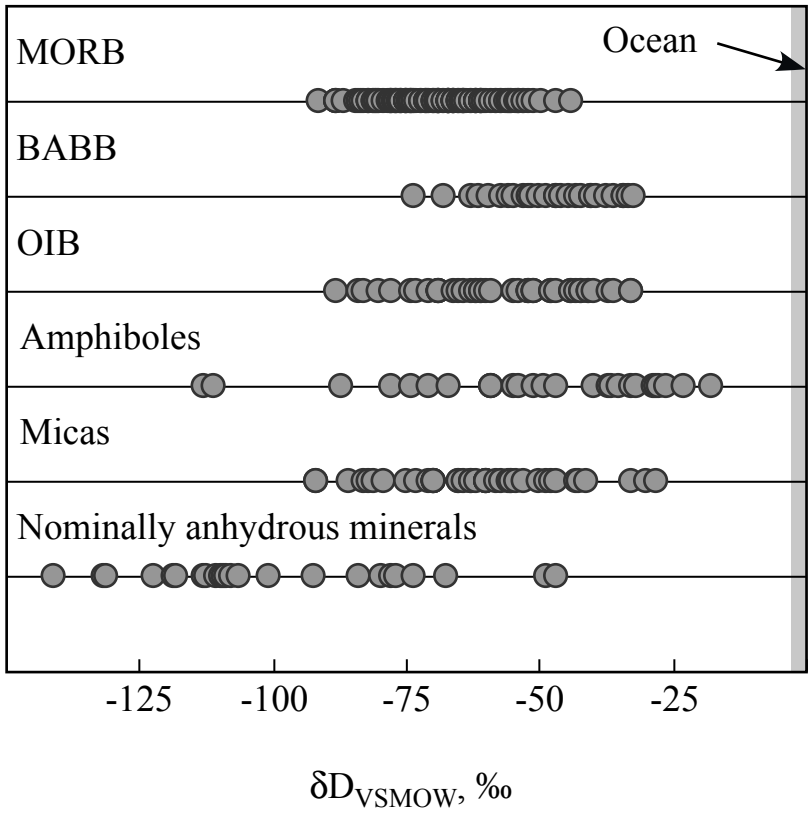

Figure 1.1 The hydrogen isotope composition of mantle materials.

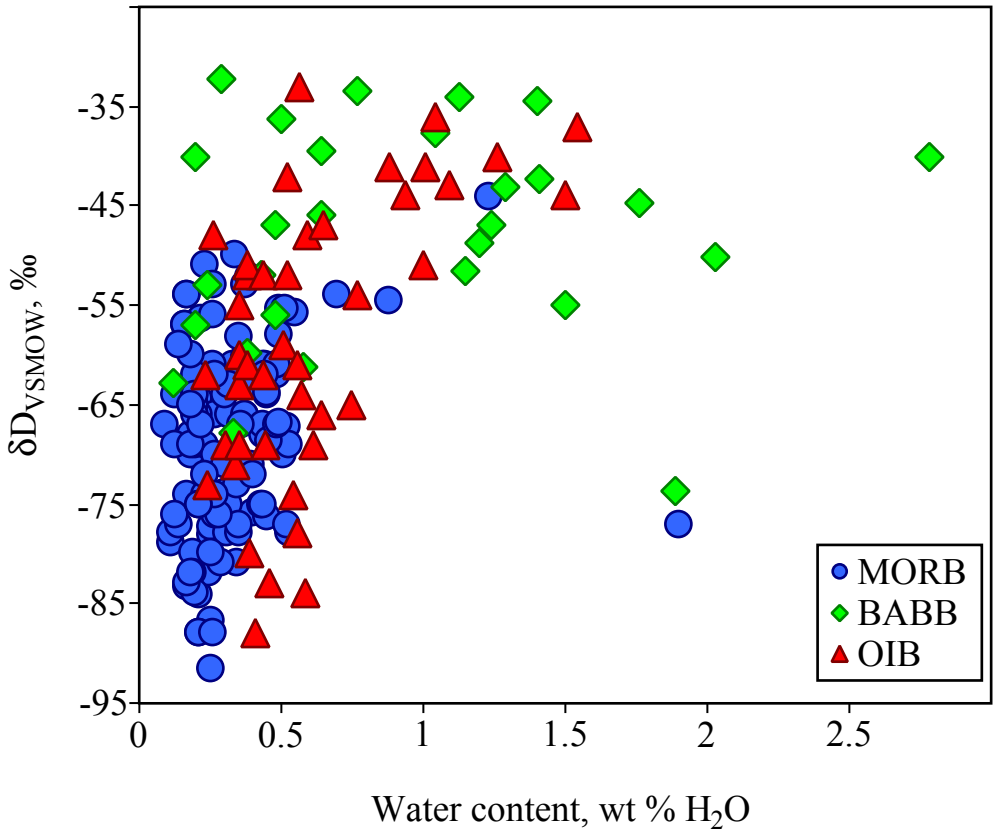

Figure 1.2 δD vs. water content for mantle derived basalts.

Chapter 2

Hydrogen and Oxygen Isotope Chemistry of Mariana Trough Basalts

Julie A. O'Leary, John M. Eiler, and Nami Kitchen

Abstract

Basaltic lavas from the Mariana Trough back arc basin vary in water content from concentrations similar to mid ocean ridge basalts (MORBs) to ten times higher. These variations plausibly reflect addition of subducted water to the mantle wedge above the subducting Pacific plate, but must also reflect variations in extent of melting of that mantle and degree of crystallization-differentiation of those melts before eruption. We report hydrogen and oxygen isotope data for lavas from the Mariana trough. These measurements, along with other geochemical data, constrain the relative proportions of subducted vs. "primitive" water in their mantle sources. Hydrogen isotope compositions in these lavas are enriched in D/H ratio by up to 35 ‰ relative to MORBs. Variations in δD correlate with geochemical indices frequently associated with fluid components, including Ba/La, Th/U, Ce/H_2O, Ce/Pb, and La/Sm. We present a forward model that constrains the characteristics and source of a slab derived fluid consistent with these trends. The data we present require that the fluid-rich component added to the mantle sources of Mariana Trough basalts came from serpentinized peridotitic sections of altered ocean lithosphere, and sampled trace elements from crustal rocks that had already undergone significant water loss underneath the arc.

Introduction

Hydrogen is a minor component of the upper mantle (averaging a few 100 ppm, by weight, as H_2O) but exerts a major influence on mantle melting and rheology and is believed to be a key to understanding mantle convection (Hirth and Kohlstedt 1996; Asimow and Langmuir 2003). The present distribution and historical cycle of mantle hydrogen are poorly understood, although the largest outputs from and inputs to the mantle can be identified. Hydrogen is principally extracted from the mantle as OH and H_2O dissolved in basaltic melts; it seems likely, based on global budgets of other trace volatiles, that this process has removed a large fraction (10's of per cent) of the mantle's primordial hydrogen inventory (Williams and Hemley 2001). Subduction adds hydrogen to the mantle in several ways: Aqueous fluids are evolved from the subducting lithosphere as a consequence of dehydration metamorphism of its hydrous rocks (metasediments, metabasaltic greenschists and amphibolites, and serpentinites; (Schmidt and Poli 1998; Kerrick and Connolly 2001; Poli and Schmidt 2002)); water rich silicate melts are evolved from the slab by partial melting of metasediments (Elliott, Plank et al. 1997; Plank and Langmiur, 1993) and, in special circumstances, metabasalts (Defant, Richerson et al. 1991); and the residues of dehydration and partial melting of subducted slabs likely contain hydrogen.

Hydrogen isotope compositions (i.e., H^2/H^1 or D/H) of mantle materials, mantle derived melts, and components of oceanic lithosphere (which presumably resemble rocks in subducting slabs, at least during the early stages of subduction) can constrain the

mantle water cycle. The hydrogen isotopic compositions of mantle minerals, reported in values of δD_{VSMOW}, range from very low values found in "nominally anhydrous" mantle garnets and clinopyroxenes (-129 to -89 ‰) (Bell and Ihinger 2000; O'Leary, J.M. et al. 2005); to variable but often deuterium enriched values in amphiboles and micas from hydrous mantle peridotites (-108 to -33 ‰) (Kuroda 1977; Boettcher 1980; Harmon 1987; Wagner 1996), and in back arc basin basalts (-70 to -32 ‰) (Poreda 1985; Honma, Kusakabe et al. 1991). Mid ocean ridge basalts (MORBs) and oceanic intraplate basalts (OIBs) are more restricted in hydrogen isotope composition with an average of -69 ‰ that has been often interpreted to be typical of mantle hydrogen (Craig and Lupton 1976; Kyser and O'Neil 1984; Poreda, Schilling et al. 1986; Garcia 1989; Chaussidon, Sheppard et al. 1991; Chaussidon and Jambon 1994; Pineau and Javoy 1994; Pineau, Shilobreeva et al. 2004) (see figure 2.1). Components of the ocean lithosphere are variable in hydrogen isotope composition but relatively deuterium enriched, on average, compared to MORB and OIB: marine cherts are lowest in average δD, -84 ± 10 ‰ (Knauth and Epstein 1975; Knauth and Epstein 1976; Kolodny and Epstein 1976), whereas hydrothermally altered oceanic basalts, gabbros, and peridotites range between -81 and -25‰ with an average of -45 ± 15‰ (Satake and Matsuda 1979; Kawahata, Kusakabe et al. 1987; Agrinier, Hekinian et al. 1995). Thus, it seems likely that additions of subducted hydrogen to mantle materials both increase their H contents and elevate their D/H ratios. The H isotope geochemistry of the mantle might resemble its O isotope geochemistry, which is characterized by a large amount of ultramafic rock having a relatively constant $\delta^{18}O$ value, and a small fraction of recycled materials that drive larger oxygen isotope variations (Eiler 2001).

However, mantle H isotope geochemistry differs in one important respect from its O isotope geochemistry: metamorphic, melting, and metasomatic processes—generally considered unimportant for most recognized oxygen isotope variations—can produce large hydrogen isotope fractionations. In fact, intramantle differentiation can produce hydrogen isotopic variations similar in magnitude to those generated by crustal recycling. These factors may be responsible for the great isotopic variability of mantle amphiboles (Boettcher 1980). One possible consequence of these fractionations is that the D/H ratio of hydrogen ultimately added to the mantle by subduction may be substantially different from D/H ratios in the components of the ocean lithosphere that are the initial sources of that subducted hydrogen. In particular, dehydration reactions in the subducting slab fractionate D/H between evolved aqueous fluids and structural OH in residual minerals, even at mantle temperatures (Suzuoki and Epstein 1976; Graham, Sheppard et al. 1980; Graham, Harmon et al. 1984; Graham, Viglino et al. 1987). Therefore, the hydrogen isotopic compositions of fluids evolved from the slab may differ from the lithologies from which those fluids are derived and the residues of dehydration reactions may differ from components of the ocean lithosphere (perhaps dramatically so when dehydration is nearly complete). For these reasons, the hydrogen isotope geochemistry of the mantle provides a potential constraint on the mantle water cycle, but only if one can understand the controls on isotopic variations.

In this study, we attempt to constrain the hydrogen isotope budget of subduction related processes through study of the H and O isotope geochemistry of seafloor basalts from the Mariana Trough, an active back arc basin in the Mariana Arc system (Stern 2002). Back arc basin basalts (BABBs) contain variable amounts of water (generally

from 0.1 to 3 wt % H_2O) that correlate with geochemical indicators of slab derived fluid and/or melt components and with indicators of the degree of melting of their mantle sources (Danyushevsky, Falloon et al. 1993; Stolper and Newman 1994; Newman and Stolper 2000; Kelley in press). Because BABB volcanic centers lie far from their associated trenches, they may sample slab derived water from subducted lithologies that have experienced extensive metamorphism and possibly partial melting; thus they provide an opportunity to examine the consequences of those processes for the hydrogen isotope budget of subduction. Furthermore, BABBs generally undergo significantly less degassing and crystallization-differentiation than do arc related lavas, simplifying the interpretation of their water contents and hydrogen isotopic composition (Gribble, Stern et al. 1998; see (Asimow 2005) for exceptions to this generalization).

Previous studies suggest that the hydrogen isotope compositions of BABBs from different spreading centers might be distinct from one another: Lau Basin BABBs have δD values closest to putative normal mantle (-69 to -43 ‰); those from the Okinawa Trough are slightly more deuterium enriched (-52 to -57 ‰); and those from the Mariana Trough are most deuterium-rich (-32 to -46 ‰) (figure 2.1). However, two of these three suites (the Lau Basin and Mariana Trough) are sparsely sampled and isotopically variable, suggesting these differences might not be representative or statistically significant. Previous work also suggests a positive correlation between water contents and δD values for the Mariana Trough and Lau Basin BABBs, although this trend was based on limited data and was violated by two out of nine samples (Poreda 1985). Regardless, this result suggests that a larger amount of deuterium rich, slab derived fluids were added to the source of Mariana BABBs than to the source of Lau BABBs.

Subsequent investigations of Mariana Trough BABBs have found a large range in water content as well as correlations between water content, extent of melting, and trace element indicators of slab contributions to mantle sources, but have not related those trends to hydrogen isotope variation (Stolper and Newman 1994; Newman and Stolper 2000; Kelley in press). This study examines a diverse, well characterized and relatively large suite of samples from one back arc basin to look for within suite variations in hydrogen isotope composition, and to relate those to variations in other geochemical properties.

A significant aspect of our study is that we determine both H and O isotope compositions for the samples. Oxygen isotope ratios of mantle derived basalts are sensitive to the addition of subducted sediments, altered crust and possibly other components of the ocean lithosphere, and thus provide an important complement to H isotope data. Oceanic lithosphere is heterogeneous in oxygen isotopic composition: sediments have $\delta^{18}O_{VSMOW}$ values of 15 to 42 ‰ (Ito and Stern 1986), altered basalts from 7 to 15 ‰ (Gregory and Taylor 1981; Kawahata, Kusakabe et al. 1987), and altered gabbros and serpentinites from 0 to 6 ‰ (Gregory and Taylor 1981). Therefore, $\delta^{18}O$ values of arc related basalts from sources influenced by slab derived components can provide some indication of the part of the slab from which those components are derived (see Eiler, Carr et al. (2005) for a recent example of such arguments).

Samples and Methods

Oxygen and hydrogen isotope measurements were made on 15 samples of vesicular, olivine-chromite-plagioclase phyric basalt (average MgO = 6.8 wt. %; average Mg# = 0.61, where Mg# is calculated as $Mg \div (Fe + Mg)$, on a molar basis assuming all Fe is Fe^{2+}) and one sample of rhyolite. These samples were dredged or collected using the ALVIN submersible from the Mariana Trough between 15 degrees N and 21 degree N (figure 2.2). All samples were collected below 3000 meters water depth, at or below the H_2O saturation depth (Newman and Stolper 2000). The petrography, major element compositions, rare earth element compositions, and volatile concentrations for all samples were determined by previous studies (Volpe 1987; Stern, Lin et al. 1990; Stolper and Newman 1994; Newman and Stolper 2000; Pearce 2005).

All materials selected for hydrogen and oxygen isotope analysis are chips of glass taken from pillow rinds. Glass separates were gently crushed in an agate mortar and dry sieved to isolate the 90-212 μm size fraction, which was then hand picked under a binocular microscope to exclude glass fragments containing visible fluid or mineral inclusions. Finally, this purified, size-sorted separate was ultra-sonicated in ethanol and dried in a 120˚C oven before analysis.

Oxygen isotope ratios were determined by laser fluorination at the California Institute of Technology using a method based on that of Sharp (1990) and Valley (1995) and recently described in Cooper, Eiler et al. (2004). Briefly, 1 to 2.5 mg aliquants of glass were reacted with BrF_5 while heating with a 50 W, 10.5 μm laser. Product O_2 was purified by cryogenic methods and passage over hot Hg, converted to CO_2 by reaction with hot graphite, and analyzed on a Finnegan MAT 251 gas source isotope ratio mass spectrometer. Samples were analyzed for $\delta^{18}O$ on 6 separate days. On each day, 5 to 10

aliquots of garnet standard, UWG2 (Valley 1995), were also analyzed with an average reproducibility of ± 0.10 ‰, 1σ, on any single day. The difference between the average measured value for this standard and its accepted value of 5.75 ‰ was applied as a correction to all sample measurements. Corrections averaged -0.18 ± 0.07 ‰, 1σ. A total of 43 aliquots of garnet were run with an overall average, pre-corrected value of 5.95 ± 0.13 ‰, 1σ. On several analysis days, aliquants of two intra-laboratory reference glasses, ALV 526-1 and AH 95:1-1, were also analyzed. Analyses of these glasses, corrected to the VSMOW scale based on measurements of UWG2 on the same day, are 5.37 ± 0.04 ‰ (n=9) for ALV 526-1, and 5.01 ± 0.1‰ (n=4) for AH 95:1-1. Previous measurements of AH95:1-1 in the USC and University of Wisconsin-Madison labs found values of 4.94 ‰ and 4.92 ‰, respectively. Previous measurements of ALV 526-1 in the Caltech lab average 5.37 ‰ for 17 analyses (Cooper, K.M., written communication).

Hydrogen isotope ratios were measured by heating glass separates in an O_2-He gas stream followed by collection and reduction of evolved water and carrier gas mass spectrometry of product H_2, using a modified version of the method described in (Eiler and Kitchen 2001). Briefly: aliquots of glass weighing between 0.1 and 1 mg are wrapped in platinum foil and placed in alumina tubes purged by a mixture of He and O_2. The loaded tubes are heated overnight at 80 ˚C to remove surface water. The tubes are then heated to 1100 ˚C using a resistance heater, driving devolatilization of the sample glass. The partial pressure of O_2 in the He purge stream is used to convert released hydrogen to H_2O rather than H_2, CH_4 or other reduced gases. Evolved water is cryogenically collected, reduced to H_2 by hot uranium metal, and passed through a capillary into a Thermo-Finnigan MAT Delta-plus XP gas source isotope ratio mass

spectrometer. This technique requires correction for blank water contributions. Blanks were measured each day by trapping water from the He stream exiting empty sample tubes for duration three times that of an analysis (to assure that enough H was recovered to precisely characterize the blank). Measured blanks, scaled to account for differences in collection time, were subtracted from all sample measurements. The accuracy and precision of our technique was characterized by analyzing two interlaboratory hydrogen isotope standards (basaltic glass Kil 2-1(δD = -62 ‰, Garcia, 1986), and a serpentine standard provided by Bruce Nelson (δD = -84.1, personal communication)) and one intralaboratory standard (basaltic glass ALV 526-1 (δD = -67 ‰)). On each analysis day, 2-3 aliquots of one or more of the three standard materials were analyzed, and 2 unknown samples were analyzed in duplicate. Data were rejected if any of the following criteria were violated:

- The blank must not exceed 10% of the sample size; the average blank contribution for accepted analyses was 6%.
- Both the blanks and intra and inter laboratory standards must be reproducible in D/H to within ± 10 ‰ during the course of an analytical session. Average standard deviation within an analytical session for ALV 526-1 was ± 4.3 ‰.
- Intra and interlaboratory standards must yield D/H within 10 ‰ of accepted values; the average daily offset was -5.8 ‰.
- The H yield must be consistent with water contents determined by FTIR analysis (Newman and Stolper 2000) within an analytical session to within 20% relative.

The external precision for replicate analyses of unknown samples averages ± 2.7 ‰ (1σ, n=2 for most samples). Measurements of KIL 2-1 standard averaged -65 ± 4.5 ‰

(n=7); ALV 526-1 averaged -72.2 ± 4.1 ‰ (n=15). Thus, we infer that analyses of unknowns have standard deviations of ±3 to 4 ‰, or typical standard errors (accounting for replicate analyses) of ± 2 to 3 ‰. Analyses of the serpentine standard averaged -91.0 ± 8 (n=2). We infer that the greater analytical uncertainty in this result could reflect isotopic heterogeneity of this standard, which we typically analyze in 10-50 µg aliquots, in contrast to the 1-5 mg aliquots analyzed by conventional means to calibrate its δD value.

Results

Hydrogen and oxygen isotope compositions

Values of δD_{VSMOW} for 15 Mariana Trough basaltic glasses vary between -74 ‰ and -34 ‰ (Table 1; figure 2.1). Despite this large range, most (11 out of 15) of the samples we examined group around an average value of -42 ± 5‰, which we suggest is typical of Mariana back arc basin basalts. The distribution of δD_{VSMOW} values is not Gaussian; the extremes are 12 ‰ above and 30 ‰ below the mode. This range extends from a minimum comparable to the average for MORBs (δD_{VSMOW} = -69 ‰) (Craig and Lupton 1976; Kyser and O'Neil 1984; Poreda, Schilling et al. 1986; Chaussidon, Sheppard et al. 1991; Pineau and Javoy 1994) to a maximum comparable to the highest values previously observed in BABBs (Poreda 1985) (figure 2.1). Previous analyses of Mariana BABBs have values of δD_{VSMOW} between -32 and -47 ‰—within our observed range but near the deuterium-enriched extreme. Our results for Mariana Trough basalt

also encompass the hydrogen isotopic compositions of BABBs from the Okinawa Trough (Honma, Kusakabe et al. 1991) and the Lau Basin (Poreda 1985), suggesting that previous indications of inter-basin differences in hydrogen isotope composition are insignificant compared to the tens of ‰ variations within a single basin.

Values of $\delta^{18}O_{VSMOW}$ for Mariana Trough basalts average 5.43 ‰ with a range from 5.01 to 5.68 ‰. This average is comparable to that found in mid ocean ridge basalts using the same laboratory and techniques (5.40 ‰), (Eiler, Gronvold et al. 2000; Cooper, Eiler et al. 2004) and 0.37 ‰ lower than the previous average for Southern Mariana Trough basalts (Macpherson, Hilton et al. 2000; Ito, Stern et al. 2003). Previous data for glasses were generated by laser fluorination at the Royal Holloway laboratories, London, reported by (Macpherson, Hilton et al. 2000) and by nickel-rod bomb at the University of Minnesota, reported by (Ito, Stern et al. 2003). This difference is a large multiple of analytical precision and suggests either that some systematic error exists in one or more of the data sets, or that our suite samples a systematically different part of the oxygen isotope distribution of Mariana Trough basalts than was sampled by previous studies. Our sample suite includes four samples previously analyzed by laser fluorination at the University of Wisconsin-Madison (Eiler, Gronvold et al. 2000). The difference between these previous results and our new results averages 0.03 ± 0.01 ‰; i.e., the relatively low $\delta^{18}O_{VSMOW}$ values characteristic of these samples are not specific to the Caltech lab. There have been no direct comparisons of measurements of $\delta^{18}O$ for basaltic glasses in the Royal Holloway and Caltech facilities, although comparisons for other phases suggest no interlaboratory bias exists. One of the samples examined here, ALV 1846-9, was also analyzed by nickel-rod bomb techniques at the University of Minnesota (Ito, Stern et al.

2003). The three determinations for ALV 1846-9 from CIT, UW, and UM are 5.66 ± 0.10, 5.56 ± 0.07 and 5.8 ± 0.30 ‰, respectively. This comparison suggests laser fluorination analyses of these samples may be systematically lower than Ni-rod bomb analyses, although the basis for this comparison is slight and previous comparisons of this sort have revealed no such systematic inter-method differences (Valley 1995; Eiler, Crawford et al. 2000). The geographic distribution of samples examined by all these studies overlap and all are basalts with MgO wt % > 6.0%, suggesting we should have observed the same oxygen isotope distribution previously found for basalts from this area. Thus, there is no satisfactory explanation for the difference in mean $\delta^{18}O$ value between our results and previous studies, and we think it most likely reflects some combination of a small (~0.1-0.2 ‰) interlaboratory difference (perhaps due to differences in sample preparation or fluorination technique for glass) and a difference in the real isotopic distributions between the sample suite examined here and those examined by (Macpherson, Hilton et al. 2000) and (Ito, Stern et al. 2003).

Oxygen isotope measurements of olivine (Eiler, Crawford et al. 2000) and clinopyroxene (Ito, Stern et al. 2003) from Mariana arc basalts average 5.15 ‰ and 5.49 ‰, respectively. Basalt glass in equilibrium with these samples would have an average $\delta^{18}O$ value of 5.51 ‰—similar to the average measured value for BABB glass reported here. Thus, previous data for mineral separates from the Mariana arc system generally support our results for glass, though this comparison might be compromised by differences in source, degrees of assimilation and/or fractional crystallization between arc and back arc basalts.

The effects of fractional crystallization on isotopic composition and major element composition

Measured values of δD_{VSMOW} and $\delta^{18}O_{VSMOW}$ for the samples examined in this study do not correlate with either Mg# (figure 2.3) or SiO_2 content (not shown, but data are available in Stern, Lin et al. (1990)), consistent with the small isotopic fractionations that are expected to accompany crystallization-differentiation of relatively magnesian basalts (Eiler 2001). However, even if differentiation does not control the isotopic variability we observe, it might have produced second-order changes that could interfere with our ability to resolve or quantify other sources of isotopic variability. Therefore, we attempt to correct for such effects before examining correlations between stable isotope compositions and other geochemical parameters.

We corrected the compositions of analyzed lavas for the effects of olivine fractionation by adding equilibrium olivine to the measured compositions of glasses until they were in equilibrium with Fo_{90} olivine, using the procedure of (Stolper and Newman 1994) modified to incorporate Mg-Fe partitioning data from (Putirka 2005). As noted by (Stolper and Newman 1994), this procedure neglects liquidus spinel and pyroxene, but its previous success in describing compositional variations of Mariana basalts suggests it is adequate for our purposes.

Once the amount of olivine fractionated from a given lava prior to its eruption was estimated using the procedure described above, we then corrected the concentrations of trace elements, H_2O, Na_2O, K_2O, and TiO_2 by assuming they are perfectly incompatible in olivine. We then corrected the oxygen isotope compositions of those

lavas using an approach similar to those described by (Eiler 2001) and (Cooper, Eiler et al. 2004). The oxygen isotope composition of each increment of olivine was calculated using known temperature dependent oxygen isotope fractionations among minerals (Chacko, Cole et al. 2001) and assuming that the reduced partition coefficient ratio of the liquid equals the weighted average for the modal constituents of that liquid (Eiler 2001). These corrections range between 0.03 and 0.08 ‰, with an average of 0.044 ‰.

Trace amounts of hydrogen are partitioned into nominally anhydrous phases during crystallization. Olivine in equilibrium with these lavas will have 2.7-38.7 ppm H_2O (Aubaud, Hauri et al. 2004), concentrations are so low that crystallization-differentiation would not generate even subtle H isotope fractionation. If magmas became water saturated at their pressures of differentiation and eruption, H_2O degassing would fractionate H isotopes. While it is possible some of the lavas we studied became saturated in water prior to eruption, previous studies of CO_2 and H_2O contents in these lavas suggest they did not undergo significant degassing of water (Newman and Stolper 2000). Therefore, we make no correction to δD values for crystallization-differentiation or degassing effects.

Correlations between fractionation-corrected stable isotope compositions and other geochemical variables

The δD values of Mariana Trough lavas correlate negatively with their K_2O contents (and similarly with concentrations of most other highly incompatible elements), Ce/Pb, Ce/H_2O, and, excepting one outlier, Na_2O/TiO_2 ratio, and positively with Ba/La,

Th/U, and La/Sm. We can think of two processes that could contribute to these correlations: (1) Slab derived fluids are suspected of being higher in δD, lower in Ce/Pb and Ce/H_2O, and higher in Ba/La than typical upper mantle peridotites, and thus trends in figures 2.4.b, c, and f might be explained by addition of slab derived fluid to the mantle sources of Mariana Trough lavas. We particularly note that Ce and H_2O have similar mineral/melt distribution coefficients (Michael 1988) and Ce is relatively insoluble in aqueous fluids below temperatures of 1000º C (Kessel, Schmidt et al. 2005), so addition of D-rich aqueous fluid should lower the Ce/H_2O ratio of the hybrid source, leading to a negative correlation in figure 2.4f, as we observe. And, (2) variations in amounts of slab derived fluids can influence variations in degrees of mantle melting, which can control variations in absolute abundances of incompatible elements (e.g., K_2O) and relative abundances of moderately incompatible elements (e.g., Na_2O/TiO_2 and La/Sm). Therefore, if a high-δD, water-rich phase is added to mantle peridotite, increasing δD should be associated with increasing degree of melting, decreasing abundances of incompatible elements such as K_2O—assuming they are not resupplied at sufficiently high concentrations by the fluid itself—and decreasing ratios of less compatible to more compatible elements such as La/Sm and Na_2O/TiO_2 (figure 2.4a, d)—again, assuming neither element has its budget dominated by the fluid. Of course, some, perhaps most, elemental abundances and abundance ratios we consider could reflect a balance between the influences of aqueous fluid addition (process 1) and degree of partial melting (process 2); in a later section of this paper we construct a model that makes quantitative and self consistent statements about the balance of these effects in explaining our observations.

Previous measurements suggest that the δD values of Mariana Trough and Lau Basin lavas exhibit a negative correlation with $1/[H_2O]$ (Poreda 1985), although 2 out of 9 samples from that study were outliers from the trend defined by the other 7 (both were considerably poorer in water than expected based on their δD values). Okinawa Trough lavas (Honma, Kusakabe et al. 1991) also deviate from the trend defined in (Poreda 1985), with water contents both lower and higher than the expected relationship, although it should be noted that the water contents reported by (Honma, Kusakabe et al. 1991) are minimum contents. Our data, while generally overlapping the previously observed range in δD and $[H_2O]$ in BABBs, degrade the expected correlation even further; to the point that one must conclude there is no systematic relationship (figure 2.5). This is somewhat surprising given the many lines of evidence suggesting water is added to the mantle sources of BABBs, and that this added water is D-rich. It is also surprising given that a plot of δD vs. Ce/H_2O for samples examined in this study yields a simple trend with the expected negative slope (figure 2.4c). One explanation for this apparent contradiction may be that the relationship between water content and hydrogen isotope composition in Mariana Trough lavas is complicated by intra basin heterogeneity in water content prior to metasomatism by slab derived fluids and/or in the productivity of fluxed melting (i.e., melt produced per increment of fluid added).

Neither H isotope composition, geochemical indicators of slab fluids, nor major element indicators of melting are correlated with oxygen isotope compositions of Mariana trough lavas (figure 2.6). The $\delta^{18}O$ values of the mantle sources of subduction zone lavas can be either increased or decreased by addition of slab derived components (Eiler, Crawford et al. 2000; Eiler, Carr et al. 2005), depending on the part of the slab

from which those components come. However, in all cases large amounts of slab derived component (several per cent) are required to generate significant oxygen isotope variations (tenths of ‰). We suggest that the lack of correlation between oxygen isotope compositions and other geochemical indices of slab derived components (e.g., Ce/Pb, δD) in our sample suite could reflect either the counterbalancing influences of additions of both high- and low-$\delta^{18}O$ slab derived components (e.g., (Eiler, Carr et al. 2005)) and/or low abundances (~ 1 % or less) of slab derived components. We consider this possibility more concretely in the discussion, below.

Discussion

Stable isotope composition of the mantle sources of Mariana Trough basalts

Correlations between δD and incompatible trace element ratios (figure 2.4) suggest that these properties may be explained by mixing between two components in the mantle sources of Mariana BABBs. Association of high δD values with enrichments in Ba and H_2O relative to other elements of similar compatibility suggest that one of these components, presumably a slab derived fluid, has a δD_{VSMOW} value of ca. –30 ‰ or higher. The high δD end member is also low in Ce/Pb, and La/Sm compared to the sources of normal MORBs (Workman and Hart 2005). With the exception of La/Sm, these are all characteristics of slab derived fluids, and so can be reasonably attributed to subduction enrichment of the mantle wedge. The D-poor component(s) must have a value of δD less than or equal to -75 ‰, and is characterized by trace element ratios more

similar to the sources of normal MORBs. It is peculiar that La/Sm of our D-rich component is lower than that of the more MORB-like component, though the difference is small and may be attributed to preferential loss of La from the slab to the arc front during subduction, resulting in a low La/Sm in slab fluids released to the back arc, similar to other fluid mobile elements in arc systems (Kelley, Plank et al. 2005; Stern, Kohut et al. 2005). A subduction derived component with high Th/U is also the opposite of what is observed in Mariana Arc lavas (Elliott, Plank et al. 1997), this is further evidence that our D-rich component, while rich relative to normal mantle in fluid mobile elements depleted in La, Pb, Ba, and U relative to fluids infiltrating the Mariana Arc mantle source region.

We have attempted to quantitatively model our results by assuming that the lavas we have studied are products of melting hybrid sources that are mixtures between peridotites resembling the sources of N-MORBs and a slab derived end member, which might be either a solute rich supercritical fluid or a water rich silicate melt (which we model as two separate cases). This calculation assumes that the trace element composition of the peridotite source prior to metasomatism by fluid or melt is the same as the depleted peridotite previously used to model the Marianas BABB source (Stolper and Newman 1994), with Ce concentrations taken from (Workman and Hart 2005) and a slightly enriched La/Sm. We chose a higher La/Sm ratio of the peridotite endmember composition to better encompass the range of La/Sm found in our dataset. The degree of melting of peridotite-fluid mixtures was calculated using a parameterization developed by (Stolper and Newman 1994) for the Mariana Trough, in which melting is controlled by the total water content of the hybrid source. The major element chemistry of the aqueous

fluid component was initially taken from (Kessel, Ulmer et al. 2005). The Na_2O, K_2O, and TiO_2 concentrations were later adjusted to best fit the data. The degree of melting of peridotite-silicate melt mixtures was calculated assuming that the silicate melt had a composition equal to experimental melts of hydrous basalt (Kessel, Ulmer et al. 2005), the peridotite end member had a major element composition equal to the DMM composition from (Workman and Hart 2005) with slight higher N_2O and lower K_2O to fit the composition range observed in Mariana BABB lavas, and a water content of 260 ppm H_2O, and using the ADIABAT_1ph interface (Smith and Asimow 2005) to the pHMELTS algorithm (Ghiorso; Asimow) to describe the degree of melting as a function of temperature, pressure and bulk composition. We assumed all melting occurred at 1 GPa at 1280º C, the pressure and temperature conditions at which the peridotite endmember partially melts by 5%. For both sets of melting calculations, fluid or melt was added to peridotite until the hybrid source had undergone 25% melting—close to the highest extents of melting inferred for the sources of Mariana BABBs (Stolper and Newman 1994; Kelley in press). This required addition of 0.38 wt % of the fluid end member or 4.5 wt % of the hydrous silicate melt end member. The trace element properties of the slab derived end members were set to fit the trends defined by our data (by iterative changes in that end member to find the minimum misfit, as in Eiler, Carr et al. (2005)). We assume the δD of the depleted mantle peridotite component is -75 ‰, similar to values typical of previous measurements of MORBs (Craig and Lupton 1976; Kyser and O'Neil 1984; Chaussidon, Sheppard et al. 1991; Chaussidon and Jambon 1994; Pineau and Javoy 1994; Pineau, Shilobreeva et al. 2004).

The forward models that best fit our H isotope data (in a least-squares sense) are illustrated in figures 2.4 and 2.6. The aqueous fluid component that best fits this dataset is enriched in most fluid mobile elements, particularly Pb and Ba, relative to elements of similar compatibility (normalized to average N-MORB source). Our model suggests that up to 0.18 wt% of this fluid phase was added to the sources of Mariana BABBs. This is broadly consistent with previous estimates (Stolper and Newman 1994), although our calculated composition has a far lower concentration of alkali elements. Our calculated fluid composition is similar to compositions of slab derived fluids proposed for the Central American (Eiler, Carr et al. 2005) and Cascade (Grove, Parman et al. 2002) arcs and its alkali and TiO_2 contents are similar to experimentally measured supercritical fluids in equilibrium with basalt (Kessel, Ulmer et al. 2005).

The best fit trace element composition of model metasomatic melt is similar in all trace element ratios and relative element enrichments to the aqueous fluid composition though the concentrations in the melt are lower in an absolute sense. Na_2O, TiO_2, and K_2O of model melt resemble experimental melts from (Kessel, Ulmer et al. 2005). Both models (i.e. hydrous melt or aqueous fluid) can adequately fit the geochemical trends defined by our data; therefore other evidence is needed to distinguish between these alternate models. The oxygen isotope compositions of Mariana BABBs exhibit a range significantly greater than analytical uncertainty, and include values well below the range typical of N-MORBs but do not exhibit any clear correlations with other easily interpreted geochemical indices. We examined the consistency of these results with models in which oxygen isotope compositions reflect mixing between typical mantle and

either of two slab-derived components: one ^{18}O rich and the other ^{18}O poor. These calculations are based on the following assumptions:

- The whole rock oxygen isotope composition of the peridotite source was set at 5.25 ‰. A whole rock having a $\delta^{18}O_{VSMOW}$ of 5.25 ‰ for a source with 54% olivine, 29% orthopyroxene, 11.8% clinopyroxene, and 4.3% spinel is in oxygen isotope equilibrium with basaltic melt that has a $\delta^{18}O_{VSMOW}$ value of 5.4 ‰ (Eiler, Crawford et al. 2000).
- The model high-$\delta^{18}O$, slab derived component is assumed to derive from sediments and/or altered basalts from the upper ca. 1/3 of the ocean crust. Such materials typically have $\delta^{18}O_{VSMOW}$ values in the range of 15 to 30 ‰ and have been previously suggested to contribute to oxygen isotope variations in the sources of N-MORBs (Eiler 2001; Cooper, Eiler et al. 2004) and some arc lavas (Ito and Stern 1986; Eiler, Crawford et al. 2000; Ito, Stern et al. 2003; Eiler, Carr et al. 2005). Mudstone, pelagic ooze, and volcaniclastic sediments from outboard of the Mariana Trench have $\delta^{18}O$ values of 23.9 ‰, 30.1‰, 16.0 ‰, respectively (Woodhead, Harmon et al. 1987). We choose 20 ‰ as a representative value for ^{18}O-rich materials from the top of the slab.
- The model low-$\delta^{18}O$, slab derived component is assumed to derive from hydrothermally altered rocks from relatively deep (≥ ca. 5 km) in the oceanic lithosphere. Phase stability arguments have been used to suggest that a major source of water in the mantle wedge of subduction zones is the breakdown of serpentine in the gabbroic and peridotitic sections of the oceanic lithosphere (Schmidt and Poli 1998; Scambelluri, Bottazzi et al. 2001; Scambelluri and Philippot 2001) and

evidence of a low $\delta^{18}O$ component in arc lavas has been attributed to dehydration of such rocks (Eiler, Carr et al. 2005). We assume such a component would have a $\delta^{18}O_{VSMOW}$ value of 1.5‰.

We performed mixing calculations among these three components, assuming the slab derived components were either aqueous fluid or silicate melt (which differ markedly in [H]/[O] ratio—aqueous fluids have a molar [H]/[O] equal to 1.35, lower than pure water due to the significant amount of solutes present, whereas hydrous melts have molar [H]/[O] of 0.29 (Kessel, Ulmer et al. 2005). Mixing curves between the mantle and either high or low $\delta^{18}O$ aqueous fluids are strongly hyperbolic and fail to fit most of the data, which include samples that are low in $\delta^{18}O$ but not exceptionally low in Ce/H_2O (see figure 2.6c). The mixing curve between mantle peridotite and the low $\delta^{18}O$ aqueous fluid is closest to the observed range, but would require addition of 1.6 wt % of H_2O fluid to explain the lowest sample. This is nine times the amount indicated by our model of the major element, trace element and H isotope geochemistry of these lavas (figure 2.4). Model mixing curves between mantle peridotite and the low-$\delta^{18}O$, low [H]/[O] hydrous melt encompass more of the data and call on amounts of slab derived component similar to those arrived at in the models fit to major element, trace element and H isotope data in figure 2.4, although they do not encompass all of the oxygen isotope data and fail to explain $\delta^{18}O$ values above the N-MORB average. Thus, our oxygen isotope data are most consistent with the slab derived component being a hydrous melt (or perhaps very solute rich supercritical fluid) derived from the serpentinized peridotite section of the altered oceanic lithosphere, but mixing relations may be complicated by addition of a second high $\delta^{18}O$, water poor component. This conclusion is similar to that reached by

(Eiler, Carr et al. 2005), regarding the oxygen isotope geochemistry of Nicaraguan arc lavas (although relationships between $\delta^{18}O$ and other geochemical variables were clearer in that case). However, we reemphasize in the case of Mariana arc BABBs there are no clear correlations between low $\delta^{18}O$ and slab signatures, and thus we leave open the possibility that low $\delta^{18}O$ lavas there instead reflect unrecognized contamination during magmatic differentiation (i.e., as has been suggested for many Hawaiian and Icelandic basalts (Wang, Eiler et al. 2004; Wang, Schauble et al. 2004)).

Hydrogen isotope and trace element evolution of the subducting oceanic crust

The data and model described above lead us to conclude that the mantle sources of Mariana BABBs were metasomatized by variable amounts of a slab derived phase that is high in δD, Ba/La and low in Ce/Pb and Ce/H_2O compared to the mantle to which it was added. Curiously, this component also appears to be low in La/Sm and high in Th/U—properties not usually associated with slab derived, water-rich components to the sources of arc related magmas. In this section, we construct a forward model of the evolution of the geochemical properties of the slab and fluid-rich phases extracted from it during subduction to explain the properties of this component and predict the properties of the residues from which it was extracted.

Our forward model first calculates the hydrogen isotope composition of fluid evolved from a subducted slab and hydrous minerals left in the residue of that fluid, based on: measured δD values of various components of the oceanic lithosphere(Wenner and Taylor 1971; Knauth and Epstein 1975; Knauth and Epstein 1976; Kolodny and

Epstein 1976; Satake and Matsuda 1979; Kawahata, Kusakabe et al. 1987; Agrinier, Hekinian et al. 1995); estimates of fractionation factors between water and hydrous minerals (Suzuoki 1973; Suzuoki and Epstein 1976; Graham and Sheppard 1980; Graham, Sheppard et al. 1980; Kuroda, Hariya et al. 1982; Graham, Harmon et al. 1984; Graham, Viglino et al. 1987; Dobson, Epstein et al. 1989; Bell and Ihinger 2000); and constraints from phase equilibria experiments and thermal models on the phase changes undergone by hydrated basalts, sediments and serpentinites during subduction (Schmidt and Poli 1998; Kerrick and Connolly 2001; Kerrick and Connolly 2001). The hydrogen isotope data, water content data, and a summary of hydrogen isotope fractionation factors are detailed in the appendix.

We divided the slab into lithospheric mantle, composed of serpentinized peridotites, and crust, composed of hydrous basalt. The temperature-pressure paths followed by each during subduction and the depths at which various dehydration reactions were crossed were taken from the experimental results and models presented by (Schmidt and Poli 1998), along the geothermal gradient calculated by (van Keken, Kiefer et al. 2002) for Pacific style subduction. At each reaction undergone on the prograde metamorphic path followed by each lithology, we calculated the amount of water released by the slab, the amounts and identities of residual hydrous phase left in the slab, and the hydrogen isotope compositions of each (based on the hydrogen isotope composition of the reactant assemblage, estimated equilibrium fractionations between residual minerals and evolved fluid and the mass balance of evolved fluid and residual phases). The residue of the first reaction undergone by each lithology then served as the reactant assemblage for the second reaction, and so forth. This approach is founded on

the experimental results of (Schmidt and Poli 1998; Poli and Schmidt 2002), although it is a simplification because some reactions are not univarient and occur gradually over a range of depths, and because there is a strong thermal gradient within the subducting slab (van Keken, Kiefer et al. 2002).

In general, each stage of dehydration serves to deplete the residue in D, and thus the slab becomes progressively distilled to lower δD values during subduction (shown for a generic subduction zone in figure 2.7). The δD value of fluid released from the oceanic crust rapidly decreases with increasing depth of subduction; when the slab has reached a depth of 75 km, residues of hydrous crustal lithologies have δD values similar to typical fresh MORBs (~-70 ‰); and deeply subducted residues are even lower in δD—comparable to values previously observed in nominally anhydrous mantle minerals (~-100 ‰; (Bell and Ihinger, 2000; Chapter 4). The lithospheric mantle section remains unmodified until deep within the subduction zone (~160 km depth), at which point it releases fluids similar in δD to Mariana BABBs and leaves a residue of nominally anhydrous minerals or phase "A" having δD values of ca. -81 ‰. This model result suggests that the primary source of high-δD fluids to the sources of Mariana BABBs is derived from dehydration of serpentinized peridotites deep within the subducted slab—a result consistent with our interpretation of the oxygen isotope compositions and trace element chemistry of these lavas.

The model presented above makes a prediction about the H isotope compositions of both metasomatic fluids released from altered oceanic crust (AOC) to the mantle wedge and dehydrated AOC mixed into the mantle. The calculated H isotope composition of dehydrated AOC is 30-50 ‰ lower than that of fluids released to the

mantle wedge, and is lower than the average value for typical MORB by 10-30 ‰, suggesting that melts of mantle mixed with recycled AOC would have a lower D/H ratio than typical MORB.

Subduction zone metamorphism also fractionates fluid mobile from fluid immobile elements, as has been described for Pb (Miller, Goldstein et al. 1994; Kelley, Plank et al. 2005), creating distinct trace element compositions for dehydrated AOC and metasomatized mantle wedge. In figure 2.8 we show calculated curves for mixing between three endmember compositions: metasomatized mantle, subducted AOC, and depleted MORB mantle (DMM) to illustrate the expected relationship between Ce/Pb and δD in mantle derived basalts. Pb concentrations in subducted AOC and the metasomatized mantle wedge for the Mariana subduction zone system were calculated by mass balance by (Kelley, Plank et al. 2005). Using the same input compilation and procedures as (Kelley, Plank et al. 2005) we calculated Ce concentrations to compute the Ce/Pb for subducted AOC and metasomatized mantle. The Ce/Pb ratio implied by this analysis for fluids added to the sources of Mariana Trough BABBs approaches our estimate for the water rich endmember of the compositional arrays in figure 2.4. The Ce/Pb ratios of fluids released from the slab in the arc (1.5) and back arc (~0) are below values found in N-MORB whereas the Ce/Pb for the residual slab (>64) are very high relative to N-MORB. The water content of AOC was set by the solubility of OH in nominally anhydrous minerals at the pressure and temperature of the last contact with a free fluid phase. The water content for metasomatized mantle assumed OH saturation in all phases at 5 GPa and 1100º C, the pressure and temperature predicted for

asthenospheric mantle above the slab at the depth serpentine breaks down and was 1497 ppm. The concentration of water in DMM was 290 ppm, and Ce/Pb was 31.

Mixing curves between DMM and both metasomatized mantle and dehydrated AOC are strongly hyperbolic, with addition of very small amounts of metasomatized mantle setting the hydrogen isotope composition to those similar to what is found in either BABB or dehydrated AOC. The concentration of H_2O in metasomatized mantle is ca. 7 times that of DMM, and the concentration of H_2O in AOC is ca. 14 times that of DMM. Mixing curves between AOC and metasomatized mantle are not as strongly curved and depend on the selected saturation conditions for olivine in the mantle wedge.

We are unaware of any MORB or OIB samples with data available for Ce, Pb, and D/H to compare to mixing curves on figure 2.8 so average values for MORB, Hawai'i (from Kilauea volcano (Coombs , Sisson et al. 2004) and Loihi volcano (Garcia, Jorgenson et al. 1995)), and Iceland (from Mohn's ridge) Ce/Pb and δD values are shown. The mean δD value for MORB is -69 ‰—10 to 40 ‰ higher than the δD of altered oceanic crust after subduction. OIBs from Iceland (Poreda, Schilling et al. 1986) and the Salas y Gomez seamount chain (Kingsley, Schilling et al. 2002) (not shown on figure 2.8) are D-enriched, while Hawai'ian lavas have a MORB-like H isotope composition (Garcia 1989) with some D-depleted melt inclusions (Hauri 2002). Though this cannot be fully addressed until there are data available for both Ce/Pb and δD from the same samples, these data appear to support our hypothesis that OIB sources rich in D are also enriched in Pb relative to MORB sources while depletions in D are associated with high Ce/Pb, suggesting that hydrogen from both AOC and the metasomatized mantle wedge are recycled in ocean island environments.

Conclusions

Hydrogen isotopic compositions of Mariana Trough basalts are variably enriched in D relative to mid ocean ridge basalts, to a degree that correlates with other geochemical indicators of slab derived aqueous fluids and degree of melting. Oxygen isotope compositions of Mariana Trough lavas are similar in average to mid ocean ridge basalts but range to 0.39 ‰ below the N-MORB average. Oxygen isotopes do no vary systematically with either hydrogen isotope composition or other geochemical indexes.

We developed a model that explains the hydrogen isotope data (and correlated geochemical data) by addition of small amounts (< 0.27 wt %) of a slab derived aqueous fluid or by larger amounts of slab derived hydrous basalt (< 2.6 wt %) to a depleted peridotite composition. Trace element ratios of the model slab derived fluid or melt are characterized by relative enrichments in fluid mobile elements (Ba, Pb, and U) but are not as high as those found in Mariana arc lavas. The range of $\delta^{18}O$ values in basalts is larger than can be accounted for by addition of a pure aqueous fluid, suggesting that the metasomatizing agent is either a supercritical fluid or hydrous melt.

We model the evolution of the hydrogen isotope and trace element compositions of altered oceanic crust, serpentinized peridotite and fluids evolved from both lithologies during subduction. The upper portion of altered ocean crust goes through a series of dehydration reactions that progressively remove D from altered basalt and gabbros. The lithospheric mantle section of oceanic crust is unmodified until deep within the subduction zone, releasing fluids upon the breakdown of chlorite and serpentine that are

similar in hydrogen isotope composition to the average of Mariana Trough basalts. The hydrogen isotope composition, anomalously low $\delta^{18}O$ values, and loss of fluid mobile trace elements relative to the arc front volcanoes indicate that the fluid released to the Mariana back arc basin source region was derived by deep dehydration of the lithospheric mantle section of altered oceanic crust. By identifying H isotope distinct subduction zone "products" that are correlated with trace element chemistry and possibly radiogenic isotope compositions we may be able to trace subducted hydrogen in OIB and MORB samples and fully describe the mantle water cycle.

Acknowledgements

We thank Bob Stern for his generosity with samples and for a thoughtful review that improved this manuscript. We thank Wang Zhengrong and Sally Newman for assistance and instruction in laboratory work during this project. We are grateful for the financial support of the Moore Foundation to J. O'Leary and to NSF.

Appendix A

The water content and hydrogen isotope composition of altered oceanic crust

Starting water contents and δD values: The oceanic lithosphere is heterogeneous in δD and water content. Because of this, our model focuses on average properties of a few major rock types, including basalts, gabbros, and serpentinized peridotites; we assume the typical δD values and water contents of these rocks equal the means of the distributions of measured values for dredge and drillcore samples.

- Cherts are the most deuterium depleted relative to ocean water, averaging -84 ‰ ± 10 ‰, with 1 ± 0.2 wt % H_2O (Knauth and Epstein 1975; Knauth and Epstein 1976; Kolodny and Epstein 1976).
- Altered basalts span a large range in deuterium content and drillcore from site 801, outboard of the Mariana trench, include the lowest-δD samples of basalt known (Alt 2003). However, the mean for all samples is much richer in deuterium, -40 ± 15 ‰, 1.92 ± 1.4 wt % H_2O (Satake and Matsuda 1979; Kawahata, Kusakabe et al. 1987).
- Gabbros are -59 ± 8 ‰, 2.03 ± 0.5 wt % H_2O (Agrinier, Hekinian et al. 1995).
- Serpentinized peridotites average -53 ± 9 ‰, 3.45 ± 2.36 wt % H_2O (Wenner and Taylor 1971). Oceanic dredge samples are dominated by chrysotile and lizardite in equilibrium with seawater at low temperature. Antigorite, formed at high temperature with an average δD_{VSMOW} = -29 ± 3‰ (Wenner and Taylor 1971) may be the dominant polymorph of serpentine in oceanic lithospheric mantle. This is supported by sulfur isotope evidence for high temperature serpentinization at mid ocean ridges (Alt and Shanks 1998). We use a value of -29 ‰ for serpentinized peridotites.

Appendix B

A summary of hydrogen isotope fractionation factors

Isotopic fractionation factors: Experimentally determined mineral-fluid hydrogen isotope fractionation factors were used when available. Fractionation factors for chlorite-H_2O_l are from Graham, Viglino et al. (1987), for amphibole-H_2O_l are from Suzuoki and Epstein (1976), for serpentine-H_2O_l, zoisite-H_2O_l, and epidote-H_2O_l are from Graham, Sheppard et al. (1980). Two of the minerals considered in the petrologic model (chloritoid and lawsonite) do not have experimentally determined fractionation factors relative to water, and so we estimate them based on principles of physical chemistry that have been previously found to predict H isotope reduced partition coefficient ratios. For chloritoid, we substituted the fractionation factors for chlorite-H_2O_l because both minerals have OH groups in octahedral coordination with Mg, Fe, and Al (Suzuoki and Epstein 1976). Lawsonite is structurally distinct from phases for which experimentally determined fractionation factors are available. We assumed there is no isotopic fractionation between the structural H_2O in lawsonite and aqueous fluid, and that the fractionation between aqueous fluid and structural OH in lawsonite resembles that between fluid and zoisite. There are no experimental or theoretical calculations of hydrogen isotope fractionations for nominally anhydrous minerals. (Dobson, Epstein et al. 1989) observed a relationship between fractionation factors of minerals and the primary hydroxyl stretching frequency which predicts fractionations of -26 ‰, -30 ‰, and -39 ‰ between olivine, clinopyroxene, orthopyroxene, respectively, and fluid. This

prediction is broadly supported by measured isotopic differences between mantle garnets, amphiboles, and micas (Bell and Ihinger 2000).

Hydrogen isotope fractionations involving water are sensitive to pressure (Driesner 1997; Horita, Driesner et al. 1999; Horita, Cole et al. 2002), particularly close to the critical point of water. This has been shown both experimentally (Horita, Driesner et al. 1999; Horita, Cole et al. 2002) and theoretically (Driesner 1997). We calculated the pressure effect on mineral-water fractionations using the experimental determinations of (Horita, Cole et al. 2002) for the brucite-water system. For each given pressure of reaction, we calculated the pressure effect on the fractionation, $\Delta_{brucite\_water}$, and then applied this correction to the fractionation factors for other mineral phases (which were generally measured near 1 kbar). We believe this approach is valid because the pressure effect stems mostly from changes in the reduced partition coefficient ratio of water rather than in those for minerals (Driesner 1997), however it should be noted that our calculation extrapolates the effect to far outside the experimentally calibrated pressure-temperature space and should be treated with caution. Pressure corrections are between 9 and 17.8 ‰ from the lowest to the highest pressure reaction. Salinity also influences the reduced partition coefficient ratio of aqueous fluids (Driesner, 2000; references therein}. The pressure, temperature, and salinity of our model fluid system overlap with those investigated by (Graham and Sheppard 1980) in the epidote-salt solution system, which showed that the effect of fluid composition is primarily a function of temperature rather than the molarity or identity of the major cation, and is negligible above 550º C. Therefore we only applied a correction for the "salt effect" for the lowest temperature dehydration reactions in basalts and gabbros, where $\Delta_{mineral\_fluid}$ is reduced by 5‰

assuming a fluid composition similar to that measured in Mariana forearc springs (Mottl, Wheat et al. 2004). It should be noted that all of the experiments referenced in this section are minerals equilibrated with either pure H_2O or brines. The fluid in subduction zones is a supercritical fluid with high concentrations of other oxides and may have different H isotope chemistry as a result.

Sample	Lattitude	Longitude	$\delta D_{,}$ ‰	1 σ	$\delta^{18}O$, ‰	1 σ	$\delta^{18}O_{9.0,}$ ‰
46:1-6	20.82	143.50	-42.3	2.3	5.24	0.22	5.23
47:1-5	20.97	143.44	-44.7	5.6	5.41	0.09	5.40
55:1-1	22.87	142.32	-45.2	0.8			
73:2-1	19.73	144.40	-51.5	5.0	5.33	0.05	5.31
80:1-3	19.12	144.67			5.17	0.04	5.14
ALV 1833-11	18.10	144.75	-48.7	14.8	5.63	0.08	5.62
ALV1846-9	18.30	144.70	-73.7	4.0	5.57	0.10	5.56
DS18:1-6	16.18	144.79	-50.2	1.9	5.64	0.10	5.62
DS22:2-1	16.96	144.78	-56.0	3.1	5.01	0.03	5.00
DS74:3-1	16.53	144.83	-34.4	0.1	5.33	0.07	5.39
DS80:25-3	15.75	144.75	-40.1	2.1	5.56	0.08	5.55
DS84:1-1	15.00	144.46	-40.1	11.7	5.68	0.12	5.66
DS86:4-1	15.09	144.50	-61.2	0.8	5.37	0.09	5.36
DS88:2-1	15.30	144.51	-37.6	3.6	5.52	0.01	5.50
DS88-3-1	15.30	144.51	-46.8	3.1			
GTVA73:2-2	16.69	144.81			5.45	0.01	5.44
WOK 28	17.64	144.90	-36.2	*	5.50	0.06	5.48
WOK16-2	18.10	144.75	-39.4	2.1	5.58	0.06	5.56

Table 2.1 Hydrogen and oxygen isotope data for Mariana Trough basalts

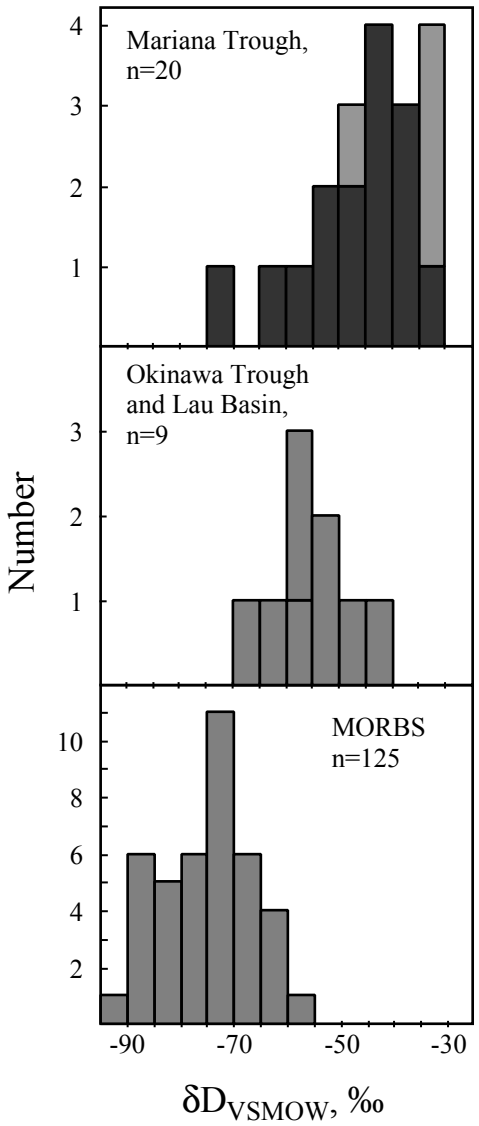

Figure 2.1. (a) Hydrogen isotopic composition of back-arc basin basalts compared with mid-ocean ridge basalts. Mid-ocean ridge data are from (Chaussidon and Jambon, 1994; Chaussidon et al., 1991; Craig and Lupton, 1976; Kyser and O'Neil, 1984; Pineau and Javoy, 1994; Poreda et al., 1986). Lau basin and previous Marianas trough data are from (Poreda, 1985a). Okinawa trough data are from (Honma et al., 1991).

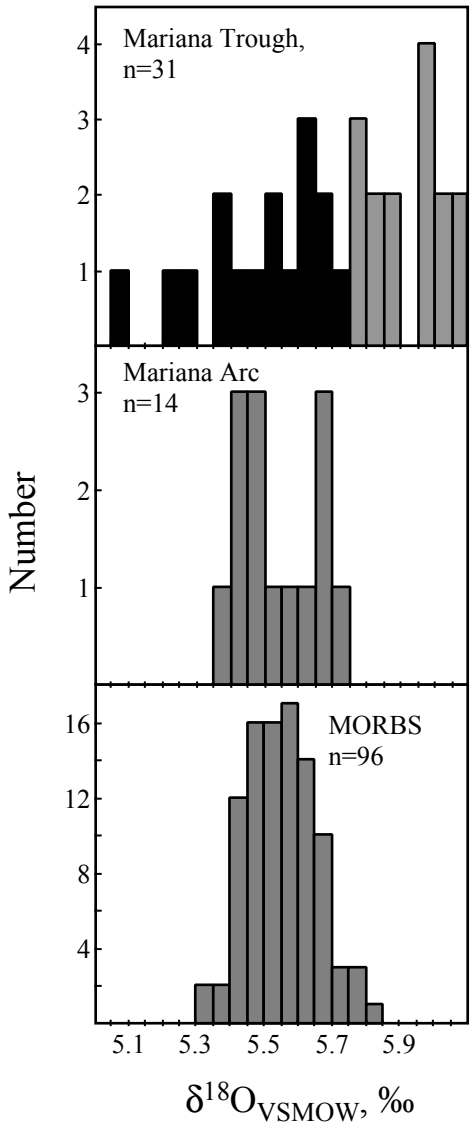

Figure 2.1.(b) Oxygen isotopic composition of back-arc basin basalts compared with mid-ocean ridge basalts and Mariana Arc basalts. Mariana Trough data are from this study (black) and Macpherson (2000). Mid-ocean ridge data are from Cooper et al., (2003) and Eiler et al., (2000c). Mariana arc data are from Eiler et al. (1998).

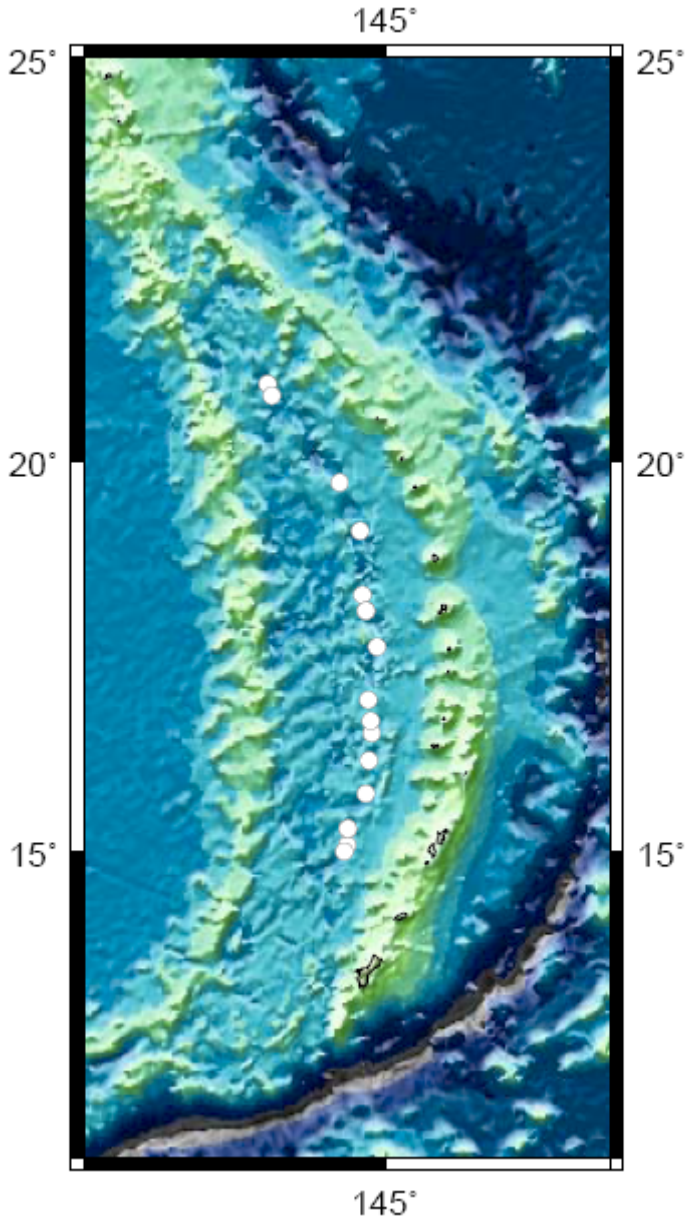

Figure 2.2 Map of the Mariana subduction zone system, prepared using GMT (Wessel and Smith, 1998).

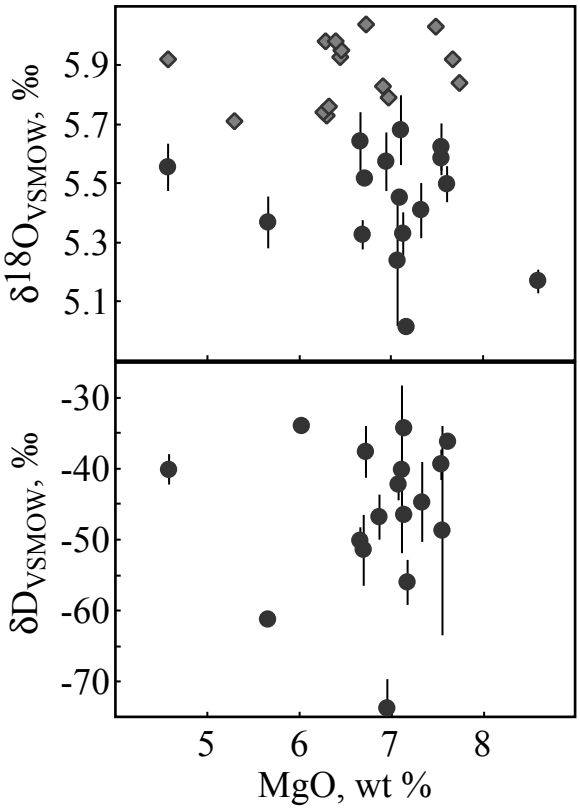

Figure 2.3. Comparison of $\delta^{18}O$ and δD with the MgO content of basalt samples. Black circles are for data from this study, gray diamonds aredata from Macpherson (2000).

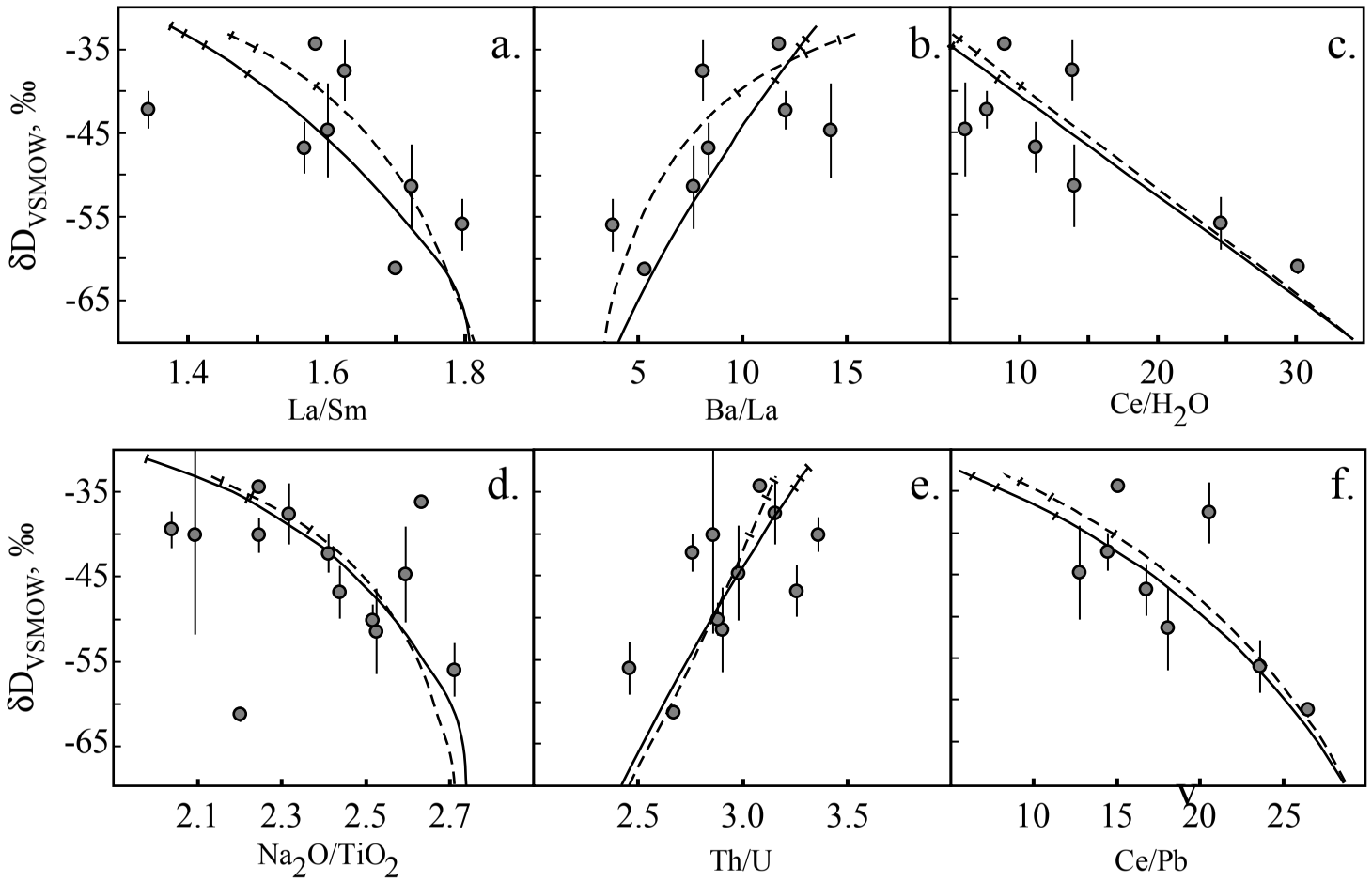

Figure 2.4. Plots of δD values vs. trace element ratios and Na_2O/TiO_2 contents. Dashed lines indicate addition of an aqueous fluid, tick marks are for every 0.1 wt % fluid added. Black curves indicate addition of melt derived from hydrous basalt with tick marks for every 1 wt % melt added.

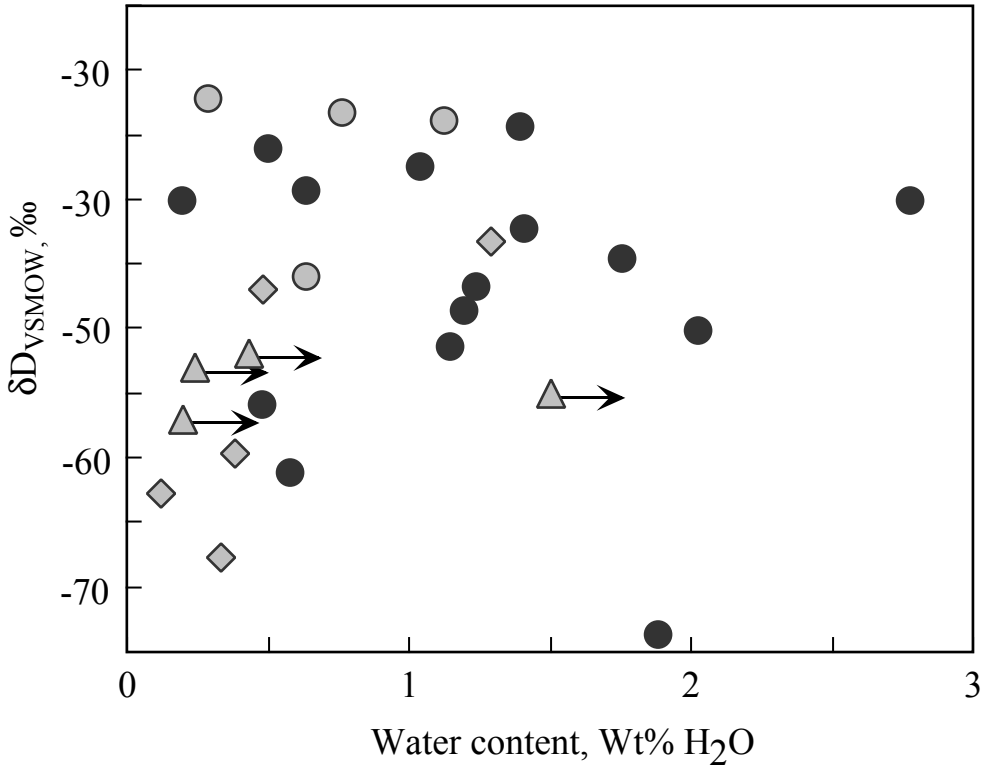

Figure 2.5. δD of glasses versus $1/H_2O$ for BABB, black symbols are from this study, gray symbols are from (Poreda, 1985b), circles are basalts from the Marianas trough, and diamonds are basalts from Lau Basin, gray triangles are from the Okinawa Trough (Honma et al., 1991). Okinawa trough water contents are minimum water contents as indicated by arrows. Water contents for Marianas glasses are from (Newman and Stolper, 2000). With the addition of this dataset, the correlation between water content and δD previously observed by (Poreda, 1985b) appears to not hold for the Mariana Trough lavas.

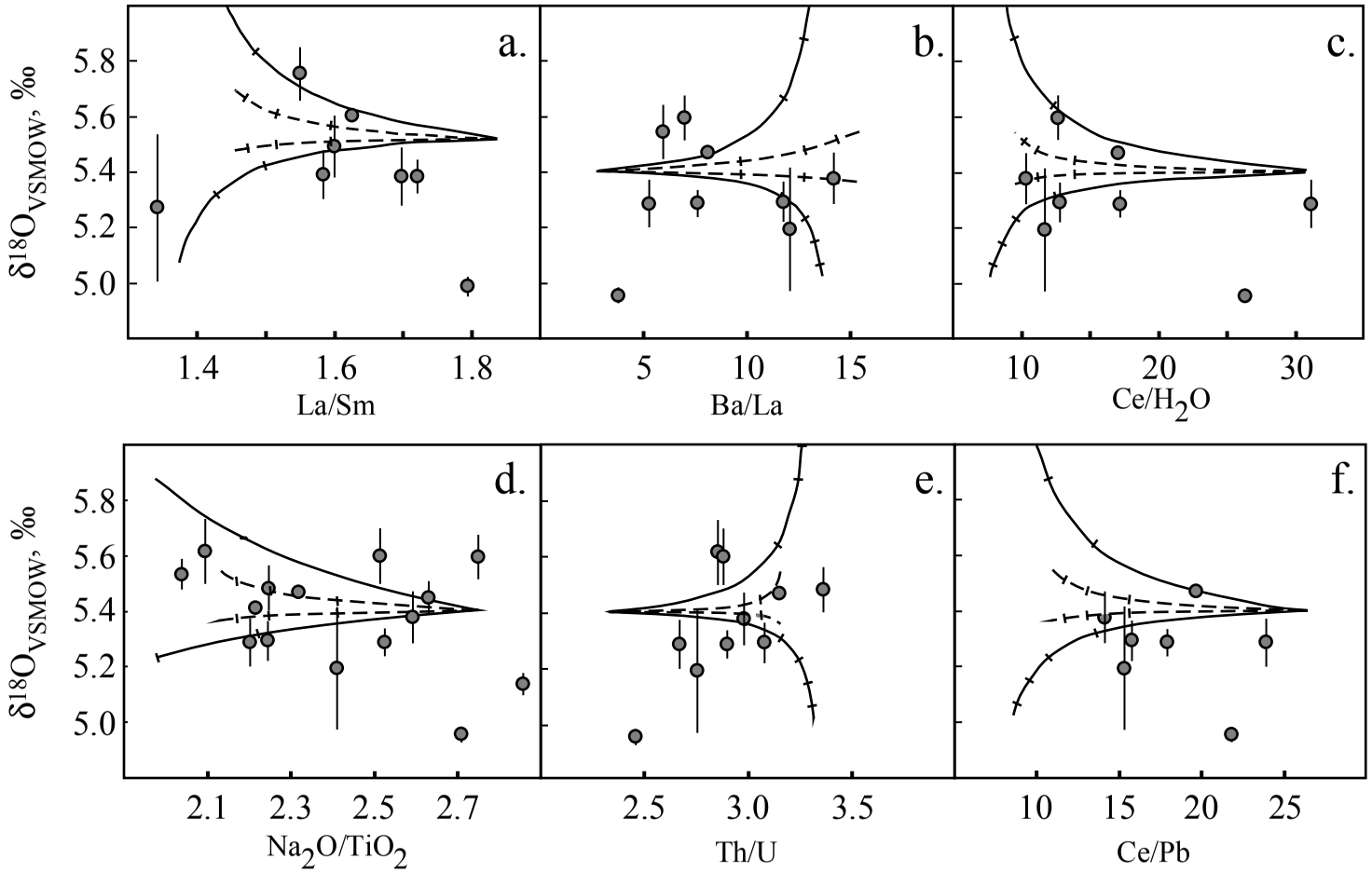

Figure 2.6. $\delta^{18}O$ of basalts vs. trace element ratios for Mariana Trough lavas. Dashed lines indicate addition of an aqueous fluid, tick marks are for every 0.1 wt % fluid added. Black curves indicate addition of melt derived from hydrous basalt with tick marks for every 1 wt % melt added. All oxygen data have been corrected for crystallization-differentiation effects.

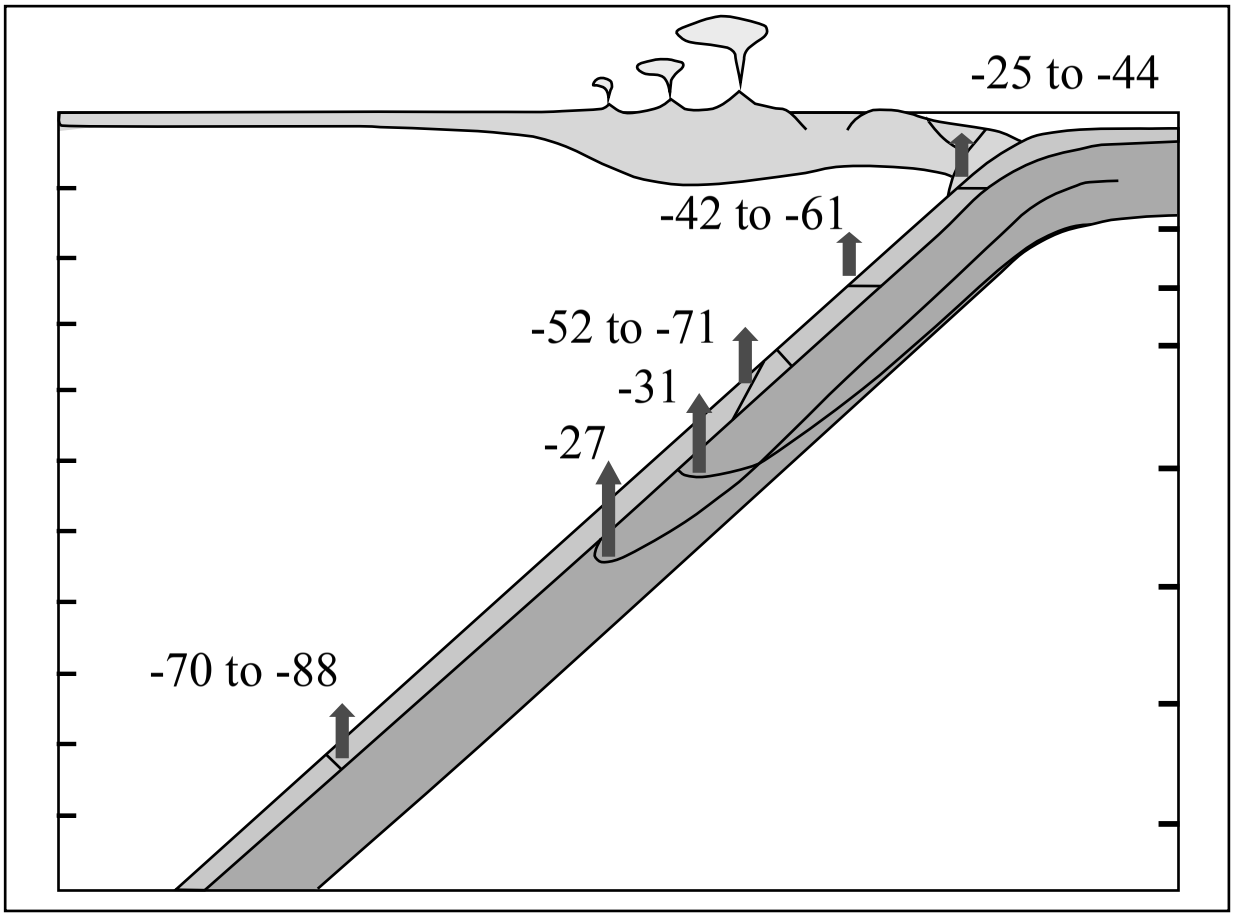

Figure 2.7. Forward model calculation of the isotopic evolution of the subducted slab. Details of the calculation are provided in the text. The line drawing and placement of reaction boundaries are after (Poli and Schmidt, 2002).

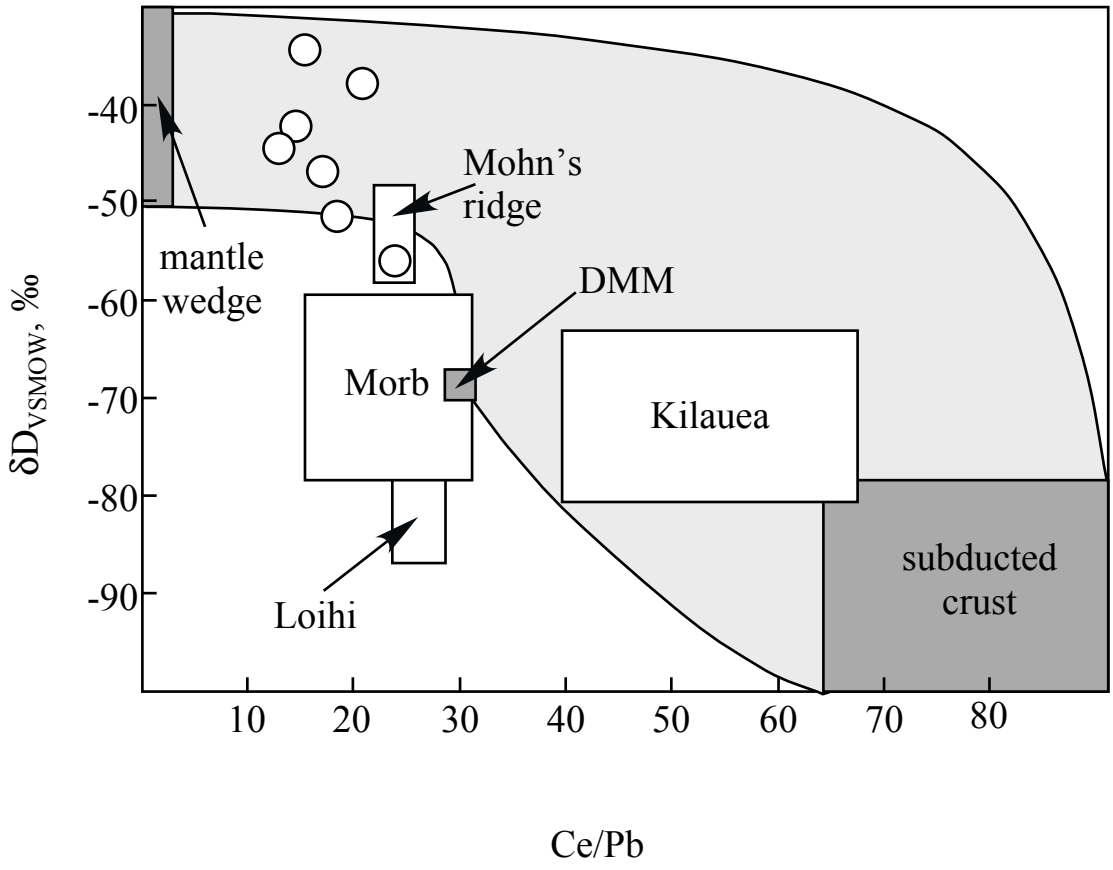

Figure 2.8. δD values vs. Ce/Pb diagram showing calculated end-member compositions for mantle metasomatized by fluids released from subducting crust, altered oceanic crust dehydrated in subduction zones, and mixing curves between those compositions and DMM. Circles show data for Mariana Trough lavas, boxes show average values of Ce/Pb and δD for MORB and available OIB lavas.

Chapter 3

Hydrogen Analysis in Minerals by Continuous-Flow Mass Spectrometry

Julie A. O'Leary, George R. Rossman, and John M. Eiler

Abstract

We present an improved method for on-line dehydration of small quantities of hydrous and nominally anhydrous minerals followed by measurement of the absolute abundance of hydrogen released from the sample by continuous-flow mass spectrometry. This method is appropriate for measuring water content between 18 ppm and 10 wt % H_2O and requires a minimum of ~ 2×10^{-8} moles of hydrogen per analysis. The hydrogen needed for an analysis corresponds to 10-200 μg of hydrous minerals or 5-40 mg of nominally anhydrous minerals. We develop measurement protocols for garnet and pyroxene, two nominally anhydrous minerals that are potentially major reservoirs of hydrogen in the mantle.

Introduction

Hydrogen is a nearly ubiquitous component of geologic materials (Aines and Rossman 1984; Skogby, Bell et al. 1990; Smyth, Bell et al. 1991; Woodhead, Rossman et al. 1991; Bell and Rossman 1992; Bell and Rossman 1992; Vlassopoulos, Rossman et al.

1993; Bell, Ihinger et al. 1995; Ingrin and Skogby 2000; Andrut, Brandstatter et al. 2003; Johnson and Rossman 2004; Bromiley and Bromiley 2006) and has a disproportionately strong effect on mineral rheology (Mackwell, Kohlstedt et al. 1985; Karato 1986), melting temperature (Hirose and Kawamoto 1995), electrical conductivity (Karato 1990) and other physical and chemical properties (Mei and Kohlstedt 2000; Mei and Kohlstedt 2000). Experimental determinations of the solubility of hydrogen in minerals at elevated temperatures and pressures have shown that common silicates (e.g., olivine, pyroxenes, feldspars and garnet) at deep-crustal and mantle conditions can contain up to thousands of ppm (weight fraction, as H_2O) (Bromiley and Bromiley 2006) (Mosenfelder, Deligne et al. 2006). However, many natural samples of these phases contain far less than their saturated hydrogen contents — a few hundred ppm is typical. Quantification of such low hydrogen contents is a challenge, particularly for materials that are precious, limited in availability, or compositionally zoned.

Hydrogen contents of minerals have been previously determined using vacuum manometry (Holdaway 1986; Rossman and Aines 1991; Ihinger 1994; Bell, Ihinger et al. 1995), infrared absorption spectroscopy (Rossman and Smyth 1990; Smyth, Bell et al. 1991; Koch-Muller, Kahlenberg et al. 2000; Koch-Muller, Fei et al. 2001; Koch-Muller, Matsyuk et al. 2004), secondary ion mass spectrometry (Holdaway 1986; Hauri 2002; Koga, Hauri et al. 2003; Aubaud, Hauri et al. 2004), and nuclear reaction analysis (NRA; (Lanford 1978; Merritt, Ricci et al. 1992; Hammer, Beran et al. 1996; Maldener, Rauch et al. 2001; Bell, Rossman et al. 2003; Maldener, Hosch et al. 2003; Bell, Rossman et al. 2004)). Each of these methods has strengths and weaknesses: vacuum manometry is quantitative (i.e., it requires no independent standardization to determine absolute

hydrogen concentrations), but has typically required ca. 1-5 μmoles of hydrogen (as H_2), corresponding to gram quantities of hydrogen-poor materials. Such large amounts of sample increase the risks of contamination and often cannot be obtained. Infrared absorption spectroscopy constrains the chemical environment of hydroxyl groups and water molecules in mineral structures, and is both sensitive and precise as a measure of hydrogen concentration, but requires independent calibration using a quantitative technique. Such calibrations are available only for a few mineral, depend on orientation, and may not be appropriate for extrapolation outside of the concentration range of their calibration (Rossman and Aines 1991; Cho and Rossman 1993). Secondary ion mass spectrometry can be sensitive and precise, consumes exceptionally small amounts of material for analysis (typically picograms (Koga, Hauri et al. 2003)), and is appropriate for studies of compositional zonation at scales down to tens of microns (or possibly smaller using nanoSIMS instrumentation (Floss, Stadermann et al. 2006)). However, it too requires independent calibration using a quantitative technique, and calibration is highly specific to mineral type and chemical composition. Nuclear reaction analysis is quantitative and can yield finely-resolved depth profiles of hydrogen concentration, but is technically difficult, not widely available, and is a near surface technique that cannot be easily compared to bulk techniques for some materials.

We present a new technique for measuring the abundance of hydrogen in minerals by extracting that hydrogen as water, reducing it to hydrogen gas, and analyzing that hydrogen gas by carrier-gas mass spectrometry. This technique is applicable to many different materials without the need for phase-specific calibrations, and can reliably

quantify hydrogen abundances as low as 20 nanomoles (corresponding to tens of ppm as H_2O in mg-quantities of sample).

Materials

Samples of garnet, clinopyroxene, orthopyroxene, olivine, and corundum were used for technique development. These samples were chosen for both the availability of high quality sample material, and for the availability of water content data. Table 2 lists the sample name, locality, variety, and nominal water content for all samples. We used anhydrous samples of two mineral, olivine and corundum to determine the blank associated with the surface area of mineral grain. IR spectroscopy was used to confirm low water contents in our anhydrous samples. The olivine sample, GRR 2014, contained 1.53 ppm H_2O using the calibration of (Bell, Rossman et al. 2003). The corundum sample, a synthetic wafer of Al_2O_3, had no detectable hydroxyl in a 2 mm thick sample. Samples of orthopyroxene, clinopyroxene, and four varieties of garnet were analyzed for water content to compare our technique to other methods; these samples range in water content from 18 to 8921 ppm H_2O. Previous water content measurements were made by vacuum manometry (Bell, Ihinger et al. 1995; Bell and Ihinger 2000), IR spectroscopy (Rossman and Aines 1991; Bell, Ihinger et al. 1995; Arredondo, Rossman et al. 2001) and NRA (Rossman, Rauch et al. 1988).

Our measured signal, though it does not require mineral specific calibrations, must be calibrated against known amounts of water. We use aliquots of a hydrous mineral, zoisite, to introduce known quantities of water into the system. Our primary

water standard is a gem quality crystal of zoisite from the Meralani Hills mine, Arusha, Tanzania. Zoisite is a hydrous mineral containing 2.01 wt % H_2O. Our standard material is near end-member zoisite ($Ca_{2.03}Mg_{0.01}Al_{2.98}(SiO_4)_{3.00}(OH)_{0.98}F_{0.02}$, see table 3.1 for a complete chemical analysis) with small amounts of Mg substituting for Ca and a minor amount of fluorine substituting for OH. Wet chemical analysis of zoisite from the Meralani Hills has determined the H_2O content to be 2.00 wt %, indistinguishable from the theoretical values (Hurlbut 1969). The crystal was ~ 5 mm across and was crushed to pieces in between 212-425 μm in diameter for analysis.

Characterization methods

Infrared spectroscopy was used to (1) measure water contents for unknown samples and (2) verify complete dehydration of samples after heating. For these measurements we collected spectra in the mid-IR region at the Mineral Spectroscopy Lab at Caltech. Measurements were made on doubly polished slabs of minerals between 72 μm and 4.2 mm. Spectra were measured in both the microscope and main compartment (depending on sample thickness) of a Nicolet 860 FTIR spectrometer. Microscope compartment measurements were made using a spot size of 50 μm, with a globar mid-IR light source, and a MCT-A detector. For main compartment measurements a spot size of 100 μm, globar light source, and a MCT-B detector were used. In both compartments 256 scans were averaged for each measurement. Unpolarized spectra were collected for garnet, an isotropic mineral. Olivine is anisotropic; spectra polarized in three perpendicular directions were collected. A $LiIO_3$ Glan-Foucault prism polarizer was used

for polarized measurements. Collected spectra were analyzed using the Omnic software package to subtract water vapor contributions, correct baselines, and calculate the integrated absorbance of the OH stretching region (ca. 3000-3600 cm^{-1}).

Raman spectra were collected on individual zoisite grains before and after analysis by step heating to confirm complete dehydration. At 1 Kbar and 550º C (Newton 1966) zoisite decomposes by the reaction:

$$zoisite \rightarrow anorthite + grossular + corundum + vapor \qquad (1)$$

Typical analysis temperatures for our technique procedure (described below) are 1120º C, more than 600º C above the temperature needed to decompose zoisite. Spectra for zoisite and dehydrated zoisite were collected on a Renishaw-Micro Raman spectrometer with a 514 nm argon ion laser on unpolished mineral chips through a 50× objective lens. Data was collected for 30 seconds, and the Raman shift was calibrated using silicon metal (520.5 cm^{-1} Raman shift) as a standard material. The collected spectra are shown along with reference spectra for anorthite, grossular, and corundum in figure 3.1. All features of a zoisite spectrum are missing and prominent peaks of the anorthite, corundum, and grossular spectra are present in the collected spectrum from a dehydrated sample, indicating complete decomposition of zoisite during an analysis.

Method description

Technique principles

We use continuous flow isotope ratio monitoring mass spectrometry (CF-IRMS) to measure the absolute amount of hydrogen in minerals. This technique is an extension of the method for D/H analysis of picoliter quantities of H_2O described in detail by (Eiler and Kitchen 2001) that is based on the principles of continuous flow mass spectrometry for isotopic ratio measurements in organic compounds (Hayes, DesMarais et al. 1977; Matthews and Hayes 1978; Merritt, Ricci et al. 1992)}. Water vapor is released from minerals by heating and transported by a stream of carrier gas through a uranium reactor at high temperature (850^o c) to form H_2 gas and UO_2. H_2 gas is then introduced into the mass spectrometer via capillary tubing. The measured current intensity for H_2^+ ions is used as a proxy for total water released from the sample. Our preparation, mineral dehydration protocols, and signal calibration methods are described in detail below. This approach has two primary advantages: signal size is dependent only on the amount of hydrogen released from the mineral, and continuous flow mass spectrometry requires ~1/1000 the absolute amount of H_2 required by vacuum manometry, making this method independent of mineral species and capable of analyzing very small quantities of minerals.

Sample preparation

Mineral grains that are free of fluid inclusions, mineral inclusions and alteration are selected for analysis using an optical microscope. Selected grains are crushed, sieved to the desired size (dependent on the mineral species), and examined again under an optical microscope to remove any remaining contaminants. Mineral separates are

sonicated in 10% HCl for 5 minutes, rinsed with deionized water, sonicated in 95% ethanol for 5 minutes, and placed in an 120º C oven until dry (2 hours-overnight). Prepared samples are loaded into platinum capsules for analysis. Small samples (less than 1 mg) are loaded into Johnson Matthey cut Pt tubes (JM/P 16110). For samples larger than 1 mg, 1/8 inch id tubing (Goodfellow, 498-125-10) is cut to the length required to fit the sample. Both size tubes are 99.95% pure platinum, tubes are annealed at 950º C for 1 hour before being used for samples to release any hydrogen in the platinum. The tube ends are loosely folded shut.

The sample mass is measured with a Cahn 29 electrobalance that has a precision of ± 0.2 μg. Balance precision was determined by measuring a class M 20 mg calibration weight ten times over the course of one day. A 20 mg calibration weight is used as platinum capsules are approximately 11 mg. The long term reproducibility of this balance is ± 1 μg (pers. communication, M. Baker). Samples masses are measured by the difference between the mass of empty platinum capsules and loaded packets. Each empty capsule is weighed twice before and after loading. Sample aliquots are between 50 μg and 40 mg (depending on anticipated water content).

Apparatus and measurement description

The apparatus used for our measurements (shown in figure 3.2) is a modification of a design described by (Eiler and Kitchen 2001) intended for isotopic analysis of picoliter amounts of water. The apparatus was modified to allow high temperature water extraction from minerals and to minimize water blanks. Letters preceding each

component description refer to the letters on figure 3.2, and are described in the order that is encountered while conducting an analysis. Arrows on figure 3.2 are in the direction of gas flow within the system.

(a) UHP He (obtained from Air Liquide) is supplied to the continuous flow system through methyl-deactivated fused silica 320 μm id capillary tubing (SGE 0624476), shown as fine lines in figure 3.2. There are two UHP He supplies to the system.

(b) Pre-treated sample tube assemblies. Each sample is analyzed in a separate assembly. The assembly is a glass tube (GE 215a fused silica glass, < 10 ppm H_2O glass) six inches long that is sealed shut at one end using a methane-oxygen torch. The glass tube is purged by two capillaries, an inlet and an outlet, attached to the open end of the glass tube. The connection is made with a custom made PEEK (poly ester ether ketone) reducing union (VICI Valvco 0.25 in to 0.0625 in reducing unions), a two-holed tubing sleeve (dual-lumen silica sealtight tubing sleeves, Upchurch Scientific) and a ferrule (Tefzel locking ferrules, Upchurch Scientific). Samples in platinum packets are placed inside the glass tubes. Prior to analysis, these assemblies are connected to a manifold supplying UHP He, and heated by heating tape to a moderate temperature (100-300°) to facilitate drying of surfaces inside the sample assembly.

(c) A supply of He with 1% O_2 (obtained from Matheson Tri-gas). The He+O_2 is also connected to the system by methyl-deactivated fused silica capillaries.

(d) A small (1 inch inner diameter, 5 inch length) molybdenum disilicide furnace (robust radiator, MHI), set for an internal temperature of 1120º C. The

temperature profile within the tube furnace is periodically checked to ensure the internal temperature remains 1120º C.

(e) A sample assembly in analysis position. The sealed end of the glass tube is inserted into the furnace hot zone.

(f) A two-way six port sample injector valve (Valvco). This valve has two positions. In the 'collect' position the gas stream from the sample assembly flows through a capillary coil submerged in liquid N_2, freezing any water vapor in the gas stream. In the 'analyze' position He from an auxiliary He supply (a) flows through the capillary coil and carries collected water to the reactor.

(g) A reactor, consisting of a 1/16 in outer diameter alumina tube (998 Al_2O_3 drawn tubing, Vesuvius McDanel) with a 0.5 mm diameter U wire inside (Goodfellow). The reactor tube is inside a SiC tube furnace set at 850º by a standard GC/TC interface from Thermo electron. The reactor tube is connected to capillary tubing with SGE fittings and Vespel ferrules.

(h) A 5 m length of 320 μm diameter capillary submerged in liquid N_2 to trap any CO_2 present in the analyte stream.

(i) A Nafion water trap.

(j) An open split set in the 'out' position.

(k) A Finnigan MAT Delta$^+$ XL gas source mass spectrometer.

All water measurements were made following the 'cryofocus' protocol of (Eiler and Kitchen 2001), with no modifications made to either the software or the mass spectrometer. In this procedure water from the sample tube (either blank water or sample

water) is collected in the Valvco sample injector for between 15-90 minutes. After collection, the valve position is changed, and the capillary coil is warmed to send the sample gas through the U reactor and into the mass spectrometer.

Analysis protocol

Each platinum sample capsule is placed in a separate glass sample assembly. The assembly is then connected to a UHP He supply and heated at between 100 and 300º C for at least 8 hours. This step is to remove surface water from both the interior of the glass tube and from the surface of mineral grains.

Each sample assembly undergoes three high temperature steps: (1) pre-heating of the glass tube, (2) blank characterization, and (3) analysis. During all high temperature steps the sample assembly is flushed by a mixture of He with 1% O_2. We add oxygen to the carrier gas to prevent evolution of H_2 or CH_4 from the sample during dehydration. The duration of each high temperature step is dependent on the length of time required to dehydrate the mineral being analyzed. Dehydration times for nominally anhydrous minerals are discussed below. During the first step, pre-heating, the sample packet is in the fitting end (the cold end) of the sample assembly. The seal end of the glass tube is heated at the analysis temperature (1120º c) to remove both surface water on the walls of the glass tube and volatile contaminants in the glass tube. The sample tube is pre-heated for the length of time needed for blank characterization and dehydration steps combined. Following pre-heating, the blank for the sample assembly is collected. During this step the position of the assembly and sample packet are the same as for pre-heating, but the

out flowing carrier gas is routed through the sample injector and water is cryogenically collected. The blank is collected for on half to three quarters of the dehydration time required for the mineral being analyzed. After analysis of the blank, the sample is dehydrated. For dehydration, the sample assembly is taken out of the furnace, the sample is moved to the sealed end of the glass tube by tipping the sample assembly down, and the glass tube is reinserted into the furnace. Evolved sample water is collected in the sample injector for 30-90 minutes (depending on the rate of water release from the mineral analyzed). The collected water is analyzed at the end of this step.

Results

Ion current calibration

The total ion current measured for M/z of + 2 (H_2^+ ions) is proportional to the moles of H released from the sample. By calibrating this signal, we can use ion current as a proxy for the water content of a sample. H_2^+ ion current is recorded as the voltage across a 10^9 ohm resistor on the Faraday cup collecting M/z of + 2. The current is recorded as a time-varying signal as the peak elutes (ca. 20-90 seconds) and is recorded in units of Volts × seconds (Vs). Peak definition and integration are performed by Finnigan Isodat 3.1 software, the endpoints are chosen based on the time derivative of the HD^+ (M/z = + 3) ion voltage using a starting slope of 0.15 mV/s, and an ending slope of 0.04 mV/s, with an integration time of 0.250 s. The background H_2^+ ion signal is typically between 200 and 250 mV, with an average standard deviation of ± 1 mV over

the time of an analysis (15-90 seconds); minimum recorded peak heights are 50 mV above the background ion signal. Sample peaks typically range from 4-100 Vs and blank peaks are between 0.5 and 5 Vs.

The sensitivity and linearity of ion current response was characterized by measuring samples of two materials of known water content, our zoisite water standard containing 2.01 wt % and a basaltic glass sample (ALV 526-1) containing 0.20 wt % H_2O. Figure 3.3a shows analyses of 14 zoisite samples between 56 and 753 μg, corresponding to 61 to 809 nanomoles of H_2O, and 3 analyses of ALV 526-1 2 wt % H_2O containing 48-86 nanomoles of H_2O. These analyses were performed over the course of 6 successive days. The measured samples define a straight line, indicating a linear relationship between the integrated voltage measured and the total moles H_2O introduced to system. The regression line, shown with a 95% confidence interval, indicates that sensitivity is 0.17 Vs/nanomole, a value that is representative for this analytical session. This sensitivity corresponds to an efficiency of ~2×10^{-6}, where efficiency is defined as:

$$S = Vs \times \varepsilon \times x_f \div A \qquad (2)$$

where Vs is the total collected charge for the H_2^+ isotopomer, ε is the ionization efficiency, x_f is the efficiency of the open split, and A is the total number of molecules introduced to the open split; see (Eiler and Kitchen 2001) for a complete discussion of the instrument sensitivity and statistical limits of precision. The efficiency of this system is considerably lower that the optimal sensitivity for systems of this kind (3×10^{-5}), and

may be improved by changing the configuration of the open split to a more sensitive setting.

Instrument sensitivity can drift over days to months with the condition of the mass spectrometer (age of the electron bombardment filament, and ion beam focus condition) and carrier gas flow rates within the continuous flow inlet system. The possibility of signal drift requires calibration standards run during each analytical session; an example instrument calibration line for a single analytical session in shown in figure 3.3b. Within each session the H_2^+ ion signal is calibrated by analyses of 4 or more aliquots of zoisite. Zoisite samples are between 30-700 mg zoisite, corresponding to 33-770 nanomoles H_2O, a range of sizes chosen to encompass the range in signal size expected during an analytical session. The signal size for this range is typically 5-75 Vs. Within daily sessions the average standard deviation for single aliquots of zoisite is 0.02 Vs/nanomole H_2O. The slope of calibration lines average 0.102 ± 0.03 Vs/nanomole H_2O and the average r^2 value for calibration lines is 0.96 ± 0.04. Daily calibration lines often do not have a zero intercept, with values between -2 and 4 Vs. Non-zero intercepts may be due to non-linearity in detector response at very low signal sizes or are associated with errors in blank correction.

Blank characterization

The effective minimum number of moles of hydrogen required for an analysis is set by the amount of water contamination evolved over the course of an analysis. The blank contribution consists of two components: water correlated with the surfaces of

mineral grains, and water derived from apparatus materials. These two components must be treated separately. The blank derived from apparatus materials can be measured for each sample assembly and subtracted from the measured signal. Any surface water contamination on mineral grains or the assembly materials cannot be corrected for, and therefore must be minimized. Background water evolved from components varies with the length of collection time. The duration of heating needed to dehydrate most nominally anhydrous minerals is long, usually 90 minutes. The step heating device described in (Eiler and Kitchen 2001) had a blank up to 1 Vs/min. We reduced this by modifying the apparatus to use the minimum number of capillary connections, and by replacing metal fitting and graphite ferrules with PEEK, ETFA, and FEP products wherever possible.

The apparatus blank is characterized by cryofocusing H_2O vapor from the He + O_2 gas stream of each sample assembly immediately prior to dehydrating the mineral grains. The average rate of blank water collected for samples of nominally anhydrous mineral samples is 0.092 Vs/min, corresponding to ~0.25 nanomoles H_2/min. Experiments replacing silica glass sample tubes with sintered polycrystalline Al_2O_3 closed end tubes initially reduced the blank, but the repeated rapid heating and cooling cycles experienced by sample tubes (greater than 800° C in under 1 minute) cracks the tubes and allows atmospheric contamination.

Nominally anhydrous minerals with low water concentrations may have high concentrations of water on the surface of mineral grains (Bell, Rossman et al. 2003). We have conducted several experiments to develop pre-heating protocols that minimize surface water present on mineral grains during an analysis. Our initial experiment was to

investigate the pattern of water released from an anhydrous mineral surface by step heating a sample of an anhydrous material, single crystal synthetic corundum. The corundum was crushed to the grain size used for nominally anhydrous minerals (the 45-90 μm sieve fraction) and heated for 15 minutes time intervals at 400° C, 636° C, 869° C, 1022° C, and 1120° C. More than 40 % of water is lost by 600° C, but 32 % of surface water is retained up to 1120° C, our typical analysis temperature (figure 3.4a). This result suggests that it is not possible to remove all surface water prior to analysis by brief heating.

Our analysis protocol calls for pre-heating samples overnight at moderate temperatures prior to analysis. To decide upon an optimum temperature for this long pre-heating step we used the release pattern determined in the corundum experiment described in the previous paragraph to choose candidate pre-heating temperatures (300º C, 500º C, and 700º C). Samples of an olivine (GRR 2014, 1.5 ppm H_2O by IR spectroscopy) were prepared by standard methods, pre-heated at the three analysis temperatures, and analyzed following normal protocol. Hydrogen yields for all three treatments were 1.0± 0.2 nanomoles H_2O/mg of sample (figure 3.4b). This result suggests that pre-heating at 300° C removes as much surface correlated water as is possible by this method but there is still a residual amount present.

To assess the total contribution of surface contamination as a function of sample mass, aliquots of San Carlos olivine between 0 mg (an empty platinum capsule) and 38 mg were measured using a 300° C pre-heating step overnight. These samples cover the mass range currently possible with our apparatus. The volume of the 38 mg sample is the maximum value that fits into the hot zone of the molybdenum disilicide furnace (letter d

on figure 3.2). The abundance of water is linearly correlated with sample mass, with a slope of 1.4 nanomoles H_2O/mg olivine and an intercept slightly below zero. The calculated water content for GRR 2014 is 21 ± 7 ppm H_2O (n = 7); we suggest this is the minimum surface water concentration, 19.5 ppm H_2O higher than the water content determined by IR spectroscopy, possible for olivine by this method. This measurement of a very low water content olivine (1.5 ppm H_2O) is similar to the measured water content for an anhydrous garnet measured by vacuum manometry (Bell and Ihinger 2000), suggesting that this is a minimum concentration possible to measure by any technique that relies on hydrogen extraction for the particle size analyzed.

Dehydration protocols

H diffusion data for many nominally anhydrous minerals indicate that > 99.9% of hydrogen will be released from a 100 μm mineral grain in 1 hour at 1100° C, including several minerals of geologic interest such as olivine (Mackwell and Kohlstedt 1990; Kohlstedt and Mackwell 1998), garnet (Wang, Zhang et al. 1996; Blanchard and Ingrin 2004; Kurka, Blanchard et al. 2005), orthopyroxene (Stalder and Skogby 2003), and clinopyroxene (Ingrin, Hercule et al. 1995; Hercule and Ingrin 1999). To verify dehydration of a sample under our laboratory conditions we used IR spectroscopy to measure the OH absorbance before and after dehydration of a sample of hydrous garnet. A 173 μm doubly-polished sample of GRR 771, a grossular with 1700 ppm H_2O was prepared. This sample is ~ 2 times as thick as the maximum dimension of sample grains analyzed normally. The large slab was broken into several pieces, each of which was

washed, wrapped in platinum foil, loaded into a sample assembly, and pre-heated as a normal sample. The first wafer was removed following pre-heating and the remaining wafers were heated to 1120° C with a wafer removed at 60 and 90 minutes. The IR spectrum between 3700 and 3500 wavenumbers was collected for each of these wafers (figure 3.6). After pre-heating there is no measurable change in the absorbance pattern in the OH stretching region, indicating that no hydroxyl is lost during pre-heating. Almost all hydroxyl is lost in the first 60 minutes, with 4% remaining in the sample. After 90 minutes hydroxyl bands are unresolved from the background. This result suggests that a sample 173 μm thick will completely dehydrate between 60 and 90 minutes. We choose to use 90 minutes as the duration of dehydration for garnets. This length of analysis is also used for pyroxenes due to the similarity in diffusion coefficients for garnet and pyroxenes. For extension of this method to other materials, particularly those with poorly known diffusion parameters, it is necessary to conduct a similar experiment to ensure both complete dehydration and no loss of water during pre-treatment procedures.

Comparisons with previous data

The data described in this section are a comparison of our analyses of water concentration measurements in nominally anhydrous minerals with measurements made by other methods. Samples for this comparison are garnets and one sample each of orthopyroxene, clinopyroxene, and olivine. The range in water contents measured are between 1.4 ppm H_2O (GRR 2014) and 8900 ppm (GRR 2094) and are listed in table 2 along with methods of previous analysis. Accepted values were obtained by a variety of

techniques: vacuum manometry (orthopyroxene, clinopyroxene, and pyrope), IR spectroscopy calibrated by manometry (grossular, almandine), and IR spectroscopy calibrated by NRA (spessartine, olivine). All measurements were made using the technique described above on aliquots of material between 0.25 mg and 38 mg in mass. Our water content measurements are close to or indistinguishable from within error to the accepted water content for most samples measured, with some exceptions discussed below (figure 3.7). Water contents are shown with 1 σ error bars, except for an unduplicated measurement of MON-9. For many samples error is within the symbol. One standard deviation for duplicate analyses varies between ± 2 ppm to ± .12 wt %, equivalent to 0.2 to 16% relative error. Deviations do not appear to be biased towards higher or lower values for any given measurement technique and we suggest that remaining differences may be specific to the sample materials. GRR 1016 (accepted H_2O = 575 ppm, measured H_2O = 852 ± 29 ppm), and GRR 2094 (accepted H_2O = 0.89 wt %, measured H_2O = 0.79 ± .12 wt %, not shown on figure 3.7) are the two significant outliers. For both samples these differences may be due to inhomogeneity in the sample garnets (Arredondo, Rossman et al. 2001). For GRR 2094 the difference may be due to inaccuracy of our measurement, or due to variations in the Beer's law absorption coefficient for spessartine at very high water content.

Summary

The results presented above suggest that continuous flow mass spectrometry can be used to accurately measure the concentration of water in mineral samples down to 18

ppm H_2O requiring as little as 30 nanomoles of hydrogen for an analysis. Though we have focused on low water content materials, this technique can be used to measure the water content of any material that dehydrates at 1100° C. Figure 3.8 illustrates the required mass of material for an analysis as a function of water content. For materials with greater than 0.2 wt % H_2O, less than 1 mg of material is required, permitting measurements of samples that are rare or precious.

Acknowledgements

We thank E. Miura Boyd, D. Bell, and M. Baker for graciously supplying sample materials. This work was supported by National Science Foundation grants # EAR-0337736 and EAR-0337816. J. O'Leary was also supported by the Gordon and Betty Moore fellowship program.

Oxide	Wt %	σ
Na_2O	0.0058	0.0062
TiO_2	0.0186	0.0121
K_2O	0.0019	0.0023
Al_2O_3	33.2925	0.0971
FeO	0.0066	0.0097
MgO	0.0599	0.0057
Cr_2O_3	0.0359	0.0186
CaO	24.9342	0.0345
SiO_2	39.5417	0.0968
MnO	0.013	0.0129
F	0.0796	0.0765
Cl	0.0016	0.0017
Total	97.991	0.196

Table 3.1. Major element chemistry of tanzanian zoisite. The formula of this zoisite sample is $Ca_{2.03}Mg_{0.01}Al_{2.98}(SiO_4)_{3.00}(OH)_{0.98}F_{0.02}$.

Sample	Mineral	Locality	Method of previous analysis	Reference	Water content, ppm H_2O		
					nominal	measured	σ
GRR 2014	forsterite olivine	unknown locality, Hebei, China	FTIR	this study	2	21	7
GRR 2009	Almandine	unkown locality	FTIR	this study	18	18	2
GRR 732	Grossular	Mindi Hills, Kenya	FTIR	Rossman et al., 1988	1089	1062	31
MON-9	Pyrope	Monastery Mine, South Afria	Hydrogen manometry	Bell et al., 1995	55	98	
GRR 43-3B	Spessartine	Rutherford # 2 mine, Amelia County, VA, USA	FTIR	Arredondo et al., 2001	1700	1716	5
GRR 72	Spessartine	unknown locality, Minas Gerais, Brazil	FTIR	Arredondo et al., 2001	104	237	8
GRR 1016	Spessartine	Little #3 mine, Ramona, San Diego County, CA, USA	FTIR	Arredondo et al., 2001	575	852	29
GRR 2094	Spessartine	Tongbei Area, Fujian Province, China	FTIR	Arredondo et al., 2001	8921	7975	1278
KBH.1 opx	orthopyroxene	Kilbourne Hole, NM, USA	Hydrogen manometry	Bell et al., 1995	187	165	20

Table 3.2. Water content of mineral samples

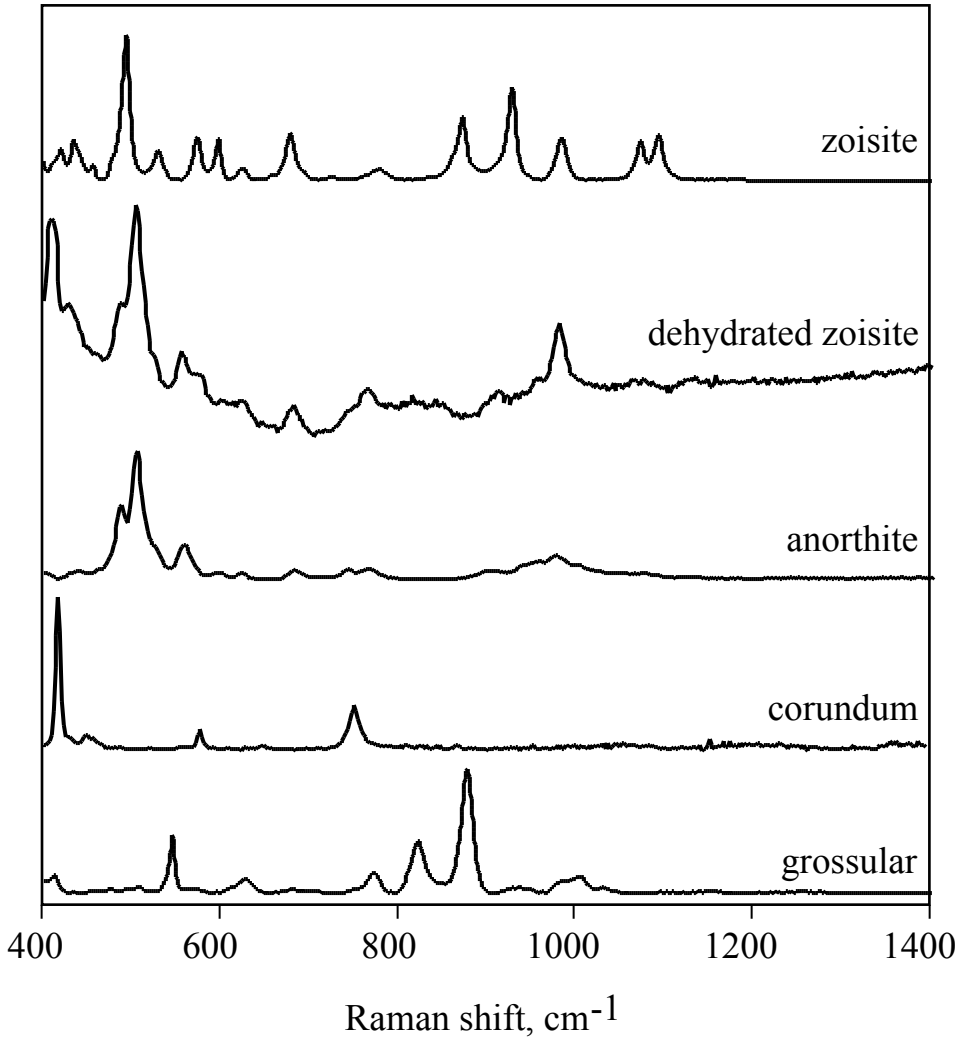

Figure 3.1. Raman spectra are shown for zoisite, residue of zoisite after hydrogen extraction, and the products of zoisite dehydration (anorthite, corundum, and grossular). Anorthite, corundum, and grossular spectra are from the Raman spectroscopy database, http://minerals.gps.caltech.edu. All prominent zoisite spectrum features are missing from the residue spectra. Features from anorthite, corundum, and grossular suggest the residue is a fine grained matrix of anorthite + corundum + grossular.

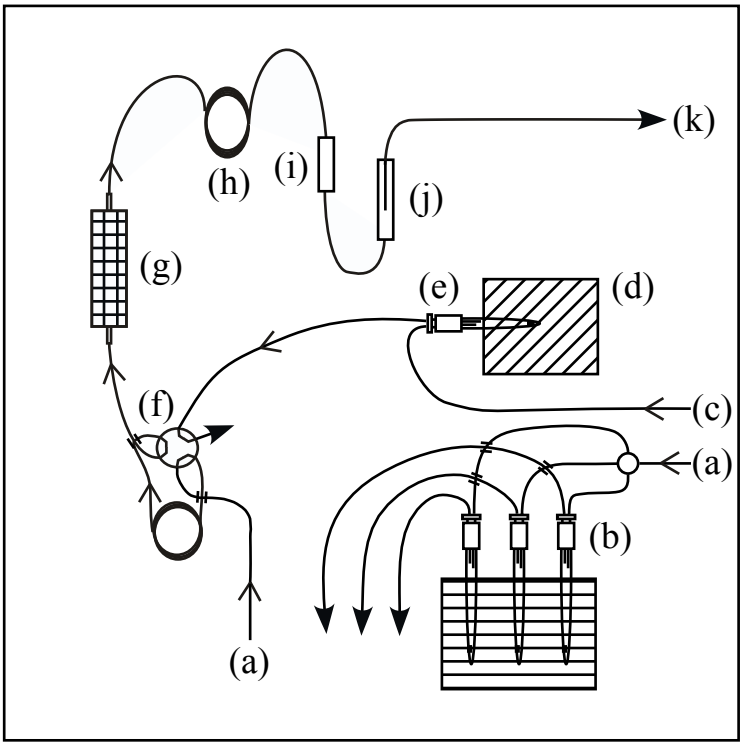

Figure 3.2. Schematic drawing of the apparatus for water extraction described in the text (modified from (Eiler and Kitchen, 2001)). All components labeled by letters are described in the text. Components a-b show sample assemblies in pre-treatment prior to analysis, c-e illustrate the high temperature water extraction line, and f-k illustrate water conversion to hydrogen for introduction into a mass spectrometer.

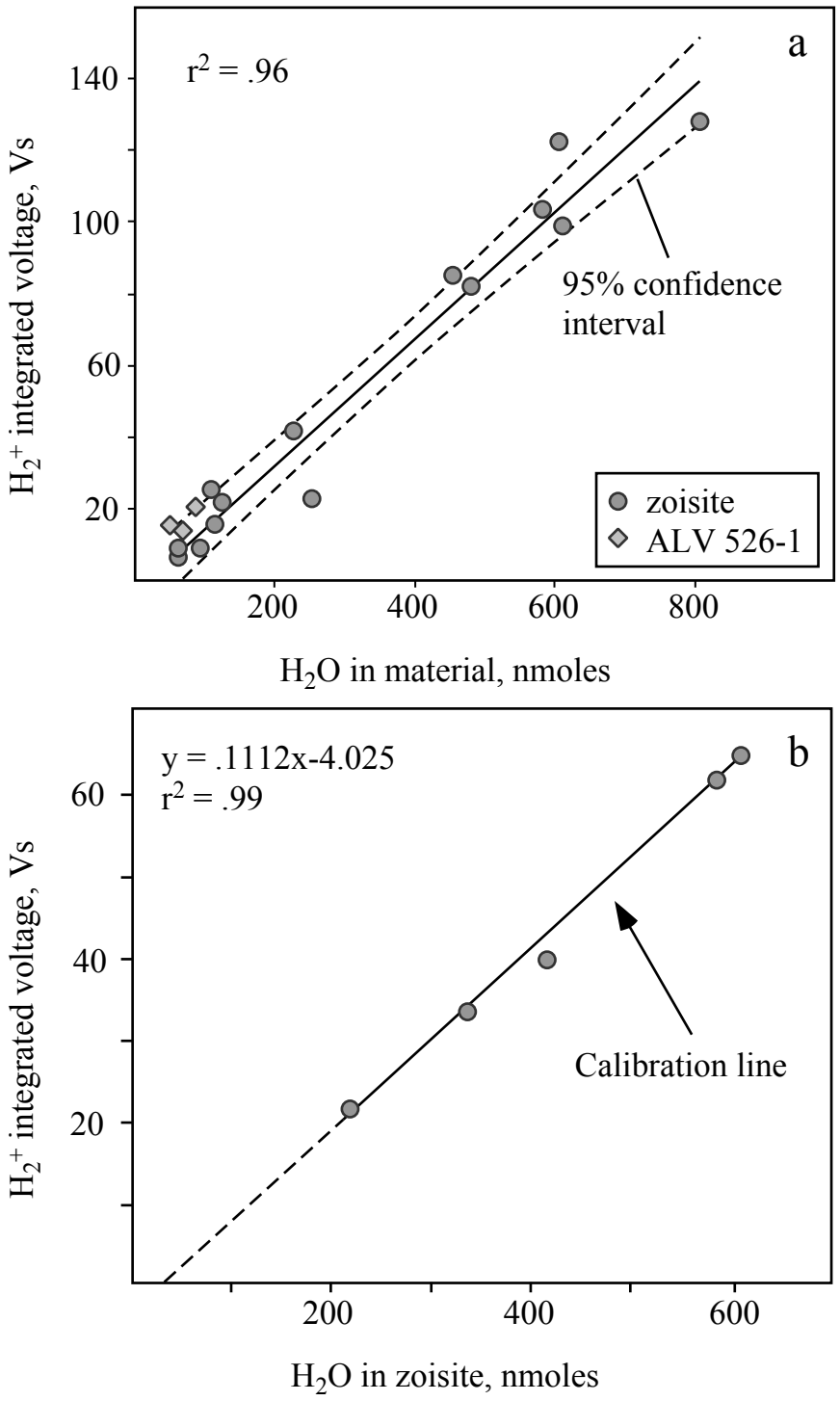

Figure 3.3. a) Analyses of zoisite and basaltic glass (ALV 526-1) over 4 days. The measured H_2^+ signal is independent of host phase. b) Example of signal response within an analytical session.

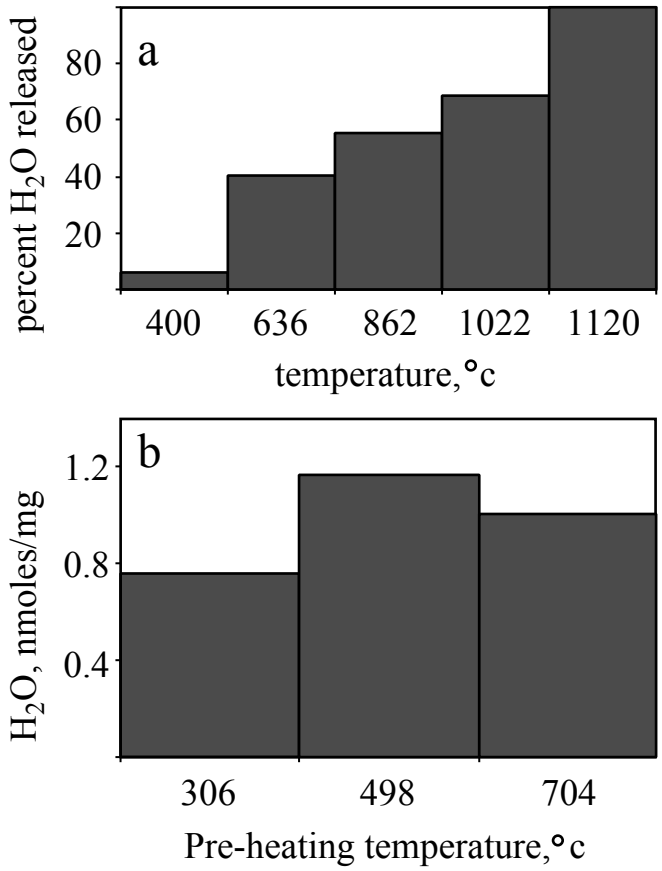

Figure 3.4. **a)** Progressive loss of surface water in temperature steps from anhydrous corundum. **b)** Water released from San Carlos olivine for three different pre-treatment temperatures, water released is not a function of pre-treatment temperature.

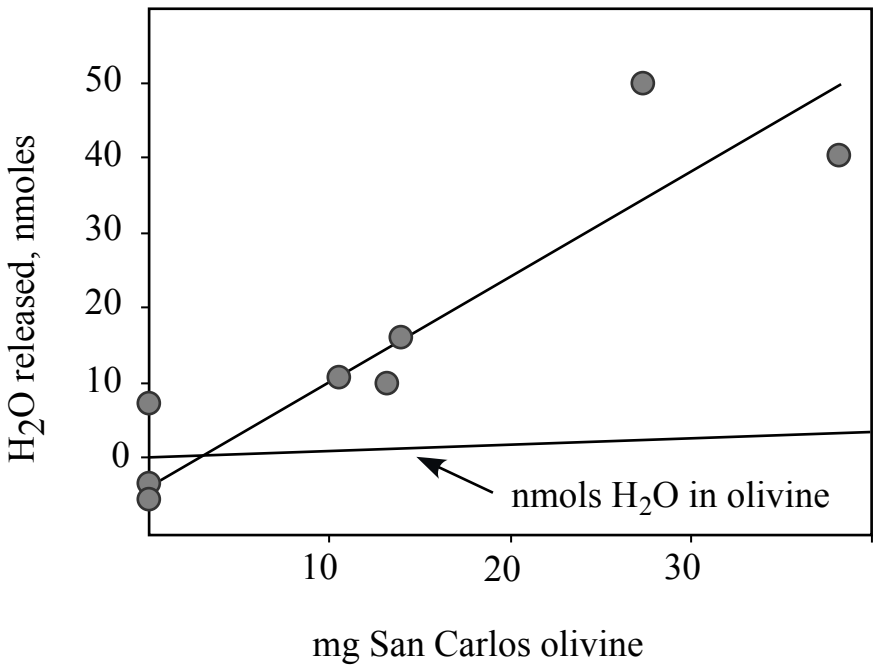

Figure 3.5. Water released, measured in nanamoles, vs. mass of San Carlos olivine, a mineral with 1.5 ppm H_2O.

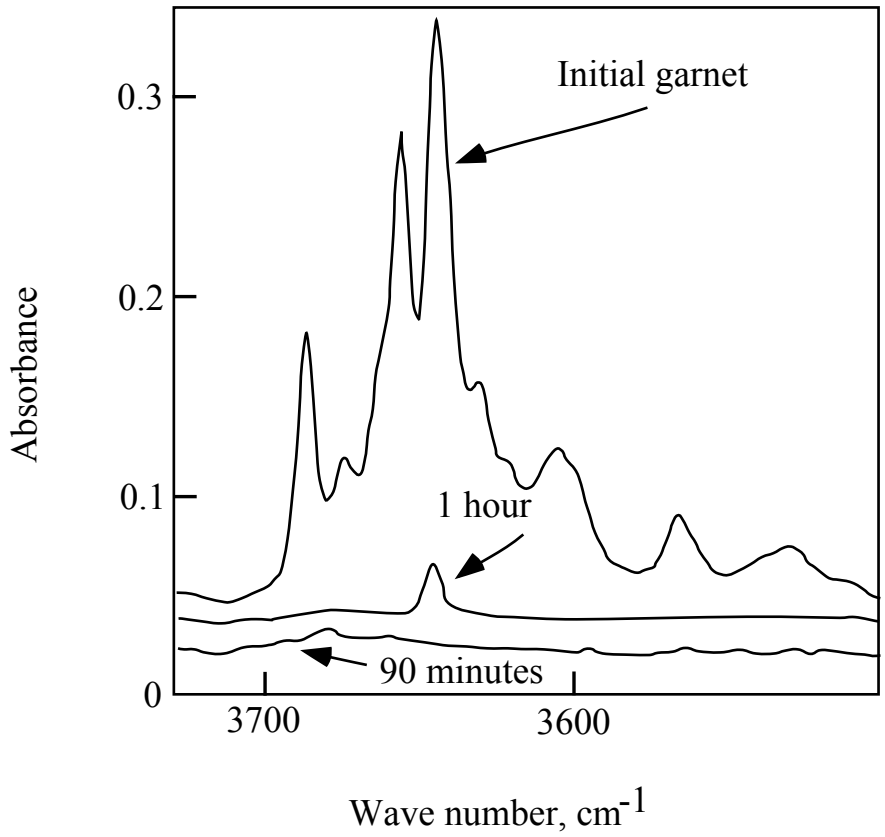

Figure 3.6. IR spectra of samples of a hydrous grossular (initial H2O = 1700 ppm) at different times during high temperature H-extraction. Spectra are vertically offset for clarity.

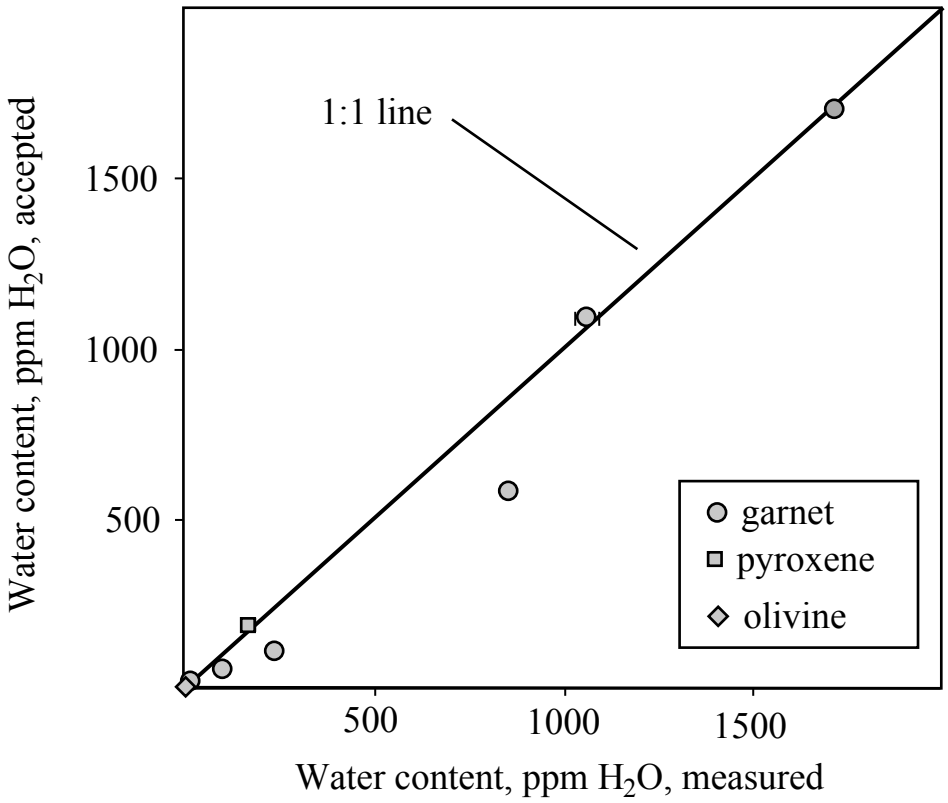

Figure 3.7. The accepted water content vs. measured water content for samples of nominally anhydrous minerals including garnet, pyroxene, and olivine.

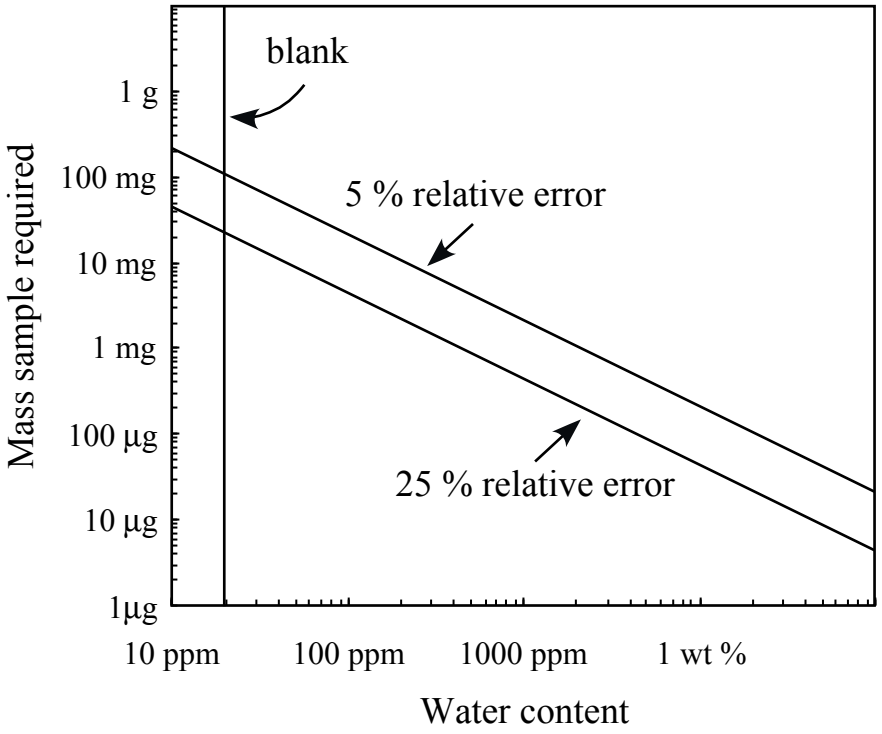

Figure 3.8. The sample size requirements for phases with between 10 ppm and 10 wt% H_2O; the required hydrogen for an analysis allows very small sample sizes (50-200 µg) for hydrous minerals, and larger sample sizes (1-30 mg) for nominally anhydrous minerals.

Chapter 4

Hydrogen Isotopic Constraints on Dehydration of Mantle Xenolith Pyroxenes

Julie A. O'Leary, John M. Eiler, and George R. Rossman

Abstract

Nominally anhydrous minerals from mantle xenoliths are the most deuterium depleted of all mantle materials, with δD values down to 53 ‰ below the average of mid-ocean ridge basalts. The low δD values of pyroxenes and garnets suggest that either large intermineral fractionations exist within the mantle, or that the hydrogen isotope composition of pyroxene does not preserve mantle conditions. We report hydrogen isotope and water content data for pyroxenes from intra-plate and sub-arc mantle xenoliths that confirm previous observations of very low δD values for xenoliths from the continental interior (δD_{cpx} = -113 ± 6, δD_{opx} = -127 ± 6) but find δD values closer to mid-ocean ridge basalts in Central American arc xenoliths (δD_{cpx} = -97 ± 12, δD_{opx} = -78 ± 1).

There is a positive correlation between the water content and δD value of intra-plate mantle pyroxenes and garnet (including data from Bell and Ihinger (2000)). Our result is consistent with H-isotope fractionation by degassing of water from nominally anhydrous minerals during emplacement in the crust. Laboratory diffusion data for OH in pyroxenes suggests hydrogen loss can occur on a timescale of hours to days at magmatic temperatures, though the lack of diffusion profiles in mantle pyroxenes and

correlations between hydrogen content and mantle derived geochemical trends (Peslier, Luhr et al. 2002) argue for at least partial preservation of the initial water content. Assuming our samples were initially in isotopic and compositional equilibrium with the depleted upper mantle, these pyroxenes have undergone 50-70 % loss of hydrogen during emplacement, suggesting that the hydrogen content of subcontinental lithosphere is similar to the source of mid-ocean ridge basalts.

Pyroxenes from sub-arc xenoliths have higher δD values than pyroxenes from intra-plate xenoliths with the same water content. This result suggests that though both subarc and intraplate pyroxenes have experienced hydrogen loss, differences in the H-isotopic composition of mantle samples may be preserved.

Introduction

Water in the upper mantle can be hosted by nominally anhydrous minerals (e.g. olivine, pyroxene, and garnet) in concentrations up to approximately 1000 ppm H_2O (Aines and Rossman 1984; Skogby, Bell et al. 1990; Smyth, Bell et al. 1991; Woodhead, Rossman et al. 1991; Bell and Rossman 1992; Bell and Rossman 1992; Vlassopoulos, Rossman et al. 1993; Bell, Ihinger et al. 1995; Ingrin and Skogby 2000; Andrut, Brandstatter et al. 2003; Johnson and Rossman 2004; Bromiley and Bromiley 2006). Though present in low concentrations, hydrogen influences the melting (Hirose and Kawamoto 1995) and deformation behavior of peridotite (Mackwell, Kohlstedt et al. 1985; Karato 1986), and may effect the dynamics of convection (Bercovici and Karato 2003). An accurate description of the water content is therefore a necessary constraint on

the evolution of the mantle. The distribution of hydrogen in the upper mantle is estimated by the water content of mantle-derived basalts and mantle xenoliths. Subcontinental lithospheric mantle xenoliths undergo a complex geologic history; the water content measured in xenoliths may not reflect equilibrium mantle conditions and could be disrupted by dehydration during transport to the surface.

The water content of normal mid-ocean ridge basalts (MORBs) suggests the depleted MORB mantle (DMM) contain 100-180 ppm H_2O (Michael 1988; Danyushevsky, Falloon et al. 1993; Danyushevsky, Eggins et al. 2000). Water contents of mantle peridotite xenoliths from continental environments are similar to the MORB-based estimate, with whole rock water contents of 28-260 ppm H_2O, and an average value of 102 ± 19 ppm H_2O (n = 19) (Bell and Rossman 1992; Peslier and Luhr 2006). Garnet lherzolite xenoliths from kimberlites are the most water-rich while sub-arc spinel peridotites contain the lowest concentrations of water. The differences in water content between geologic environments may be due to either variation in initial water content or to the proportion of hydrogen lost during transport to the surface by different mechanisms. For olivine, water content variability appears to be a consequence of preservation. Olivines from subarc xenoliths are zoned in water content along diffusion profiles that indicate extensive hydrogen loss (Demouchy, Jacobsen et al. 2006; Peslier and Luhr 2006) while megacrysts from kimberlites are unzoned and contain concentrations of hydrogen only possible at pressure greater that 3 GPa (Bell, Rossman et al. 2004). Hydrogen loss from olivine is consistent with diffusion rates for hydrogen transport in olivine that predict dehydration can occur on a timescale of hours to days at magmatic temperatures (Mackwell and Kohlstedt 1990; Demouchy and Mackwell 2003).

Water contents of pyroxene from both kimberlite (Bell, Rossman et al. 2004) and basalt hosted xenoliths (Peslier, Luhr et al. 2002) are correlated with the major element chemistry of the minerals and are not zoned in water content (Skogby, Bell et al. 1990; Peslier, Luhr et al. 2002). These results suggest that clinopyroxene and orthopyroxene preserve initial mantle water contents in all geologic environments, despite laboratory diffusion data that predict significant loss of hydrogen on timescales similar to hydrogen loss from olivine (Ingrin, Hercule et al. 1995; Hercule and Ingrin 1999; Blanchard and Ingrin 2004).

The hydrogen isotope ratio of water in nominally anhydrous minerals may provide constraints on the source of water content heterogeneity in mantle xenoliths. The hydrogen isotopic compositions of mantle pyroxenes and garnets, reported in values of δD_{VSMOW}, are the lowest of any mantle material, ranging between -129 and -89 ‰ (Bell and Ihinger 2000). The average of all mantle xenolith garnets and pyroxenes is deuterium depleted by more than 40 ‰ relative to both MORB (Craig and Lupton 1976; Kyser and O'Neil 1984; Poreda, Schilling et al. 1986; Chaussidon, Sheppard et al. 1991; Chaussidon and Jambon 1994; Pineau and Javoy 1994; Pineau, Shilobreeva et al. 2004) and micas in mantle xenoliths (Kuroda 1977; Boettcher 1980) (figure 4.1). MORBs span a restricted range of hydrogen isotopic compositions with an average of -69 ‰, similar to the average of mantle derived mica (-62 ‰), values that are thought to represent typical mantle hydrogen. Basalts derived from geochemically enriched regions of the mantle are variably D enriched relative to MORB, ranging in δD_{VSMOW} from -88 to -33 ‰ (Poreda 1985; Poreda, Schilling et al. 1986; Garcia 1989; Kingsley, Schilling et al. 2002, chapter

2). High δD values in back-arc basin basalts and ocean island basalts are interpreted as resulting from the addition of D-rich hydrogen from subducted ocean crust (chapter 2).

D-depleted hydrogen in nominally anhydrous mantle minerals may be generated by intramantle processes. Hydrogen isotope fractionation factors are large (typically 10-50 ‰ between water and hydrous silicates) and persist to mantle temperatures and pressures (Cole, Mottl et al. 1987; Horibe and Craig 1995). Bell and Ihinger (2000) interpret low δD values of mantle pyroxenes and garnets as equilibrium distribution of isotopes between hydrous and nominally anhydrous silicate minerals. In this study, we attempt to further constrain the processes that determine the water content and hydrogen isotopic composition of nominally anhydrous mantle minerals by study of pyroxenes from subarc and subcontinental mantle xenoliths.

Samples and methods

We measured the δD values and water contents for 5 mantle pyroxenes from two spinel lherzolites and one pyroxenite; sample names and localities are shown in table 4.1. Sample KBH-1 is an alkali-basalt hosted xenolith consisting of granoblastic spinel lherzolite from Kilbourne Hole, New Mexico. Mantle xenoliths from Kilbourne hole are from between 40-70 km depth, with equilibration temperatures of 1000-1200° C (Thompson, Ottley et al. 2005). Water content and H isotope data for orthopyroxene from KBH-1 was previously reported by (Bell and Ihinger 2000). One lherzolite sample and a pyroxenite sample are from Cerro Mercedes volcano located in the volcanic front of the Nicaraguan arc system and are thought to be from the asthenospheric wedge (M.

Carr, pers. communication). Major element chemistry for Cerro Mercedes pyroxene samples are shown in table 4.2.

Mineral separates of clinopyroxene and orthopyroxene for each sample were selected from 2-5 mm sized grains. Pyroxene separates were crushed in an alumina mortar and sieved to isolate mineral grains between 45 and 90 mm in maximum dimension. Crushed mineral grains were sonicated in a 10% HCl solution for 5 minutes followed by multiple rinses with deionized water to remove any surface contamination. Following acid cleaning, samples were ultra-sonicated in 95% ethanol for 5 minutes and placed in a 120° C oven to dry overnight. The washed mineral grains were inspected under a binocular microscope to remove any visible alteration or inclusions of fluids and minerals.

Hydrogen isotope ratios and water contents were measured by continuous flow mass spectrometry at the California Institute of Technology using methods modified from those described by (Eiler and Kitchen 2001) to measure absolute water abundance and hydrogen isotope ratios in nominally anhydrous minerals (see chapter 3). In brief, aliquants of pyroxene between 2.5 and 8.9 mg were placed in platinum tubes folded shut at each end. The sample tubes were placed in silica glass tubes purged by a mixture of He and O_2. Loaded sample assemblies were heated overnight at 300º C to remove surface water. Samples were heated to 1120º C for 90 minutes to drive complete dehydration of the pyroxenes. Our protocols for pre-treatment, pre-heating sample tubes, blank characterization, and dehydration (described in detail in chapter 3) are intended to minimize contamination by surface correlated water and to ensure complete dehydration of pyroxene. Hydrogen diffusion in pyroxenes is rapid enough that a 100 μm diameter

grain of either clinopyroxene or orthopyroxene heated at 1100° C for 90 minutes will lose > 99.97 % of hydrogen. Pyroxene grains inspected after analysis were not melted at these conditions. Evolved water was cryogenically collected, reduced to H_2 by reaction with hot uranium metal, and passed through a capillary into a Thermo-Electron MAT Delta-plus XP gas source isotope ratio mass spectrometer.

This technique requires correction for blank water contributions. The size of the blank correction is time dependent and must be characterized for each sample assembly. Immediately prior to analysis, a blank is measured by collecting water from the sample gas stream of for 60 minutes. The size of the blank is scaled to the total analysis time, and used to correct both the water content and hydrogen isotopic composition of each sample. Full procedural blanks were measured using a low water content olivine sample (GRR 2014, 1.5 ppm H_2O). This blank experiment, described in full in chapter 3, found a contribution of 1.4 nanomoles/mg material. For the sample masses used in this study this would contribute 3.5-12.4 nanomoles H_2, or the equivalent of 21 ppm H_2O per sample. The water content and δD values have not been corrected for this additional blank component.

Analyses for this study were run in three separate sessions. For each session 3 or 4 aliquants of an absolute water content standard were analyzed. We use zoisite, a hydrous mineral that contains 2.01 wt% H_2O, to calibrate the ion current generated for H_2^+ ions. Calibration lines for sessions had an average r^2 = .987. Our zoisite standard material has also been calibrated as an isotopic standard against an in-house basaltic glass hydrogen isotope standard, ALV 526-1. The average δD value of zoisite is -37.5 ± 1.2 ‰ (n = 14). The average for zoisite standards analyses during this study was -26 ± 5 ‰ (n =

9), with an average daily standard deviation of ± 4 ‰. The isotopic composition of samples were adjusted by the average offset of standards, this correction averaged -12 ‰.

Results

Water contents of clinopyroxene samples range from 144-264 ppm H_2O and water contents of orthopyroxene samples range from 158-165 ppm H_2O (shown in table 4.1). Water contents for coexisting clinopyroxene and orthopyroxene (shown on figure 4.2 in gray) are close to the distribution predicted by experimental partition coefficient for pyroxenes. Both samples fall within the range previously observed for pyroxenes from mantle xenoliths, though the Cerro Mercedes lherzolite sample is at the low water content range for clinopyroxene samples. Water content values for olivine were not determined for these samples, precluding an estimate of the whole rock water content.

The hydrogen isotope composition for 5 mantle pyroxenes is between -127 and -79 ‰, with an average value of -102 ‰ (shown in figure 4.1). This distribution confirms the deuterium depleted isotopic values observed by (Bell and Ihinger 2000) in nominally anhydrous minerals. Including all measurements, the δD_{VSMOW} for nominally anhydrous minerals is -100 ‰. This average is -31 ‰ below the average for MORBS and is 10 ‰ lower than any MORB measured (Craig and Lupton 1976; Kyser and O'Neil 1984; Poreda, Schilling et al. 1986; Chaussidon, Sheppard et al. 1991; Chaussidon and Jambon 1994; Pineau and Javoy 1994; Pineau, Shilobreeva et al. 2004). The hydrogen isotopic fractionation between coexisting orthopyroxene and clinopyroxene is not consistent for samples KBH-1 and 2-CM2003-3-2a #58. For the Kilbourne Hole lherzolite sample Δ_{cpx-}

$_{opx}$ = 14 ‰ while the Cerro Mercedes lherzolite sample $\Delta_{cpx\text{-}opx}$ = -36 ‰. Measured δD_{VSMOW} values from Cerro Mercedes are the highest among mantle pyroxenes from xenoliths, and may reflect the addition of deuterium enriched fluids to the subarc mantle, an effect that is observed in back arc basin basalts (Poreda 1985, Chapter 2).

Averaged by sample, the δD_{VSMOW} values of mantle pyroxenes are not correlated with water content (figure 4.3b). When each analysis is considered separately, it appears that there is a correlation between the absolute water content and the isotopic composition of the samples (figure 4.4). This suggests that there is heterogeneity within samples. Orthopyroxene from KBH-1 was measured in both this study and (Bell and Ihinger 2000). The average isotopic composition of KBH-1 orthopyroxene for duplicate measurements from each study are -127 ± 6‰ (this study) and -112 ± 2‰ (Bell and Ihinger 2000), a difference larger than error. Though there are not enough overlapping data to rule out inter-laboratory differences between these measurements, the differences in isotopic composition may reflect heterogeneous isotopic compositions in the xenolith. (Bell and Ihinger 2000) used 650 and 1300 mg of orthopyroxene to make an isotopic analysis by dual inlet mass spectrometry. Our continuous flow measurements used 8.49 and 8.98 mg for KBH-1 orthopyroxene, and may reveal heterogeneities not observed in larger samples.

Discussion

Correlations between water content and hydrogen isotopic composition of mantle pyroxenes

Positive correlations between δD_{VSMOW} and the water content of mantle pyroxenes suggest that hydrogen isotopes can be used to test for the origin and preservation of mantle hydrogen in nominally anhydrous minerals. Mineral-fluid hydrogen fractionation factors remain large at magmatic temperatures; degassing can produce > 50 ‰ variation in arc lavas (Pineau, Semet et al. 1999). We consider three explanations for correlation between water content and isotope composition: (1) Nominally anhydrous minerals are in isotopic equilibrium with hydrous phases in the upper mantle. (2) The isotopic composition of nominally anhydrous minerals results from mantle melting processes. (3) The isotopic composition of pyroxenes is a result of degassing during ascent to the surface.

Equilibrium distribution of isotopes among mantle phases

Micas in hydrous mantle xenoliths have δD values between –92 and –61 ‰ (Kuroda 1977; Boettcher 1980; Wagner 1996), a range similar to that found in MORB that is likely to represent the isotopic composition of deep-seated water. Bell and Ihinger (2000) conclude that low δD values in nominally anhdryous mantle minerals are in isotopic equilibrium with hydrous phases of “normal” mantle H isotope composition. There are no experimentally determined hydrogen fractionation factors for nominally anhydrous minerals. Bell and Ihinger (2000) estimates mineral-water fractionation factors based on an empirical relationship observed between the primary OH stretching frequency of a mineral and $\Delta_{mineral\text{-}water}$ (Dobson, Epstein et al. 1989), this relationship

predicts a fractionation of 15 ‰ between phlogopite and clinopyroxene, and a fractionation of 22 ‰ between phlogopite and orthopyroxene. Clinopyroxene and orthopyroxene in equilibrium with the most D-depleted mica from mantle xenoliths would be -107 and -113 ‰, similar to H isotope compositions found in mantle xenoliths. However, pyroxenes in equilibrium with the average δD value of micas would be -76 and -83 ‰, almost 20 ‰ higher than the average δD value of nominally anhydrous mantle minerals. Furthermore, our samples from Kilbourne Hole and Cerro Mercedes do not contain hydrous phases (though it is possible there were hydrous minerals present mantle source regions) suggesting that the whole rock isotopic composition is low in δD relative to other mantle materials.

If pyroxenes are in equilibrium with hydrous mantle phases, positive correlations between the water content and hydrogen isotope composition of pyroxene may be the result of mixing between a component with an isotopic composition similar to MORB and a D-depleted, low water content component. Altered oceanic crust that was dehydrated during subduction may be depleted in D and could serve as the source of hydrogen to nominally anhydrous minerals (Chapter 2), but these correlations are not apparent when averaged by xenolith. Preserving isotopic and water content heterogeneity on the hand specimen scale over mantle timescales is not possible, suggesting a late stage process is responsible for the observed correlation.

Hydrogen isotope chemistry of mantle melting

If mantle xenoliths are representative of the composition of the upper mantle, the hydrogen isotope composition of pyroxenes and garnets in mantle xenoliths should be related to the δD_{VSMOW} values found in MORB. The similarity in water content between mantle xenoliths (28-260 ppm) (Bell and Rossman 1992; Peslier and Luhr 2006) and the source of normal MORB (100-190 ppm in depleted MORB mantle, DMM) (Michael 1988) suggests that the H isotopic composition of xenoliths might be similar to DMM. Water behaves as a moderately incompatible species duing melting, with $D^{cpx/melt} = 0.023$ and $D^{opx/melt} = 0.019$ (Aubaud, Hauri et al. 2004), so most water is partitioned into the melt. To illustrate the effect of batch melting on H isotopic composition we calculate the isotope fractionation as a function of melt fraction. Melting calculations were done using the Adiabat_1ph interface (Smith and Asimow 2005) for pHMELTS (Ghiorso, Hirschmann et al. 2002; Asimow, Dixon et al. 2004) to simulate batch melting at a mid-ocean ridge between pressures of 3 GPa and 1 GPa, assuming an initial composition of from (Workman and Hart 2005), with an adjusted Na_2O content of 2.8 wt %, without constraining fO_2, and assuming an initial bulk water content of 180 ppm. Distribution coefficients used for hydrogen partitioning into olivine from Mosenfelder, Deligne et al. (2006). The H contents of pyroxenes are calculated using the mineral-mineral distribution coefficients from Hirth and Kohlstedt (1996). The H isotope composition of all phases were calculated using the phase proportions, concentration of hydrogen in each mineral, and equilibrium hydrogen fractionation factors for all phases. Hydrogen isotope fractionation factors for nominally anhydrous minerals and basalt were estimated using the Dobson et al. (1989) empirical relationship described above and experimentally determined fractions in the basalt-water system (Cole, Mottl et al. 1987). The predicted

fractionation factors (shown in table 4.3) are: $\Delta_{olivine\text{-}basalt}$ = -25 ‰, $\Delta_{orthopyroxene\text{-}basalt}$ = -13 ‰, and $\Delta_{clinopyroxene\text{-}basalt}$ = -21 ‰. This method of estimating fractionation factors for nominally anhydrous minerals was first suggested by Bell and Ihinger (2000). The average of all mantle-derived pyroxenes and garnets (-100 ± 25 ‰) was used as the initial hydrogen isotope composition. Figure 4.3a shows a curve for the isotopic composition of the liquid and of the residual solid. The δD value of the liquid is initially 11 ‰ higher than the bulk δD but rapidly approaches the initial bulk composition as melting proceeds and is never close to the average isotopic composition for MORB. This suggests that mantle xenoliths are not similar to the isotopic composition of DMM, and that the isotopic composition of the upper mantle is similar to δD_{VSMOW} values of MORB.

An alternative is that hydrogen in mantle xenoliths is residual to a batch or fractionational melting event of an initially DMM-like isotopic composition. To investigate this possibility we calculate the water content and δD values of liquid and residual solids for batch and fractional melting of a source with an initial δD_{VSMOW} equal to the average of MORB, 69 ‰. These calculations were done using the same whole rock composition and methods as described above. Curves for the isotopic composition and water content of liquid, clinopyroxene, orthopyroxene, and olivine are shown on figure 4.3b along with isotopic data for pyroxenes from mantle xenoliths, averaged by sample. The water contents of mantle xenolith pyroxenes are too high to have undergone even small amounts of melting (< 1%). The hydrogen isotopic composition does not evolve to the low values found in nominally anhydrous minerals until large extents of melting, when there is essentially no water left in the either pyroxene or olivine.

Degassing effects on hydrogen isotope composition

Correlations between water content and δD value of individual pyroxene samples may be caused by the loss of a deuterium rich component during degassing. Isotopic fractionation by volatile loss is sensitive to both the species of hydrogen lost and the mechanism of hydrogen transport. Figure 4.5a illustrates fractionation trends for four possible mechanisms of hydrogen loss from pyroxenes. Diffusive loss of H^+ ions or water molecules will preferentially remove H^+ or H_2O relative to D^+ or HDO, driving the δD of pyroxene higher than then initial value. Curves for diffusive loss were calculated assuming the relative rates of diffusion for isotopologues are inversely proportional to the square roots of isotopologue mass. The development of an isotopic gradient by diffusion requires that hydrogen is extracted faster than H-D exchange within the crystal. Diffusion coefficients for hydrogen extraction and incorporation in clinopyroxene are ~ 2-3 orders of magnitude slower than the diffusion rates for H-D substitution (Hercule and Ingrin 1999) suggesting that an isotopic gradient cannot be maintained within pyroxene crystals.

Hydrogen loss from pyroxenes by reaction to either H_2 or H_2O will also fractionate the isotopic composition of residual hydrogen. Assuming the conditions of Raleigh distillation apply, loss of hydrogen as H_2 produces large positive shifts in δD due to large predicted fractionation between H_2 and clinopyroxene ($\Delta_{H2\text{-}clinopyroxene}$ = - 140 ‰). Rayleigh fractionation of H_2O from pyroxenes predicts a positive relationship between water content and δD, similar to what is observed in mantle pyroxenes. Rayleigh fractionation assumes instantaneous equilibrium between an isotopically homogeneous

reservoir of hydrogen in pyroxene and an incremental amount of water that is immediately removed from the system, conditions that are unlikely in a natural environment. This model, though simple and idealized, would approximate natural conditions of a mineral in which H^+ diffuses to a reaction site, reacts to form water, and is rapidly lost from the system (see figure 4.5b).

To quantify the effect of hydrogen loss by Rayleigh distillation of H_2O we calculate degassing trends for orthopyroxene and clinopyroxene, shown as curves in figure 4.4. The initial hydrogen content and isotopic composition were chosen as an equilibrium distribution of hydrogen isotopes in a peridotite with a δD_{VSMOW} = -69 ‰, the mean δD_{VSMOW} value of MORB. Hydrogen partitioning was calculated for a peridotite containing 54% olivine, 23% orthopyroxene, 18% clinopyroxene, and 5% spinel using distribution coefficients from (Aubaud, Hauri et al. 2004), and hydrogen isotope fractionation factors between pyroxenes and fluid that were determined as described above for pyroxene-melt fractionation factors (listed in table 4.3). Two curves were calculated, one for peridotite initially containing 180 ppm H_2O (to represent a N-MORB water content) and one for 450 ppm H_2O (representing an E-MORB water content). Our calculated relationship between hydrogen isotope composition and water content are similar to the trends defined by alkali basalt and kimberlite hosted xenoliths. Deuterium-enriched samples from Cerro Mercedes arc xenoliths have similar water contents to other samples, suggesting that they may have originated from an initially D-rich hydrogen isotope composition relative to DMM. This result would be consistent with data for back arc basins that indicate the asthenospheric wedge is fluxed by a high δD fluid ($\delta D_{VSMOW} \approx$ -30 ‰) (Poreda, 1985, Chapter 2).

A trend similar to what we observe in pyroxenes in mantle xenoliths is found in augite phenocrysts from the Dish Hill basanite (Dyar 1996). Dish Hill pyroxenes have high water contents (0.05 to 0.86 wt % H_2O) and low δD_{VSMOW} values (-34 to -154 ‰) that are correlated with water content. Low δD values for these samples were attributed to assimilation of meteoric water. These data can also be described by water loss from pyroxenes. The curve shown in figure 4.6 is dehydration of a pyroxene, starting from an initial water content of 8500 ppm H_2O, the highest water content in the dataset. These data are consistent with a dehydration trend, suggesting the water loss and H isotopic fractionation is common during eruption or within a magma chamber.

Timing of hydrogen loss from mantle pyroxenes

Hydrogen diffusion in pyroxenes is 5-6 orders of magnitude faster than any other cation; experimentally determined hydrogen diffusion rates predict a loss of 50% of hydrogen in less than 15 hours at 900° C from a 1 mm diameter grain (Ingrin, Hercule et al. 1995; Hercule and Ingrin 1999; Stalder and Skogby 2003). Despite this, diffusion profiles are only rarely found at the edges of pyroxene grains (Peslier, Luhr et al. 2002). For a pyroxene grain to lose 40-60 % of hydrogen without evidence of a diffusion profile would require either a two-stage process with an initial loss of hydrogen followed by relaxation of the diffusion profile or that hydrogen loss from pyroxenes is rate limited by reaction rates at grain boundaries rather than H diffusion through a crystal, preventing formation of a diffusion profile.

Diffusion profiles in olivine from sub-arc xenoliths are consistent with loss of 80% of the initial hydrogen concentration (Demouchy, Jacobsen et al. 2006; Peslier and Luhr 2006). Diffusion rates for hydrogen extraction and incorporation in pyroxenes are 1-2 orders of magnitude slower than the rate of metastable hydrogen transport in olivine ($D \approx 10^{-10}$ m^2/sec) (Mackwell and Kohlstedt 1990; Kohlstedt and Mackwell 1998). The expected relationships between olivine concentration profiles and pyroxene concentration profiles can be calculated using equations 6.18 from (Crank 1975) for diffusion in a sphere. Assuming fast diffusion rate for olivine, an 80% dehydration of olivine from mantle xenoliths (Peslier and Luhr 2006), and using diffusion coefficients for all minerals at 900° c, same size grains of clinopyroxene would retain 80 % of hydrogen and orthopyroxene would retain 60 % of initial hydrogen content. These calculations suggest that zoning should exist in the outer rim of pyroxene grains. The absence of diffusion profiles in both clinopyroxenes and orthopyroxenes suggest that the loss of hydrogen is rate limited by a reaction along the grain boundary, and no diffusion profile created within the sample.

The water content and hydrogen isotope composition of the upper mantle

We conclude from these comparisons that mantle pyroxenes have undergone extensive water loss and hydrogen isotopic fractionation during emplacement in the crust. Water loss trends in the previous section were calculated assuming an initial δD value and water content similar to the source of N-MORB and E-MORB, a choice that produced an estimate of 40-60% hydrogen loss from most mantle pyroxene. Water

content estimates for xenoliths based on the H_2O content of nominally anhydrous minerals suggest bulk rock compositions of between 28 and 260 ppm H_2O, with an average of 102 ± 19 ppm H_2O (Bell and Rossman 1992; Peslier, Luhr et al. 2002). These measurements are consistent with water content estimates for DMM (50-180 ppm H_2O) though are lower than estimates for E-MORB and OIB sources (200-450 ppm H_2O). If these calculations are recalculated assuming that the pyroxenes have lost 50% of their initial hydrogen content, the range in nominally anhydrous mantle xenoliths may be approximately 400-500 ppm H_2O and average about 200 ppm H_2O. This result suggests that the water content of mantle peridotite without the presence of hydrous minerals is high enough to be a source for enriched mantle melts.

Conclusions

We present hydrogen isotope and water content measurements on 5 mantle pyroxenes that confirm that nominally anhydrous minerals from mantle xenoliths are deuterium depleted by approximately 30 ‰ relative to other mantle materials. Correlations between δD_{VSMOW} value and water content in clinopyroxene and orthopyroxene suggest that the exotic hydrogen isotope composition of nominally anhydrous minerals is related to processes that determine water content of xenoliths. The low δD of pyroxenes in mantle xenoliths cannot be explained by equilibrium partitioning between mantle phases, or by isotopic fractionation produced by melting during formation of mid-ocean ridge basalts. Upper mantle with the isotopic composition measured in these xenoliths can neither generate MORB nor be residual to MORB

formation. The isotopic composition of mantle pyroxenes is best explained by degassing of hydrogen from samples, suggesting that these mantle pyroxenes have lost > 50% of hydrogen during ascent to the surface and that the initial isotopic composition of nominally anhydrous minerals is similar to other mantle materials.

Acknowledgements

We thank Alan Brandon, Michael Carr, Michael Baker, and David Bell for their generosity with sample materials. We are grateful to NSF for financial support through grants # EAR-0337736 and EAR-0337816. J. O'Leary was also supported by the Gordon and Betty Moore fellowship program.

Sample	Mineral species	Locality	Rock type	δD	1 σ	H_2O, ppm	1 σ
KBH1	Al-enstatite	Kilbourne Hole, SW US	spinel lherzolite	-127	7	165	20
KBH1	Ti-Al augite	Kilbourne Hole, SW US	spinel lherzolite	-113	7	264	37
2-CM2003-3-2a #58	Al-augite	Cerro Mercedes, Nicaragua	spinel lherzolite	-105	6	144	44
2-CM2003-3-2a #58	Al-enstatite	Cerro Mercedes, Nicaragua	spinel lherzolite	-79	1	158	57
2-CM2003-3-2a #68	Ti-Al augite	Cerro Mercedes, Nicaragua	pyroxenite	-84		169	

Table 4.1. Hydrogen isotope and water content data and sample descriptions

Name	Na_2O	TiO_2	K_2O	Al_2O_3	FeO	MgO	Cr_2O_3	CaO	SiO_2	MnO	Total
2-CM2003-3-2a #68, cpx	0.27	0.14	0.01	2.94	4.10	16.58	0.49	22.75	52.08	0.12	99.48
2-CM2003-3-2a #58, opx	0.02	0.04	0.00	1.92	7.53	38.97	0.33	0.50	51.19	0.15	100.65
2-CM2003-3-2a #58, cpx	0.64	0.21	0.00	3.48	2.67	16.58	1.03	22.70	52.86	0.08	100.25

Table 2. Major element chemistry of Cerro Mercedes pyroxenes

Mineral	$\alpha_{min/H2O}$	$\alpha_{min/melt}$	$\Delta_{min-H2O}$	$\Delta_{min-melt}$
clinopyroxene	0.970	0.985	-30	-15
orthopyroxene	0.962	0.977	-39	-24
olivine	0.974	0.988	-26	-11
garnet	0.972	0.987	-28	-13

Table 4.3. Estimated fractionation factors used for calculations

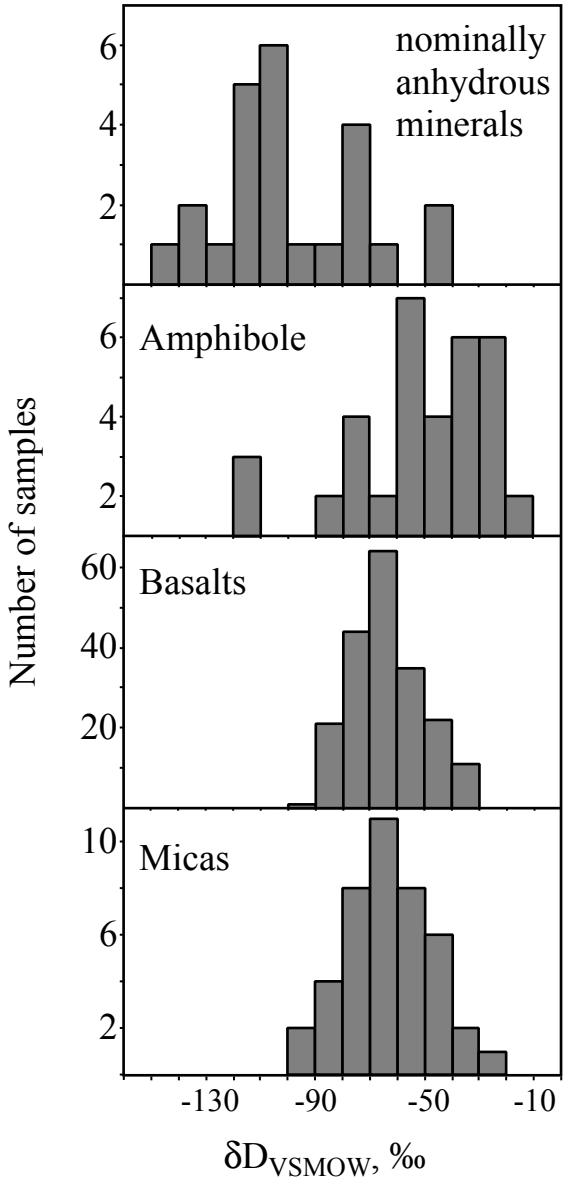

Figure 4.1. The distribution of hydrogen isotope compositions in mantle derived materials. Basalts (Craig and Lupton 1976; Kyser and O'Neil 1984; Poreda, Schilling et al. 1986; Chaussidon, Sheppard et al. 1991; Chaussidon and Jambon 1994; Pineau and Javoy 1994; Pineau, Shilobreeva et al. 2004) and micas (Kuroda 1977; Boettcher 1980) have similar distributions with averages of -69 ‰ and -61 ‰, and range between -92 and -41 ‰. These samples represent continental (micas) and oceanic (basalt) environments, suggesting the upper mantle has a homogeneous isotopic composition. Amphiboles, many from the same environments as micas, are not as close to a Gaussian distribution, with a larger range between -113 and 8 ‰ (Kuroda 1977; Boettcher 1980; Wagner 1996). Mantle garnets and pyroxene (Bell and Ihinger, 2000; this study) are deuterium depleted relative to other mantle materials with an average of -100 ‰.

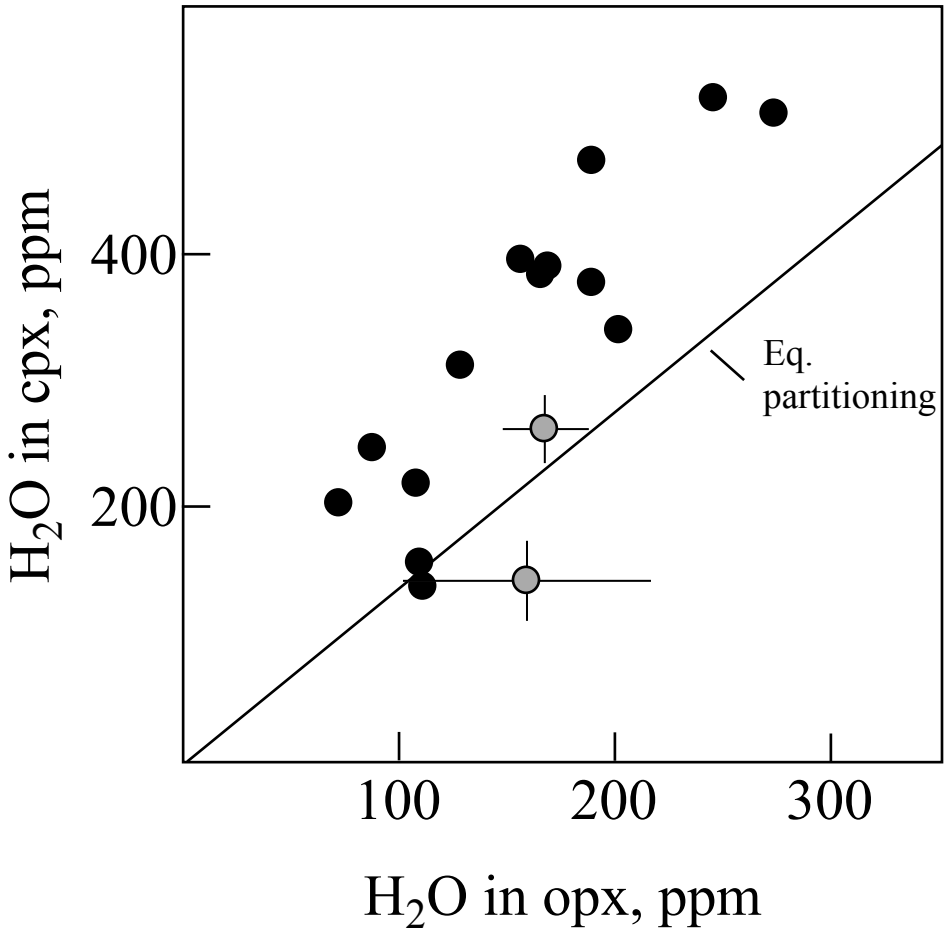

Figure 4.2. Water contents of coexisting mantle clinopyroxenes and orthopyroxenes. Data shown in black are from (Bell and Rossman 1992; Peslier, Luhr et al. 2002), data shown in grey are from this study. Water concentrations in mantle pyroxenes do not correspond to hydrogen partitioning data; they are skewed towards higher concentrations in clinopyroxene.

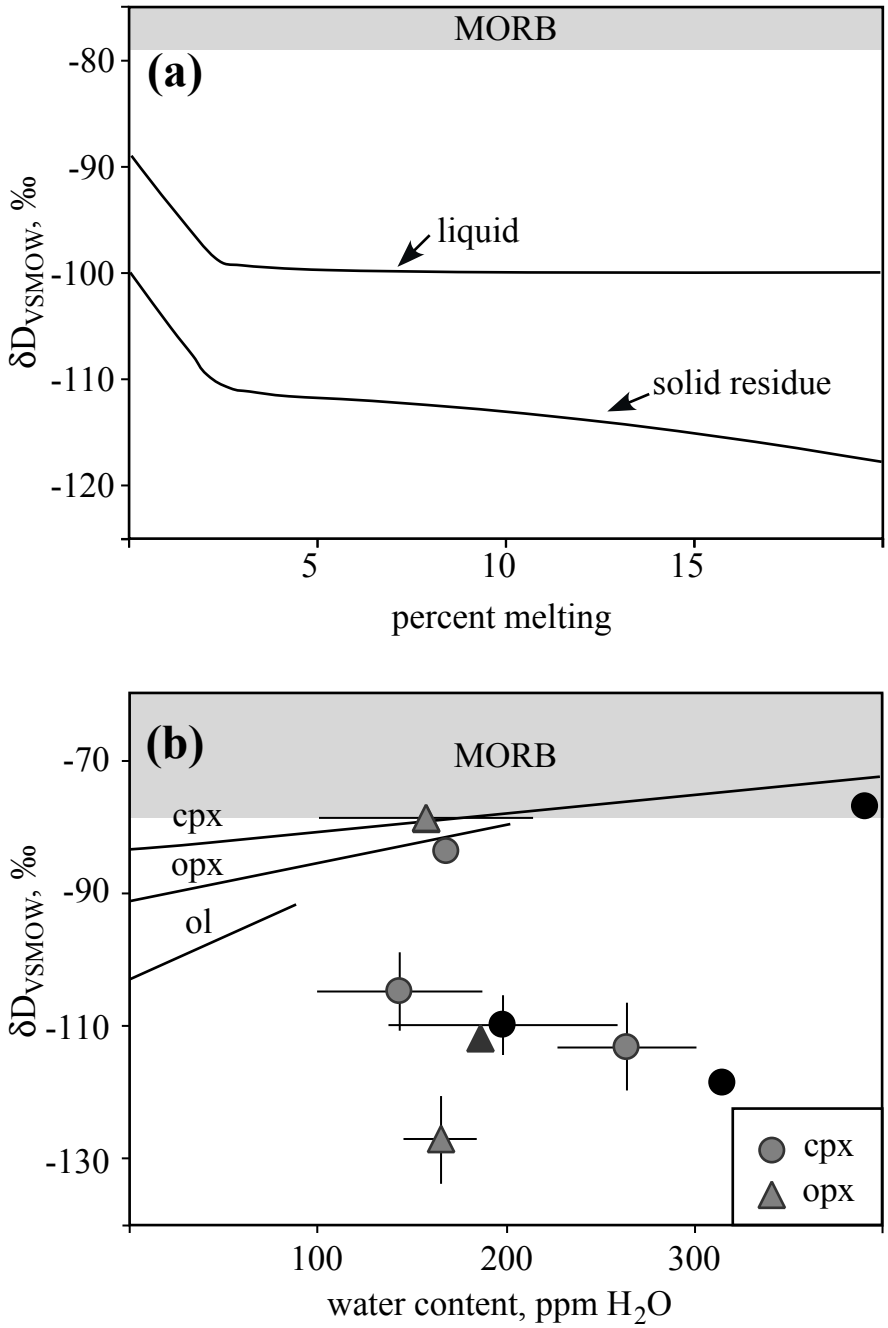

Figure 4.3. **(a)** Calculated δD values for liquid and solid residue of a peridotite source undergoing batch partial melting from an initial isotopic composition equal to the average of nominally anhydrous minerals from mantle xenoliths. **(b)** δD values vs. water content for clinopyroxene, orthopyroxene, and olivine. Curves show the calculated composition of nominally anhydrous minerals in a peridotite residue during partial melting. The initial isotopic composition of the source is set at the average of MORB. Data shown in black are from Bell and Ihinger (2000), data shown in grey are from this study. The isotopic composition of natural samples is lower than is likely in a peridotite residue.

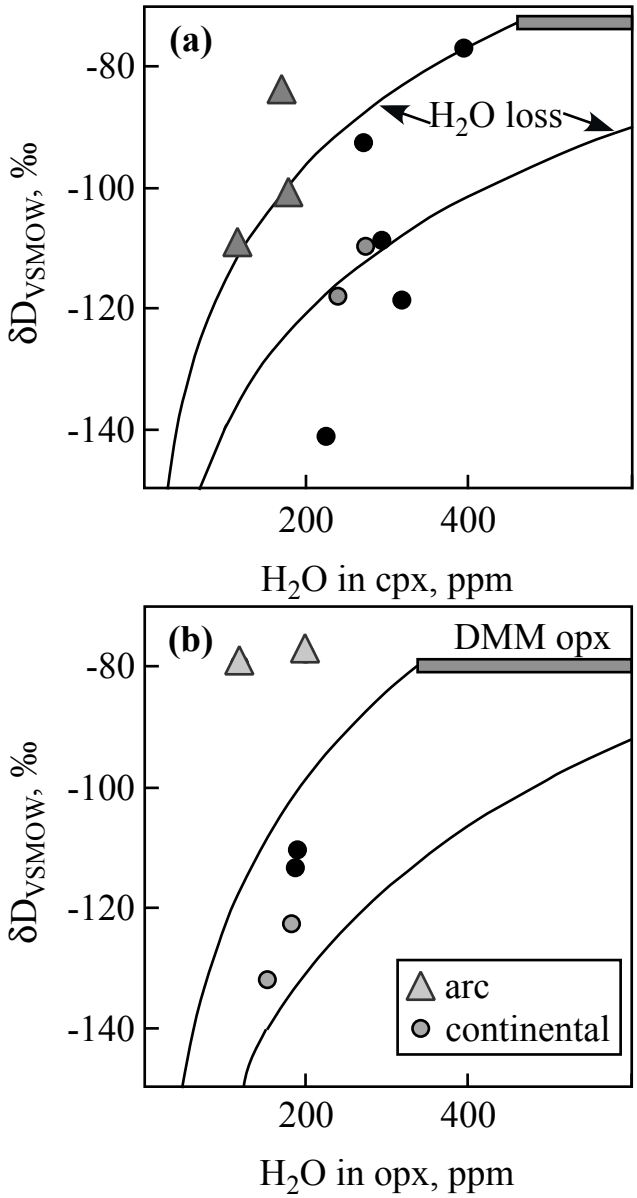

Figure 4.4. (a) The δD values vs. water content for individual samples on mantle clinopyroxenes. Curves mark calculated change in the isotope composition as a function of water loss from initial compositions of either water rich or water poor clinopyroxene in MORB-source mantle. Data shown in black are from Bell and Ihinger (2000), data shown in gray are from this study. **(b)** Hydrogen isotopic composition vs. water content for orthopyroxenes from mantle xenoliths. Model calculations are described in the text.

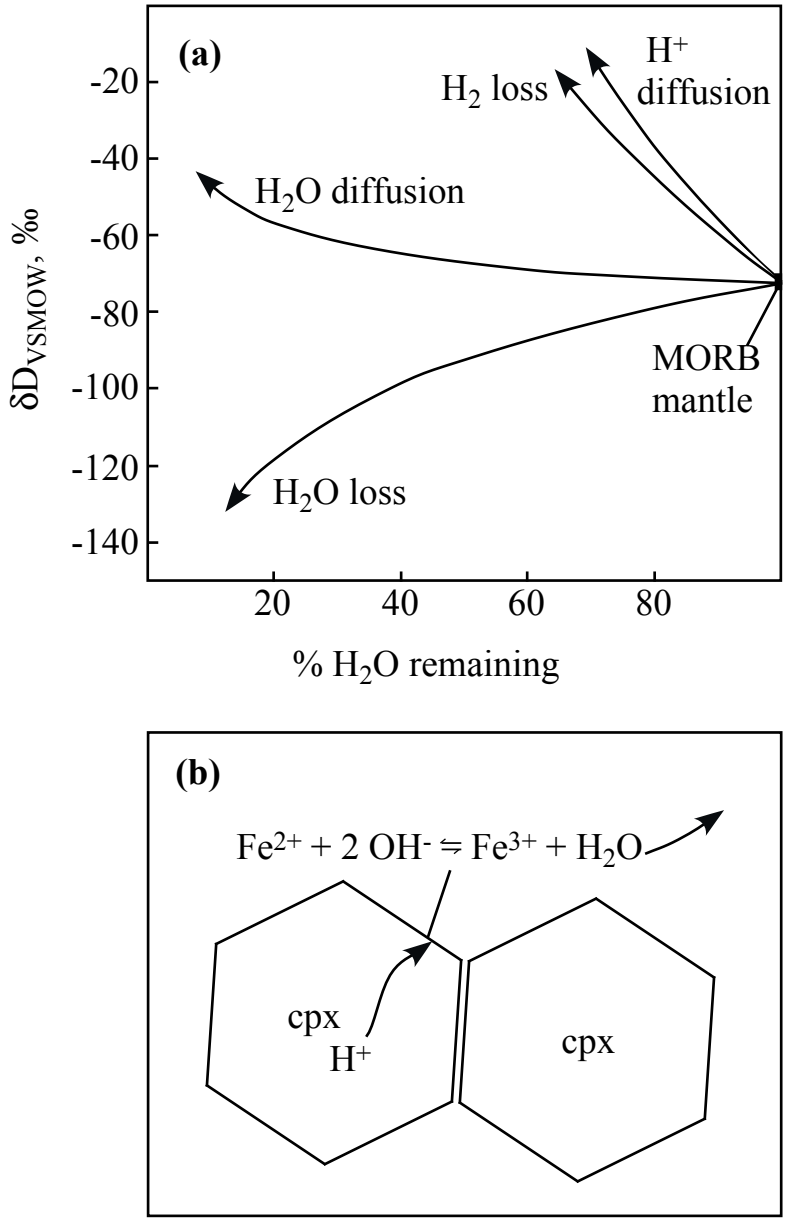

Figure 4.5. (a) Calculated isotopic composition of clinopyroxene with an initial composition in equilibrium with MORB source mantle undergoing different mechanisms of hydrogen loss. **(b)** Schematic drawing of our preferred mechanism for hydrogen loss. Hydrogen is lost by formation of water molecules that are in isotopic equilibrium with a well-mixed reservoir of hydrogen within a diffusion domain of pyroxene. After formation, water is lost from the system by rapid diffusion.

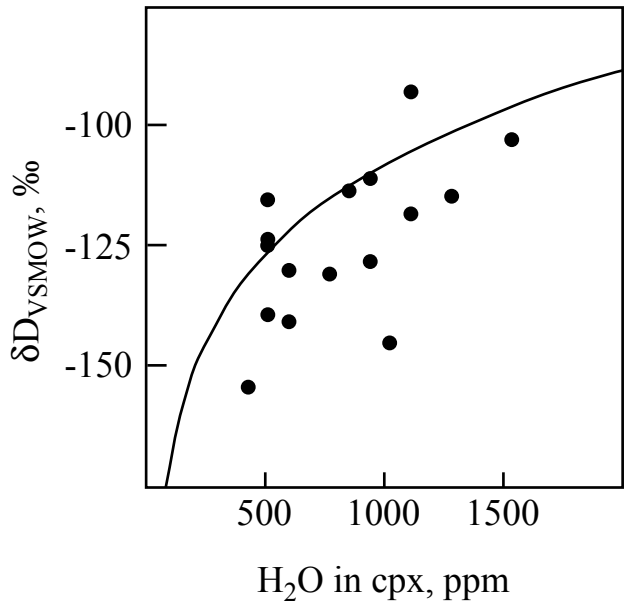

Figure 4.6. The δD_{VSMOW} vs. the water content in augite samples from the Dish Hill basanite. Data are from Dyar (1996). Model curve is of a Rayleigh style loss of water from a water-rich (8500 ppm H2O) initial composition with an isotopic composition in equilibrium with DMM.

Appendix 1

Protocols for D/H and Water Content Analysis of Hydrous Materials

Introduction

This appendix presents procedures for the preparation, pre-treatment, and dehydration of mineral samples for hydrogen isotope and water content measurements and two examples of the data treatment methods. These protocols were created using literature reports of the thermal stability and hydrogen loss rates of minerals and by methods described in Chapter 3 of this thesis. The apparatus for these measurements is also described in Chapter 3.

General procedure

All measurements require two steps, a pre-treatment heating step at low temperatures to remove atmospheric contamination and a dehydration step at high temperatures. The ideal pre-treatment option is to heat samples for longer than 12 hours at a temperature of 300 º C, conditions shown to produce the lowest blank contribution from sample materials. However, these conditions may cause partial water loss from some even high temperature materials (e.g. basalt glass, amphiboles) that undergo oxidation of iron at low temperatures in an oxidizing environment. Table A1.1 presents conditions of pre-treatment for materials that have been analyzed at the time of this

writing. Within this list conditions for garnet, basalt glass, zoisite, rutile, and tourmaline have been confirmed by spectroscopic characterization of sample materials following analysis.

The minimum duration used for high temperature dehydration is 30 minutes. During dehydration sample assemblies are purged by a flow of He and O_2 gas at a rate of 13 cm^3/minute and released water is continuously collected. The internal volume of standard sample assemblies is approximately 6.5 cm^3. In a 30 minute sample collection time the sample assembly is purged 60 times. This allows for complete collection of all water released from the sample. Samples that require longer times for dehydration include most nominally anhydrous minerals. The dehydration times for these minerals were determined using H diffusion data from literature sources and verification of dehydration by IR spectroscopy.

Table A1.1. Analysis conditions for materials of interest

Material	**Grain size**	**Pretreatment**		**Dehydration**	
		time, hours	**temp, ° C**	**time, minutes**	**temp, ° C**
basalt glass	90-212	8-24 hours	120	30	1120
biotite	90-212	8-24 hours	120	30	1120
amphibole	90-212	8-24 hours	120	30	1120
zoisite	212-425	8-72 hours	300	30	1120
tourmaline	212-425	8-72 hours	300	30	1120
garnet	45-90	8-72 hours	300	90	1120
clinopyroxene	45-90	8-72 hours	300	90	1120
orthopyroxene	45-90	8-72 hours	300	90	1120
olivine	45-90	8-72 hours	300	90	1120

During a standard water content or hydrogen isotope analysis data are recorded using the Isodat software package. Each sample requires two measurements recorded in

separate Isodat records: (1) a record that corresponds to a measurement of the blank associated with the sample assembly and (2) a record that corresponds to measurement of water released from the sample. The total H_2^+ signal and δD value of both the blank and the total sample are calculated using standard Isodat routines. These total H_2^+ signal and δD value must be corrected for blank contribution for final data reduction. An example spreadsheet of this is included on the supplementary CD of this thesis. Blank correction is scaled to the time of sample collection according to the following equations. The total H_2^+ signal collected for the sample ($H^+_{2\,sample}$) is corrected by:

$$H^+_{2\,corr} = \left(\frac{H^+_{2\,sample}}{Time_{sample}} - \frac{H^+_{2\,blank}}{Time_{blank}}\right) \times Time_{sample}$$

Where $Time_{sample}$ and $Time_{blank}$ are the length of time the sample and the blank were collected and $H^+_{2\,sample}$ and $H^+_{2\,blank}$ are the total H_2^+ signal collected for the sample and the blank, respectively. The proportion of the total H_2^+ signal due to hydrogen from the sample is then:

$$P = \frac{H^+_{2\,sample}}{H^+_{2\,corr}}$$

The measured δD value can then be corrected by:

$$D/H_{corr} = D/H_{sample} - P = \frac{D/H_{sample} - (D/H_{blank} \times (1-P))}{P}$$

These corrections must be made using isotope ratios rather than δD values.

Appendix 1

Protocols for D/H and Water Content Analysis of Hydrous Materials

Introduction

This appendix presents procedures for the preparation, pre-treatment, and dehydration of mineral samples for hydrogen isotope and water content measurements and two examples of the data treatment methods. These protocols were created using literature reports of the thermal stability and hydrogen loss rates of minerals and by methods described in Chapter 3 of this thesis. The apparatus for these measurements is also described in Chapter 3.

General procedure

All measurements require two steps, a pre-treatment heating step at low temperatures to remove atmospheric contamination and a dehydration step at high temperatures. The ideal pre-treatment option is to heat samples for longer than 12 hours at a temperature of 300 º C, conditions shown to produce the lowest blank contribution from sample materials. However, these conditions may cause partial water loss from some even high temperature materials (e.g. basalt glass, amphiboles) that undergo oxidation of iron at low temperatures in an oxidizing environment. Table A1.1 presents conditions of pre-treatment for materials that have been analyzed at the time of this

writing. Within this list conditions for garnet, basalt glass, zoisite, rutile, and tourmaline have been confirmed by spectroscopic characterization of sample materials following analysis.

The minimum duration used for high temperature dehydration is 30 minutes. During dehydration sample assemblies are purged by a flow of He and O_2 gas at a rate of 13 cm^3/minute and released water is continuously collected. The internal volume of standard sample assemblies is approximately 6.5 cm^3. In a 30 minute sample collection time the sample assembly is purged 60 times. This allows for complete collection of all water released from the sample. Samples that require longer times for dehydration include most nominally anhydrous minerals. The dehydration times for these minerals were determined using H diffusion data from literature sources and verification of dehydration by IR spectroscopy.

Table A1.1. Analysis conditions for materials of interest

Material	**Grain size**	**Pretreatment**		**Dehydration**	
		time, hours	**temp, ° C**	**time, minutes**	**temp, ° C**
basalt glass	90-212	8-24 hours	120	30	1120
biotite	90-212	8-24 hours	120	30	1120
amphibole	90-212	8-24 hours	120	30	1120
zoisite	212-425	8-72 hours	300	30	1120
tourmaline	212-425	8-72 hours	300	30	1120
garnet	45-90	8-72 hours	300	90	1120
clinopyroxene	45-90	8-72 hours	300	90	1120
orthopyroxene	45-90	8-72 hours	300	90	1120
olivine	45-90	8-72 hours	300	90	1120

During a standard water content or hydrogen isotope analysis data are recorded using the Isodat software package. Each sample requires two measurements recorded in

separate Isodat records: (1) a record that corresponds to a measurement of the blank associated with the sample assembly and (2) a record that corresponds to measurement of water released from the sample. The total H_2^+ signal and δD value of both the blank and the total sample are calculated using standard Isodat routines. These total H_2^+ signal and δD value must be corrected for blank contribution for final data reduction. An example spreadsheet of this is included on the supplementary CD of this thesis. Blank correction is scaled to the time of sample collection according to the following equations. The total H_2^+ signal collected for the sample ($H^+_{2\,sample}$) is corrected by:

$$H^+_{2\,corr} = \left(\frac{H^+_{2\,sample}}{Time_{sample}} - \frac{H^+_{2\,blank}}{Time_{blank}}\right) \times Time_{sample}$$

Where $Time_{sample}$ and $Time_{blank}$ are the length of time the sample and the blank were collected and $H^+_{2\,sample}$ and $H^+_{2\,blank}$ are the total H_2^+ signal collected for the sample and the blank, respectively. The proportion of the total H_2^+ signal due to hydrogen from the sample is then:

$$P = \frac{H^+_{2\,sample}}{H^+_{2\,corr}}$$

The measured δD value can then be corrected by:

$$D/H_{corr} = D/H_{sample} - P = \frac{D/H_{sample} - (D/H_{blank} \times (1-P))}{P}$$

These corrections must be made using isotope ratios rather than δ notation.

Appendix 2

Summary of hydrogen isotope measurements

Introduction

This appendix presents a summary of hydrogen isotope and water content measurements collected during this thesis. Table A2.1 contains a summary of isotopic standard measurements for data used in chapters 2, 3, 4. Standard data collected during technique development periods and recognized periods of instrument maintenance periods are excluded from this compilation.

Standard name	Material	δD_{VSMOW}, continuous flow (per mil)	1 σ	n	δD_{VSMOW}, dual inlet (per mil)
NBS 30 biotite	biotite	-69	5	19	-67
Serpentine	serpentine	-86	9	19	-84
ALV 526-1 basalt glass	basalt glass	-72	4	15	-
zoisite	zoisite	-37*	5	14	-

Table A2.1. Summary of standard analyses during data collection for Chapter 2, 3, and 4.

* Zoisite standard summary excludes data collected during completion of Chapter 4 analyses. Chapter 4 standard analyses were shifted to a composition of -27 ± 5, n = 9, these measurements were excluded based on evidence that the internal reference gas was isotopically shifted during those analytical sessions.

Table A2.2 contains hydrogen isotope measurements on basalt glass collected for Chapter 2. This table includes all data collected including data from rejected days. For each sample the sample name, mass of material analyzed, time of collection, raw total sample signal, raw δD value, corrected total sample signal, and corrected δD value are presented.

Sample name	analysis #	Sample mass (mg)	Collection time (minutes)	Total $H_2^+{}_{raw}$ (Vs)	δD_{raw} (per mil)	% of signal from sample	Total $H_2^+{}_{corr}$ (Vs)	δD_{corr} (per mil)	Notes
KIL 2-1	5561	331.7	15	16.83	-64.86	0.90	15.07	**-62.9**	
WOK16-2	5562	436.9	15	28.18	-40.04	0.94	26.42	**-37.3**	
serpentine	5564	29.2	15	38.65	-84.15	0.95	36.89	**-84.3**	
WOK16-2	5566	306.7	17	22.41	-45.12	0.91	20.41	**-41.6**	
KIL 1-9	5570	509	15	27.83	-63.2	0.95	26.53	**-60.8**	
DS86:4-1	5571	305.9	15	17.04	-61.84	0.92	15.74	**-57.6**	
ALV1846-9	5573	140	15	27.89	-71.71	0.95	26.59	**-69.7**	
DS86:4-1	5575	443	15	26.73	-67.22	0.95	25.43	**-64.9**	
ALV1846-9	5576	121.2	15	23.82	-79.63	0.95	22.52	**-77.7**	
serpentine	5580	32.5	15	37.57	-89.15	0.97	36.50	**-88.8**	
KIL 2-1	5581	432.9	15	20.2	-63.36	0.95	25.77	**-61.3**	
DS84:1-1	5582	565.8	15	13.1	-57	0.92	12.03	**-53.2**	
DS18:1-6	5583	153.8	15	29.37	-48.94	0.96	28.30	**-47.0**	
serpentine	5585	25.5	15	34.21	-99.81	0.97	33.14	**-99.8**	
DS84:1-1	5586	799.1	15	17.97	-57.56	0.94	16.90	**-54.9**	
DS18:1-6	5587	102.7	15	19.53	-55.83	0.95	18.46	**-53.3**	
serpentine	5590	31.9	15	35.83	-77.89	0.92	33.02	**-77.6**	*
WOK 28	5591	314	15	14.24	-49.48	0.80	11.43	**-41.5**	*
KIL 2-1	5593	385.1	15	18.01	-60.93	0.84	15.20	**-57.1**	*
serpentine	5595	35.4	15	44.33	-98.23	0.94	41.52	**-99.3**	*
Wok 28	5596	326.9	15	15.86	-32.19	0.82	13.05	**-21.5**	*

Table A2.2. All analyses collected during the completion of chapter 2. This table includes rejected data. The reasons for data rejection are indicated by code, * idicates a day was reject due to either isotopically shifted or unreproducible standards, ** indicates sample yield was too low.

Sample name	analysis #	Sample mass (mg)	Collection time (minutes)	Total $H_2^+{}_{raw}$ (Vs)	δD_{raw} (per mil)	% of signal from sample	Total $H_2^+{}_{corr}$ (Vs)	δD_{corr} (per mil)	Notes
ALV1833-11	5597	290.5	15	33.07	-39.08	0.92	30.26	**-35.1**	*
ALV 526-1	5599	917	15	17.71	-67.84	0.94	16.66	**-68.9**	
D54	5600	191.9	15	16.3	-35.07	0.94	15.25	**-33.9**	
KIL 2-1	5603	380.7	15	14.78	-69.78	0.93	13.73	**-71.2**	
D54	5604	131.7	16	11.99	-40.44	0.91	10.87	**-39.3**	
DS88-3-1	5605	287.7	15	28.77	-49.99	0.96	27.72	**-49.9**	
ALV1833-11	5606	332.7	15	32.37	-59.28	0.97	31.32	**-59.5**	
ALV 526-1	5609	907.6	15	15.025	-70.98	0.96	14.45	**-68.9**	
46:1-6	5610	205.3	15	29.406	-46.98	0.98	28.83	**-45.5**	
WOK 28	5611	792.4	20	33.085	-38.3	0.98	32.31	**-36.3**	
ALV 526-1	5612	988.4	15	17.428	-57.13	0.97	16.85	**-54.9**	
46:1-6	5613	663	15	87.25	-34	0.99	86.67	**-33.4**	
DS74:3-1	5736	368.4	15	49.48	-38.28	0.96	47.49	**-36.5**	
ALV 526-1	5737	755.6	15	39.285	-75.29	0.95	37.30	**-74.9**	
DS80:25-3	5737	409.2	18	95.49	-43.76	0.98	93.11	**-42.8**	
ALV 526-1	5738	1050	18	25.52	-48.51	0.91	23.14	**-45.1**	
DS88:2-1	5739	630.5	20	80.784	-32.96	0.97	78.14	**-31.3**	
DS74:3-1	5740	298.7	20	42.674	-35.36	0.94	40.03	**-32.3**	
DS80:25-3	5741	409.2	18	96.95	-25.99	0.98	94.57	**-24.6**	
DS88:2-1	5742	212.3	20	36.588	-43.54	0.93	33.94	**-40.6**	
ALV 526-1	5743	640.1	20	19.51	-70	0.86	16.86	**-68.2**	
ALV 526-1	5747	613.4	20	12.688	-89.28	0.86	10.85	**-94.4**	*

Table A2.2.continued All analyses collected during the completion of chapter 2. This table includes rejected data. The reasons for data rejection are indicated by code, * idicates a day was reject due to either isotopically shifted or unreproducible standards, ** indicates sample yield was too low.

Sample name	analysis #	Sample mass (mg)	Collection time (minutes)	Total $H_2^+{}_{raw}$ (Vs)	δD_{raw} (per mil)	% of signal from sample	Total $H_2^+{}_{corr}$ (Vs)	δD_{corr} (per mil)	Notes
55:1-1	5748	377.2	20	60.389	-40.79	0.97	58.56	**-40.2**	*
ALV 1833-11	5749	372.2	20	41.95	-43.79	0.96	40.12	**-43.1**	*
ALV 526-1	5750	707.4	20	16.11	-66.48	0.89	14.28	**-67.4**	*
55:1-1	5751	146.9	20	19.5	-63	0.91	17.67	**-63.4**	*
ALV 526-1	5950	756.9	21	20.54	0.93	0.77	15.87	**27.6**	*
ALV 526-1	5952	832.9	21	20.83	-3.44	0.78	16.16	**21.4**	*
ALV1833-11	5953	373.45	20	39.72	-33.15	0.89	35.27	**-26.0**	*
ALV1833-11	5954	342.6	20	37.72	-20.99	0.88	33.27	**-11.8**	*
ALV 526-1	5955	798.7	20	21.82	-4.07	0.80	17.37	**17.8**	*
ALV 526-1	5960	639	21	14.61	2.51	0.51	7.49	**113.9**	*
ALV 526-1	5962	1101.2	20	24.65	-4.05	0.72	17.87	**37.9**	*
DS 88:25-3	5963	154.25	21	34.34	-12.99	0.79	27.22	**13.6**	*
serpentine	5970	31.9	15	46.009	-78.94	0.95	43.61	**-79.8**	
serpentine	5971	46.1	17	60.222	-74.85	0.95	57.51	**-75.4**	
KIL 2-1	5972	319.7	20	16.533	-35.22	0.81	13.34	**-28.3**	**
serpentine	5988	411	15	25.78	-67.61	0.92	23.72	**-65.6**	*
ALV 526-1	5989	720.5	16	13.29	-55.04	0.83	11.09	**-47.9**	*
ALV 1833-11	5990	368	20	41.02	-24.12	0.93	38.27	**-19.3**	*
ALV 1833-11	5991	295.7	20	36.22	-54.53	0.92	33.47	**-51.5**	*
ALV 526-1	5992	957.2	20	25.27	-69.37	0.89	22.52	**-66.7**	*
serpentine	5993	29.5	20	31.65	-69.16	0.91	28.90	**-67.1**	*
46:1-6	5995	230	20	38.55	-49.91	0.93	35.80	**-46.8**	*

Table A2.2.continued All analyses collected during the completion of chapter 2. This table includes rejected data. The reasons for data rejection are indicated by code, * idicates a day was reject due to either isotopically shifted or unreproducible standards, ** indicates sample yield was too low.

Sample name	analysis #	Sample mass (mg)	Collection time (minutes)	Total $H_2^+{}_{raw}$ (Vs)	δD_{raw} (per mil)	% of signal from sample	Total $H_2^+{}_{corr}$ (Vs)	δD_{corr} (per mil)	Notes
46:1-6	5998	260	20	41.23	-19.46	0.93	38.48	**-14.4**	*
ALV 526-1	6012	992.4	16	28.1	-78.7	0.93	26.07	**-78.7**	
KIL 2-1	6013	610.3	16	33.42	-71.9	0.94	31.39	**-71.5**	
ALV 526-1	6014	837.7	16	23.27	-79.2	0.91	21.24	**-79.3**	
DS80:25-3	6015	165.7	20	44.05	-54.46	0.94	41.51	**-53.0**	
DS80:25-3	6016	169.5	20	21.09	-91.61	0.88	18.55	**-93.4**	**
KIL 2-1	6018	634.5	20	37.39	-68.46	0.93	34.85	**-67.7**	
ALV 526-1	6019	1035	22	35.77	-69.9	0.92	32.98	**-69.2**	
DS22:2-1	6020	713.1	22	39.2	-57.75	0.93	36.41	**-56.1**	
DS22:2-1	6021	726.7	22	43.03	-57.34	0.94	40.24	**-55.9**	
ALV 526-1	6024	835.9	20	23.83	-70.4	0.93	22.14	**-68.2**	
ALV 526-1	6025	980.3	20	26.056	-71.04	0.94	24.37	**-69.1**	
55:1-1	6026	262.9	20	50.55	-46.17	0.97	48.86	**-44.3**	
55:1-1	6027	151.1	20	33.49	-60.89	0.95	31.80	**-58.9**	**
55:1-1	6028	186	20	36.624	-48.4	0.95	34.94	**-46.0**	
KIL 2-1	6029	436	20	25.011	-65.04	0.93	23.32	**-62.6**	
ALV 526-1	6030	787.2	20	21.947	-74.51	0.92	20.26	**-72.5**	
DS 88:2-1	6031	395.7	24	51.167	-39.85	0.96	49.14	**-37.4**	
DS 88:2-1	6032	282	31	41.568	-44.89	0.94	38.95	**-41.3**	
ALV 526-1	6036	920.5	20	30.417	-77.23	0.88	26.80	**-70.5**	
KIL 2-1	6037	646.5	20	39.91	-67.67	0.91	36.29	**-61.8**	
47:1-5	6038	246.4	20	64.09	-55.26	0.94	60.47	**-51.0**	

Table A2.2.continued All analyses collected during the completion of chapter 2. This table includes rejected data. The reasons for data rejection are indicated by code, * idicates a day was reject due to either isotopically shifted or unreproducible standards, ** indicates sample yield was too low.

Sample name	analysis #	Sample mass (mg)	Collection time (minutes)	Total $H_2^+{}_{raw}$ (Vs)	δD_{raw} (per mil)	% of signal from sample	Total $H_2^+{}_{corr}$ (Vs)	δD_{corr} (per mil)	Notes
ALV 526-1	6041	937.7	20	36.77	-79.71	0.90	33.15	**-74.6**	
47:1-5	6039	218.7	21	51.77	-51.81	0.93	47.97	**-45.9**	
47:1-5	6042	224.8	20	48.04	-44.08	0.92	44.42	**-37.3**	
46:1-6	6043	315.1	20	52.86	-45.96	0.93	49.24	**-40.0**	
46:1-6	6044	259.7	20	47.07	-50.87	0.92	43.45	**-44.5**	
ALV 526-1	6045	854	21	28.51	-61.43	0.87	24.71	**-51.4**	
ALV 526-1	6048	897.6	20	27.53	-93.72	0.92	25.37	**-94.4**	
ALV 1833-11	6049	382	23	52.194	-45.41	0.95	49.71	**-43.4**	
73:2-1	6050	212.8	24	34.074	-58.71	0.92	31.49	**-56.5**	
ALV 1833-11	6051	343.8	22	54.523	-36.16	0.96	52.15	**-33.9**	
ALV 526-1	6052	910.9	23	25.969	-103.35	0.90	23.49	**-105.2**	
73:2-1	6053	333.1	20	48.607	-48.2	0.96	46.45	**-46.4**	
DS 80: 25-3	6054	136.3	20	41.327	-52.55	0.95	39.17	**-50.7**	*
ALV 526-1	6419	595.5	20	28.36	-95.69	0.58	16.34	**-80.0**	*
WOK 16-2	6420	411.2	21	42.33	-81.19	0.70	29.71	**-66.0**	*
DS80:25-3	6421	157.2	20	52.36	-79.79	0.77	40.34	**-68.7**	*
serpentine	6422	30.9	20	58.3	-90.24	0.79	46.28	**-83.3**	*
GTVA 73:2-2	6423	247.6	21	46.65	-67.36	0.73	34.03	**-49.0**	*
ALV 526-1	6463	614.8	20	18.36	-96.95	0.78	14.26	**-78.7**	
ALV 1846-9	6464	575.8	22	69.56	-76.96	0.94	65.05	**-71.2**	
GTVA 73:2-2	6465	192.3	21	31.68	-88.37	0.86	27.37	**-77.1**	
ALV 526-1	6473	714	26	20.71	-99.72	0.71	14.67	**-97.1**	
GTVA 73:2-2	6474	732.8	20	114.37	-58.98	0.96	109.72	**-57.0**	
DS 18:1-6	6475	201	20	51.67	-63.89	0.91	47.02	**-59.7**	

Table A2.2.continued All analyses collected during the completion of chapter 2.

Sample name	analysis #	Sample mass (mg)	Collection time (minutes)	Total $H_2^+{}_{raw}$ (Vs)	δD_{raw} (per mil)	% of signal from sample	Total $H_2^+{}_{corr}$ (Vs)	δD_{corr} (per mil)	Notes
DS 80:25-3	6476	366.2	20	100.39	-66.21	0.95	95.74	**-64.3**	
DS 80:25-3	6480	170	20	54	-75.02	0.91	49.35	**-72.1**	
GTVA 73:2-2	6481	234.4	25	46.32	-89.39	0.87	40.51	**-87.0**	
ALV 526-1	6482	571.8	20	37.67	-107.21	0.88	33.02	**-107.4**	
ALV 526-1	6484	586.5	20	16.04	-105.12	0.80	12.88	**-97.9**	*
DS 22:2-1	6485	360.3	21	21.45	-85.76	0.85	18.14	**-76.8**	*
DS 84:1-1	6486	881.7	24	21.69	-88.54	0.83	17.90	**-78.8**	*
ALV 526-1	6487	551.5	21	12.98	-77.38	0.74	9.67	**-57.8**	*
DS 80:25-3	6488	532.4	22	118.25	-73.46	0.97	114.78	**-71.6**	*
ALV 526-1	6495	606.7	20	13.94	-96.85	0.90	12.48	**-97.9**	*
80:1-3	6496	44.4	30	31.95	-109.23	0.93	29.76	**-110.8**	*
80:1-3	6497	338.9	38	22.3	-126.77	0.71	15.90	**-116.3**	*
ALV 526-1	6498	516.8	21	16.81	-101.58	0.79	13.28	**-87.9**	*
DS 88:3-1	6499	214	20	58.32	-75.88	0.94	54.95	**-71.2**	*
DS 88:3-1	6500	446.8	20	29.24	-99.92	0.88	25.87	**-93.0**	*
DS 88:3-1	6501	302.7	23	25.76	-115.53	0.85	21.89	**-108.9**	*
ALV 526-1	6503	1246	20	35.57	-113.6	0.91	32.20	**-109.5**	*
ALV 526-1	6566	1077	20	33.05	-88.69	0.88	28.95	**-78.5**	
DS 84:1-1	6567	884.2	20	26.55	-84.84	0.85	22.45	**-71.1**	
DS 84:1-1	6568	604.5	20	24.4	-100.98	0.83	20.30	**-89.0**	
ALV 526-1	6569	402.4	20	14.51	-106.91	0.72	10.41	**-85.9**	
DS 84:1-1	6570	1440.3	21	42.57	-92.53	0.90	38.26	**-84.9**	

Table A2.2. All analyses collected during the completion of chapter 2. This table includes rejected data. The reasons for data rejection are indicated by code, * idicates a day was reject due to either isotopically shifted or unreproducible standards, ** indicates sample yield was too low.

Appendix 3

Database of mineral spectroscopy measurements

Introduction

This database consists of Raman and IR spectra of samples studied during this thesis. Not all of this data is presented in the thesis. Data are organized by mineral group, then sample name within the excel spreadsheet, appendix 3. Many of these samples were part of experiments or were heat treated prior to measurement. These samples are noted in the table, and a link to a brief description of the experiment is also presented.

BIBLIOGRAPHY

Agrinier, P., R. Hekinian, et al. (1995). "O and H stable isotope compositions of oceanic crust and upper mantle rocks exposed in the Hess Deep near the Galapagos Triple Junction." Earth and Planetary Science Letters **136**(3-4): 183-196.

Ahrens, T. J. (1989). "Water storage in the mantle." Nature **342**: 122-123.

Aines, R. D. and G. R. Rossman (1984). "Water-content of mantle garnets." Geology **12**(12): 720-723.

Alt, J. C. (2003). "Stable isotopic composition of upper oceanic crust formed at a fast spreading ridge, ODP Site 801." Geochemistry Geophysics Geosystems **4**.

Alt, J. C. and W. C. Shanks (1998). "Sulfur in serpentinized oceanic peridotites: Serpentinization processes and microbial sulfate reduction." Journal of Geophysical Research-Solid Earth **103**(B5): 9917-9929.

Andrut, M., F. Brandstatter, et al. (2003). "Trace hydrogen zoning in diopside." Mineralogy and Petrology **78**(3-4): 231-241.

Arredondo, E. H., G. R. Rossman, et al. (2001). "Hydrogen in spessartine-almandine garnets as a tracer of granitic pegmatite evolution." American Mineralogist **86**(4): 485-490.

Asimow, P. D., J. E. Dixon, et al. (2004). "A hydrous melting and fractionation model for mid-ocean ridge basalts: Application to the Mid-Atlantic Ridge near the Azores." GeochemistryGeophysics Geosystems **5**(1): Q01E16, doi:10.1029/2003GC000568.

Asimow, P. D., Langmuir C.H., and the Kilo Moana 0417 Shipboard Science Party (2005). "Effect of water on magma and crustal density: Highly fractionated lavas in the Lau Basin and other wet spreading centers." Geochemica et Cosmochemica Acta **69a**: #2578.

Asimow, P. D. and C. H. Langmuir (2003). "The importance of water to oceanic mantle melting regimes." Nature **421**(6925): 815-820.

Aubaud, C., E. H. Hauri, et al. (2004). "Hydrogen partition coefficients between nominally anhydrous minerals and basaltic melts." Geophysical Research Letters **31**(20): ISI:000224881700005.

Bell, D. R. and P. D. Ihinger (2000). "The isotopic composition of hydrogen in nominally anhydrous mantle minerals." Geochimica et Cosmochimica Acta **64**(12): 2109-2118.

Bell, D. R., P. D. Ihinger, et al. (1995). "Quantitative-analysis of trace OH in garnet and pyroxenes." American Mineralogist **80**(5-6): 465-474.

Bell, D. R. and G. R. Rossman (1992). "The distribution of hydroxyl in garnets from the subcontinental mantle of Southern Africa." Contributions to Mineralogy and Petrology **111**(2): 161-178.

Bell, D. R. and G. R. Rossman (1992). "Water in Earth's mantle - the role of nominally anhydrous minerals." Science **255**(5050): 1391-1397.

Bell, D. R., G. R. Rossman, et al. (2003). "Hydroxide in olivine: A quantitative determination of the absolute amount and calibration of the IR spectrum." Journal of Geophysical Research-Solid Earth **108**(B2).

Bell, D. R., G. R. Rossman, et al. (2004). "Hydroxide in kyanite: A quantitative determination of the absolute amount and calibration of the IR spectrum." American Mineralogist **89**(7): 998-1003.

Bell, D. R., G. R. Rossman, et al. (2004). "Abundance and partitioning of OH in a high-pressure magmatic system: Megacrysts from the Monastery kimberlite, South Africa." Journal of Petrology **45**(8): 1539-1564.

Bercovici, D. and S.-i. Karato (2003). "Whole-mantle convection and the transition-zone water filter." **425**(6953): 39-44.

Blanchard, M. and J. Ingrin (2004). "Hydrogen diffusion in Dora Maira pyrope." Physics and Chemistry of Minerals **31**(9): 593-605.

Blanchard, M. and J. Ingrin (2004). "Kinetics of deuteration in pyrope." European Journal of Mineralogy **16**(4): 567-576.

Boettcher, A. B., O'Neil, J.R. (1980). "Stable isotope, chemical, and petrogrphic studies of high-pressure amphiboles and micas: evidence for metasomatism in the mantle source regions of alkali basalts and kimberlites." American Journal of Science **280**(A): 594-621.

Bromiley, G. D. and F. A. Bromiley (2006). "High-pressure phase transitions and hydrogen incorporation into $MgSiO_3$ enstatite." American Mineralogist **91**(7): 1094-1101.

Chacko, T., D. R. Cole, et al. (2001). Equilibrium oxygen, hydrogen and carbon isotope fractionation factors applicable to geologic systems. Stable Isotope Geochemistry. Washington D.C., The Mineralogical Society of America. **43:** 1-81.

Chaussidon, M. and A. Jambon (1994). "Boron content and isotopic composition of oceanic basalts - geochemical and cosmochemical implications." Earth and Planetary Science Letters **121**(3-4): 277-291.

Chaussidon, M., S. M. Sheppard, et al. (1991). " Hydrogen, sulphur, and neodymium isotope variations in the mantle beneath the EPR at 12 deg 50 min N." Journal of the Geological Society **3**: 325 -337.

Cho, H. and G. R. Rossman (1993). "Single-crystal NMR-studies of low-concentration hydrous species in minerals - grossular garnet." American Mineralogist **78**(11-12): 1149-1164.

Cole, D. R., M. J. Mottl, et al. (1987). "Isotopic exchange in mineral-fluid systems 2. oxygen and hydrogen isotopic investigation of the experimental basalt-seawater system." Geochimica et Cosmochimica Acta **51**(6): 1523-1538.

Coombs , M. L., T. W. Sisson, et al. (2004). "Ultra-high chlorine in submarine Kilauea glasses: Evidence for direct assimilation of brine by magma." Earth and Planetary Science Letters **217**: 297-313.

Cooper, K. M., J. M. Eiler, et al. (2004). "Oxygen isotope evidence for the origin of enriched mantle beneath the mid-Atlantic ridge." Earth and Planetary Science Letters **220**(3-4): 297-316.

Craig, H. and J. E. Lupton (1976). "Primordial neon, helium, and hydrogen in oceanic basalts." Earth and Planetary Science Letters **31**(3): 369-385.

Crank, J. (1975). The Mathamatics of Diffusion. Oxford, Oxford Science Publications.

Danyushevsky, L. V., S. M. Eggins, et al. (2000). "H_2O abundance in depleted to moderately enriched mid-ocean ridge magmas; Part I: Incompatible behaviour, implications for mantle storage, and origin of regional variations." Journal of Petrology **41**(8): 1329-1364.

Danyushevsky, L. V., T. J. Falloon, et al. (1993). "The H_2O content of basalt glasses from southwest Pacific back-arc basins." Earth and Planetary Science Letters **117**(3-4): 347-362.

Defant, M. J., P. M. Richerson, et al. (1991). "Dacite genesis via both slab melting and differentiation - petrogenesis of La-Yeguada Volcanic Complex, Panama." Journal of Petrology **32**(6): 1101-1142.

Demouchy, S., S. D. Jacobsen, et al. (2006). Rapid magma ascent recorded by water diffusion profiles in mantle olivine. **34:** 429-432.

Demouchy, S. and S. J. Mackwell (2003). "Water diffusion in synthetic iron-free forsterite." Physics and Chemistry of Minerals **30**: 486-494.

Dixon, J. E., L. Leist, et al. (2002). "Recycled dehydrated lithosphere observed in plume-influenced mid-ocean-ridge basalt." Nature **420**(6914): 385-389.

Dobson, P. F., S. Epstein, et al. (1989). "Hydrogen isotope fractionation between coexisting vapor and silicate-glasses and melts at low-pressure." Geochimica et Cosmochimica Acta **53**(10): 2723-2730.

Driesner, T. (1997). "The effect of pressure on deuterium-hydrogen fractionation in high-temperature water." Science **277**(5327): 791-794.

Driesner, T. and T. M. Seward (2000). "Experimental and simulation study of salt effects and pressure/density effects on oxygen and hydrogen stable isotope liquid-vapor fractionation for 4-5 molal aqueous NaCl and KCl solutions to 400 degrees C." Geochimica et Cosmochimica Acta **64**(10): 1773-1784.

Dyar, M. D. (1996). Crystal chemistry of Fe^{3+}, H^{+}, and D/H in mantle-reived augite from Dish Hill: Implications for alteration during transport. Mineral Spectroscopy: A Tribute to Roger G Burns. M. D. Dyar, McCammon C., Schaefer, M.W., The Geochemical Society. **No. 5**.

Eiler, J. M. (2001). Oxygen isotope variations of basaltic lavas and upper mantle rocks. Stable Isotope Geochemistry. J. W. Valley and D. R. Cole. Washington D.C., The Mineralogical Society of America. **43:** 319-364.

Eiler, J. M., M. J. Carr, et al. (2005). "Oxygen isotope constraints on the sources of Central American arc lavas." Geochemistry Geophysics Geosystems **6**(7): Q07007, doi:10.1029/2004GC000804.

Eiler, J. M., A. Crawford, et al. (2000). "Oxygen isotope geochemistry of oceanic-arc lavas." Journal of Petrology **41**(2): 229-256.

Eiler, J. M., K. Gronvold, et al. (2000). "Oxygen isotope evidence for the origin of chemical variations in lavas from Theistareykir volcano in Iceland's northern volcanic zone." Earth and Planetary Science Letters **184**(1): 269-286.

Eiler, J. M. and N. Kitchen (2001). "Hydrogen-isotope analysis of nanomole (picoliter) quantities of H_2O." Geochimica et Cosmochimica Acta **65**(24): 4467-4479.

Elliott, T., T. Plank, et al. (1997). "Element transport from slab to volcanic front at the Mariana arc." Journal of Geophysical Research-Solid Earth **102**(B7): 14991-15019.

Floss, C., F. J. Stadermann, et al. (2006). "Identification of isotopically primitive interplanetary dust particles: A NanoSIMS isotopic imaging study." Geochimica et Cosmochimica Acta **70**(9): 2371-2399.

Garcia, M. O., B. A. Jorgenson, et al. (1995). "Geochemical and isotopic evolution of Loihi volcano, Hawaii." Journal of Petrology **36**: 1647-1674.

Garcia, M. O., Muenow, David W., and Aggrey Kwesi E. (1989). "Major element, volatile, and stable isotope geochemistry of Hawaiian submarine tholeiitic glasses." Journal of geophysical Research **94**(B8): 10525-10538.

Ghiorso, M. S., Hirschmann, M.M., Reiners P.W., and Kress V.C. (2002). "The pMELTS: A revision of MELTS for improved calculation of phase relations and major element partitioning related to partial melting of the mantle to 3 GPa." Geochemistry Geophysics Geosystems **3**(5): art. no. 1030 DOI 2001GC000217.

Graham, C. M., R. S. Harmon, et al. (1984). "Experimental hydrogen isotope studies - hydrogen isotope exchange between amphibole and water." American Mineralogist **69**(1-2): 128-138.

Graham, C. M. and S. M. F. Sheppard (1980). "Experimental hydrogen isotope studies .2. fractionations in the systems epidote-NaCl-H_2O, epidote-$CaCl_2$-H_2O and epidote-seawater, and the hydrogen isotope composition of natural epidotes." Earth and Planetary Science Letters **49**(2): 237-251.

Graham, C. M., S. M. F. Sheppard, et al. (1980). "Experimental hydrogen isotope studies .1. systematics of hydrogen isotope fractionation in the systems epidote-H_2O, zoisite-H_2O and AlO(OH)-H_2O." Geochimica et Cosmochimica Acta **44**(2): 353-364.

Graham, C. M., J. A. Viglino, et al. (1987). "Experimental-study of hydrogen-isotope exchange between aluminous chlorite and water and of hydrogen diffusion in chlorite." American Mineralogist **72**(5-6): 566-579.

Gregory, R. T. and H. P. Taylor (1981). "An oxygen isotope profile in a section of Cretaceous oceanic crust, Samail opholite, Oman: Evidence for d18O buffering of the oceans by deep > 5km) seawate-hydrothermal circulation at mid-oceanic ridges." Journal of Geophysical Research **86**: 2737-2755.

Gribble, R. F., R. J. Stern, et al. (1998). "Chemical and isotopic composition of lavas from the Northern Mariana Trough: Implications for magmagenesis in back-arc basins." Journal of Petrology **39**(1): 125-154.

Grove, T. L., S. W. Parman, et al. (2002). "The role of an H_2O-rich fluid component in the generation of primitive basaltic andesites and andesites from the Mt. Shasta

region, N California." Contributions to Mineralogy and Petrology **142**(4): 375-396.

Hagemann, R., Nief, G., Roth, E. (1970). "Absolute isotopicscale for deuterium analysis of natural waters. Absolute D/H ratio for SMOW." Tellus **22**(712-715).

Hammer, V. M. F., A. Beran, et al. (1996). "OH concentrations in natural titanites determined by FTIR spectroscopy and nuclean reaction analysis." European Journal of Mineralogy **8**: 281-288.

Harmon, R. S., Hoefs J., and Wedepohl K.H. (1987). "Stable isotope (O,H,S) relationships in Tertiary basalts and their mantle xenoliths from the Northern Hessian Depression, W.-Germany." Contributions to Mineralogy and Petrology **95**: 350-369.

Hauri, E. (2002). "SIMS analysis of volatiles in silicate glasses, 2: isotopes and abundances in Hawaiian melt inclusions." Chemical Geology **183**(1-4): 115-141.

Hayes, J. M., D. J. DesMarais, et al. (1977). "High precision stable isotope ratios from microgram samples." Advances in Mass Spectrometry **7**(A): 475-480.

Hercule, S. and J. Ingrin (1999). "Hydrogen in diopside: Diffusion, kinetics of extraction-incorporation, and solubility." American Mineralogist **84**(10): 1577-1587.

Hirose, K. and T. Kawamoto (1995). "Hydrous partial melting of Iherzolite at 1 Gpa - the effect of H_2O on the genesis of basaltic magmas." Earth and Planetary Science Letters **133**(3-4): 463-473.

Hirschmann, M. M., C. Aubaud, et al. (2005). "Storage capacity of H_2O in nominally anhydrous minerals in the upper mantle." Earth and Planetary Science Letters **236**(1-2): 167-181.

Hirth, G. and D. L. Kohlstedt (1996). "Water in the oceanic upper mantle: Implications for rheology, melt extraction and the evolution of the lithosphere." Earth and Planetary Science Letters **144**(1-2): 93-108.

Holdaway, M. J., Dultrow, B.L., Borthwick, J., Shore, P., Harmon, R.S. (1986). "H content of staurolite as determined by H extraction line and ion microprobe." American Mineralogist **71**: 1135-1141.

Honma, H., M. Kusakabe, et al. (1991). "Major and trace-element chemistry and D/H, $^{18}O/^{16}O$, $^{87}Sr/^{86}Sr$ and $^{143}Nd/^{144}Nd$ ratios of rocks from the spreading center of the Okinawa Trough, a marginal back-arc basin." Geochemical Journal **25**(2): 121-136.

Horibe, Y. and H. Craig (1995). "D/H fractionation in the system methane-hydrogen-water." Geochimica Et Cosmochimica Acta **59**(24): 5209-5217.

Horita, J., D. R. Cole, et al. (2002). "Experimental and theoretical study of pressure effects on hydrogen isotope fractionation in the system brucite-water at elevated temperatures." Geochimica et Cosmochimica Acta **66**(21): 3769-3788.

Horita, J., T. Driesner, et al. (1999). "Pressure effect on hydrogen isotope fractionation between brucite and water at elevated temperatures." Science **286**(5444): 1545-1547.

Hurlbut, C. S. J. (1969). "Gem zoisite from Tanzania." American Mineralogist **54**(5-6): 702-709.

Ihinger, P. D., Hervig, R.L. and McMillan, G.L. (1994). Analytical methods for volatiles in glasses. Rviews in Mineralolgy. M. R. a. H. Carroll, J.R. . Washington D.C., Mineralogical Society of America. **30:** 67-121.

Ingrin, J., S. Hercule, et al. (1995). "Diffusion of hydrogen in diopside - results of dehydration experiments." Journal of Geophysical Research-Solid Earth **100**(B8): 15489-15499.

Ingrin, J. and H. Skogby (2000). "Hydrogen in nominally anhydrous upper-mantle minerals: concentration levels and implications." European Journal of Mineralogy **12**(3): 543-570.

Ito, E., Harris, D.M., Anderson, J.A.T. (1983). "Alteration of oceanic crust and geologic cycling of chlorine and water." Geochemica et Cosmochemica Acta **47**: 1613-1624.

Ito, E. and R. J. Stern (1986). "Oxygen-isotopic and strontium-isotopic investigations of subduction zone volcanism - the case of the Volcano Arc and the Marianas Island-Arc." Earth and Planetary Science Letters **76**(3-4): 312-320.

Ito, E., R. J. Stern, et al. (2003). "Insights into operation of the subduction factory from the oxygen isotopic values of the southern Izu-Bonin-Mariana Arc." Island Arc **12**(4): 383-397.

Jambon, A. (1994). Earth Degassing and Large-Scale Geochemical Cycling of Volatile Elements. Volatiles in Magmas. **30:** 479-517.

Jambon, A. and J. L. Zimmermann (1990). "Water in Oceanic Basalts - Evidence for Dehydration of Recycled Crust." Earth and Planetary Science Letters **101**(2-4): 323-331.

Johnson, E. A. and G. R. Rossman (2004). "A survey of hydrous species and concentrations in igneous feldspars." American Mineralogist **89**(4): 586-600.

Karato, S., Paterson, M.S. and Gerald, F. (1986). "Rheology of synthetic olivne aggregates: influence of grain size and water." Journal of Geophysical Research **91**: 8151-8176.

Karato, S. I. (1990). "The role of hydrogen in the electrical conductivity of the upper mantle." Nature **347**: 272-273.

Kawahata, H., M. Kusakabe, et al. (1987). "Strontium, oxygen, and hydrogen isotope geochemistry of hydrothermally altered and weathered rocks in DSDP hole-504b, Costa-Rica Rift." Earth and Planetary Science Letters **85**(4): 343-355.

Kelley, K. A., T. Plank, et al. (2005). "Subduction cycling of U, Th, and Pb." Earth and Planetary Science Letters **234**(3-4): 369-383.

Kelley, K. A., Plank, T, Grove T.L., Stolper E.M., Newman, S., Hauri E. (in press). "Mantle melting as a function of water content beneath back-arc basins." Journal of Geophysical Research.

Kerrick, D. M. and J. A. D. Connolly (2001). "Metamorphic devolatilization of subducted marine sediments and the transport of volatiles into the Earth's mantle." Nature **411**(6835): 293-296.

Kerrick, D. M. and J. A. D. Connolly (2001). "Metamorphic devolatilization of subducted oceanic metabasalts: implications for seismicity, arc magmatism and volatile recycling." Earth and Planetary Science Letters **189**(1-2): 19-29.

Kessel, R., M. W. Schmidt, et al. (2005). "Trace element signature of subduction-zone fluids, melts and supercritical liquids at 120-180 km depth." Nature **437**(7059): 724-727.

Kessel, R., P. Ulmer, et al. (2005). "The water-basalt system at 4 to 6 GPa: Phase relations and second critical endpoint in a K-free eclogite at 700 to 1400 degrees C." Earth and Planetary Science Letters **237**(3-4): 873-892.

Kingsley, R. H., J. G. Schilling, et al. (2002). "D/H ratios in basalt glasses from the Salas y Gomez mantle plume interacting with the East Pacific Rise: Water from old D-rich recycled crust or primordial water from the lower mantle?" Geochemistry Geophysics Geosystems **3**: art. no.-1025.

Knauth, L. P. and S. Epstein (1975). "Hydrogen and oxygen isotope ratios in silica from the JOIDES Deep Sea Drilling Project." Earth and Planetary Science Letters **25**(1): 1-10.

Knauth, L. P. and S. Epstein (1976). "Hydrogen and oxygen isotope ratios in nodular and bedded cherts." Geochemica et Cosmochemica Acta **40**(9): 1095-1108.

Koch-Muller, M., Y. Fei, et al. (2001). "Location and quantitative analysis of OH in coesite." Physics and Chemistry of Minerals **28**(10): 693-705.

Koch-Muller, M., V. Kahlenberg, et al. (2000). "Location of OH groups and oxidation processes in triclinic chloritoid." Physics and Chemistry of Minerals **27**(10): 703-712.

Koch-Muller, M., S. S. Matsyuk, et al. (2004). "Hydroxyl in omphacites and omphacitic clinopyroxenes of upper mantle to lower crustal origin beneath the Siberian platform." American Mineralogist **89**(7): 921-931.

Koga, K., E. Hauri, et al. (2003). "Hydrogen concentration analyses using SIMS and FTIR: Comparison and calibration for nominally anhydrous minerals." Geochemistry Geophysics Geosystems **4**: art. no.-1019.

Kohlstedt, D. L. and S. J. Mackwell (1998). "Diffusion of hydrogen and intrinsic point defects in olivine." Zeitschrift Fur Physikalische Chemie-International Journal of Research in Physical Chemistry & Chemical Physics **207**: 147-162.

Kolodny, Y. and S. Epstein (1976). "Stable isotope geochemistry of deep sea cherts." Geochimica et Cosmochimica Acta 40(10) **40**(10): 1195-1209.

Kurka, A., M. Blanchard, et al. (2005). "Kinetics of hydrogen extraction and deuteration in grossular." Mineralogical Magazine **69**(3): 359-371.

Kuroda, Y. (1977). "Hydrogen isotope composition of deep-seated water." Contributions to Mineralogy and Petrology **60**: 311-315.

Kuroda, Y., Y. Hariya, et al. (1982). "D/H Fractionation between water and the melts of quartz, K-feldspar, albite and anorthite at high-temperature and pressure." Geochemical Journal **16**(2): 73-78.

Kyser, T. K. and J. R. O'Neil (1984). "Hydrogen isotope systematics of submarine basalts." Geochimica et Cosmochimica Acta **48**(10): 2123-2133.

Lanford, W. A. (1978). "^{15}N Hydrogen profiling: Scientific applications." Nuclear Instruments and methods in physics research **149**(Sect. B): 1-8.

Mackwell, S. J. and D. L. Kohlstedt (1990). "Diffusion of hydrogen in olivine - implications for water in the mantle." Journal of Geophysical Research-Solid Earth and Planets **95**(B4): 5079-5088.

Mackwell, S. J., D. L. Kohlstedt, et al. (1985). "The role of water in the deformation of olivine single-crystals." Journal of Geophysical Research-Solid Earth and Planets **90**(NB13): 1319-1333.

Macpherson, C. G., D. R. Hilton, et al. (2000). "Evidence for an O-18-depleted mantle plume from contrasting O- 18/O-16 ratios of back-arc lavas from the Manus Basin and Mariana Trough." Earth and Planetary Science Letters **176**(2): 171-183.

Maldener, J., A. Hosch, et al. (2003). "Hydrogen in some natural garnets studied by nuclear reaction analysis and vibrational spectroscopy." Physics and Chemistry of Minerals **30**(6): 337-344.

Maldener, J., F. Rauch, et al. (2001). "OH absorption coefficients of rutile and cassiterite deduced from nuclear reaction analysis and FTIR spectroscopy." Mineralogy and Petrology **71**(1-2): 21-29.

Matthews, D. E. and J. M. Hayes (1978). "Isotope-ratio-monitoring gas chromatography-mass spectrometry." Analytical Chemistry **50**(11): 1465-1473.

Mei, S. and D. L. Kohlstedt (2000). "Influence of water on plastic deformation of olivine aggregates 1. Diffusion creep regime." Journal of Geophysical Research-Solid Earth **105**(B9): 21457-21469.

Mei, S. and D. L. Kohlstedt (2000). "Influence of water on plastic deformation of olivine aggregates 2. Dislocation creep regime." Journal of Geophysical Research-Solid Earth **105**(B9): 21471-21481.

Merritt, D. A., M. P. Ricci, et al. (1992). "Isotope-ratio-monitoring techniques for hydrogen isotopic analyses." Abstracts of papers of the American Chemical Society **203. 90-Geoc, Part 1**.

Michael, P. J. (1988). "The concentration, behavior and storage of H_2O in the suboceanic upper mantle: Implications for mantle metasomatism." Geochemica et Cosmochemica Acta **55**: 555-566.

Miller, D. M., S. L. Goldstein, et al. (1994). "Cerium lead and lead-isotope ratios in arc magmas and the enrichment of lead in the continents." Nature **368**(6471): 514-520.

Mosenfelder, J. L., N. I. Deligne, et al. (2006). "Hydrogen incorporation in olivine from 2-12 GPa." American Mineralogist **91**(2-3): 285-294.

Mottl, M. J., C. G. Wheat, et al. (2004). "Chemistry of springs across the Mariana forearc shows progressive devolatilization of the subducting plate." Geochimica Et Cosmochimica Acta **68**(23): 4915-4933.

Newman, S. and E. Stolper (2000). "H_2O and CO_2 in magmas from the Mariana arc and back arc systems." Geochemistry Geophysics Geosystems **1**: 1999GC000027.

Newton, R. C. (1966). "The thermal stability of zoisite." Journal of Geology **73**: 431-441.

O'Leary, J. A., E. J.M., et al. (2005). "Hydrogen isotope geochemistry of nominally anhydrous minerals." Geochemica et Cosmochemica Acta **69**(10): A745-A745 Supplement S.

Pearce, J. A., Stern Robert J, Bloomer, Sherman H., Fryer, Patty (2005). "Geochemical mapping of the Mariana arc-basin system: Implications for the nature and distribution of the subduction components." Geochemistry Geophysics Geosystems **6**(7): Q07006, doi:10.1029/2004GC000895.

Peslier, A. H. and J. F. Luhr (2006). "Hydrogen loss from olivines in mantle xenoliths from Simcoe (USA) and Mexico: Mafic alkalic magma ascent rates and water budget of the sub-continental lithosphere." Earth and Planetary Science Letters **242**(3-4): 302-319.

Peslier, A. H., J. F. Luhr, et al. (2002). "Low water contents in pyroxenes from spinel-peridotites of the oxidized, sub-arc mantle wedge." Earth and Planetary Science Letters **201**(1): 69-86.

Pineau, F. and M. Javoy (1994). "Strong degassing at ridge crests - the behavior of dissolved carbon and water in basalt glasses at 14-Degrees-N, Mid- Atlantic Ridge." Earth and Planetary Science Letters **123**(1-4): 179-198.

Pineau, F., M. P. Semet, et al. (1999). "The genesis of the stable isotope (O, H) record in arc magmas: the Kamtchatka's case." Chemical Geology **153**(1-4): 93-124.

Pineau, F., S. Shilobreeva, et al. (2004). "Deep-sea explosive activity on the Mid-Atlantic Ridge near 34 degrees 50 ' N: a stable isotope (C, H, O) study." Chemical Geology **211**(1-2): 159-175.

Plank, T. and C. Langmuir (1993). "Tracing trace elements from sediment input to volcanic output at subduction zones." Nature **362**: 799-742.

Poli, S. and M. W. Schmidt (2002). "Petrology of subducted slabs." Annual Review of Earth and Planetary Sciences **30**: 207-235.

Poreda, R. (1985). "Helium-3 and deuterium in back-arc basalts: Lau Basin and the Mariana Trough." Earth and Planetary Science Letters **73**: 244-254.

Poreda, R., J. G. Schilling, et al. (1986). "Helium and hydrogen isotopes in ocean-ridge basalts north and south of Iceland." Earth and Planetary Science Letters **78**(1): 1-17.

Putirka, K. (2005). "Mantle potential temperatures at Hawaii, Iceland, and the mid-ocean ridge system, as inferred from olivine phenocrysts: Evidence from thermally driven mantle plumes." Geochemistry Geophysics Geosystems **6**(5): 10.1029/2005GC000915.

Rossman, G. R. and R. D. Aines (1991). "The hydrous components in garnets - grossular-hydrogrossular." American Mineralogist **76**(7-8): 1153-1164.

Rossman, G. R., F. Rauch, et al. (1988). "Nuclear reaction analysis of hydrogen in almandine, pyrope, and spessartite garnets." Neues Jahrbuch fuer Mineralogie. Monatshefte(4): 172-178.

Rossman, G. R. and J. R. Smyth (1990). "Hydroxyl contents of accessory minerals in mantle eclogites and related rocks." American Mineralogist **75**(7-8): 775-780.

Rupke, L. H., J. P. Morgan, et al. (2004). "Serpentine and the subduction zone water cycle." Earth and Planetary Science Letters **223**(1-2): 17-34.

Satake, H. and J. Matsuda (1979). "Strontium and hydrogen isotope geochemistry of fresh and metabasalt dredged from the Mid-Atlantic Ridge." Contributions to Mineralogy and Petrology **70**(2): 153-157.

Scambelluri, M., P. Bottazzi, et al. (2001). "Incompatible element-rich fluids released by antigorite breakdown in deeply subducted mantle." Earth and Planetary Science Letters **192**(3): 457-470.

Scambelluri, M. and P. Philippot (2001). "Deep fluids in subduction zones." Lithos **55**(1-4): 213-227.

Schmidt, M. W. and S. Poli (1998). "Experimentally based water budgets for dehydrating slabs and consequences for arc magma generation." Earth and Planetary Science Letters **163**(1-4): 361-379.

Sharp, Z. D. (1990). "A laser-based microanalytical method for the in situ determination of oxygen isotope ratios of silicates and oxides." Geochemica et Cosmochemica Acta **54**: 1353-1357.

Skogby, H., D. R. Bell, et al. (1990). "Hydroxide in pyroxene - variations in the natural-environment." American Mineralogist **75**(7-8): 764-774.

Smith, P. M. and P. D. Asimow (2005). "Adiabat_1ph: A new public front-end to the MELTS, pMELTS, and pHMELTS models." Geochemistry Geophysics Geosystems **6**: art. no. Q02004, doi 10.1029/2004GC000816.

Smyth, J. R., D. R. Bell, et al. (1991). "Incorporation of hydroxyl in upper-mantle clinopyroxenes." Nature **351**(6329): 732-735.

Stalder, R. and H. Skogby (2003). "Hydrogen diffusion in natural and synthetic orthopyroxene." Physics and Chemistry of Minerals **30**(1): 12-19.

Stern, R. J. (2002). "Subduction zones." Reviews of Geophysics **40**(4).

Stern, R. J., E. Kohut, et al. (2005). "Subduction factory processes beneath beneath the Guguan cross-chain, Mariana Arc: no role for sediments, are serpentinites important." Contributions to Mineralogy and Petrology **151**: 202-221.

Stern, R. J., P. N. Lin, et al. (1990). "Enriched back-arc basin basalts from the Northern Mariana Trough - implications for the magmatic evolution of back-arc basins." Earth and Planetary Science Letters **100**(1-3): 210-225.

Stolper, E. and S. Newman (1994). "The role of water in the petrogenesis of Mariana trough magmas." Earth and Planetary Science Letters **121**: 293-325.

Suzuoki, T. and S. Epstein (1976). "Hydrogen isotope fractionation between OH-bearing minerals and water." Geochimica et Cosmochimica Acta **40**(10): 1229-1240.

Suzuoki, T., Kimura T (1973). "D/H and $^{18}O/^{16}O$ fractionation in ice-water system." Mass Spectrometry **21**: 229-233.

Thompson, R. N., C. J. Ottley, et al. (2005). "Source of the quaternary alkalic basalts, picrites and basanites of the Potrillo Volcanic Field, New Mexico, USA: Lithosphere or convecting mantle?" Journal of Petrology **46**(8): 1603-1643.

Valley, J. W., Kitchen, N., Kohn, M.J., Niendorff, C.R., and Spicuzza, M.J. (1995). "Strategies fpr high precision oxygen isotope analysis by laser fluorination." Geochemica et Cosmochemica Acta **59**: 5223-5231.

van Keken, P. E., B. Kiefer, et al. (2002). "High-resolution models of subduction zones: Implications for mineral dehydration reactions and the transport of water into the deep mantle." Geochemistry Geophysics Geosystems **3**.

Vlassopoulos, D., G. R. Rossman, et al. (1993). "Coupled substitution of H and minor elements in rutile and the implications of high OH contents in Nb-rich and Cr-rich rutile from the upper mantle." American Mineralogist **78**(11-12): 1181-1191.

Volpe, A. M., McDougall, J.D., and Hawkins, J.W. (1987). "Mariana Trough basalts (MTB): Trace element and Sr-Nd isotopic evidence for mixing between MORB-like and arc-like melts." Earth and Planetary Science Letters **82**: 241-254.

Wagner, C., Deloule, E., Mokhtari, A. (1996). "Richterite-bearing peridotites and MARID-type inclusions in lavas from North Eastern Morocco: mineralogy and D/H isotopic studies." Contributions to Mineralogy and Petrology **124**: 406-421.

Wang, L. P., Y. X. Zhang, et al. (1996). "Diffusion of the hydrous component in pyrope." American Mineralogist **81**(5-6): 706-718.

Wang, Z., J. Eiler, et al. (2004). "Oxygen isotope composition of olivine phenocrysts from Koolau Scientific Drilling Project (KSDP)." Geochimica Et Cosmochimica Acta **68**(11): A557-A557.

Wang, Z. G., E. A. Schauble, et al. (2004). "Equilibrium thermodynamics of multiply substituted isotopologues of molecular gases." Geochimica Et Cosmochimica Acta **68**(23): 4779-4797.

Wenner, D. B. and H. P. Taylor (1971). "Temperatures of serpentinization of ultramafic rocks based on $^{18}O/^{16}O$ fractionation between coexisting serpentine and magnetite." Contributions to Mineralogy and Petrology **32**(3): 165-&.

Wessel, P. and W. H. F. Smith (1998). "New, improved version of Generic Mapping Tools released." Eos Transactions American Geophysical Union **79 (47)**: 579.

Williams, Q. and R. J. Hemley (2001). "Hydrogen in the deep earth." Annual Review of Earth and Planetary Sciences **29**: 365-418.

Woodhead, J. A., G. R. Rossman, et al. (1991). "Hydrous species in zircon." American Mineralogist **76**(9-10): 1533-1546.

Woodhead, J. D., R. S. Harmon, et al. (1987). "O, ,S, Sr, Pb, isotope variations in volcanic rocks from the Northern Mariana Islands: implications for crustal recycling in intra-oceanic arcs." Earth and Planetary Science Letters **83**: 39-52.

Workman, R. K. and S. R. Hart (2005). "Major and trace element composition of the depleted MORB mantle (DMM)." Earth and Planetary Science Letters **231**(1-2): 53-72.